

## Porous organic framework (POF) membranes for CO<sub>2</sub> separation

Shan, Meixia

**DOI**

[10.4233/uuid:c4ca2469-1bf2-458d-b944-c76c7d061abe](https://doi.org/10.4233/uuid:c4ca2469-1bf2-458d-b944-c76c7d061abe)

**Publication date**

2018

**Document Version**

Final published version

**Citation (APA)**

Shan, M. (2018). *Porous organic framework (POF) membranes for CO<sub>2</sub> separation*. [Dissertation (TU Delft), Delft University of Technology]. <https://doi.org/10.4233/uuid:c4ca2469-1bf2-458d-b944-c76c7d061abe>

**Important note**

To cite this publication, please use the final published version (if applicable).  
Please check the document version above.

**Copyright**

Other than for strictly personal use, it is not permitted to download, forward or distribute the text or part of it, without the consent of the author(s) and/or copyright holder(s), unless the work is under an open content license such as Creative Commons.

**Takedown policy**

Please contact us and provide details if you believe this document breaches copyrights.  
We will remove access to the work immediately and investigate your claim.

# **Porous organic framework (POF) membranes for CO<sub>2</sub> separation**

**Meixia Shan**



# Porous organic framework (POF) membranes for CO<sub>2</sub> separation

Proefschrift

ter verkrijging van de graad van doctor  
aan de Technische Universiteit Delft,  
op gezag van de Rector Magnificus prof.dr.ir. T.H.J.J. van der Hagen,  
voorzitter van het College voor Promoties,  
in het openbaar te verdedigen op  
Woensdag, 24 oktober, 2018 om 15:00 uur

door

**Meixia SHAN**

Master of Engineering in Materials Science and Engineering, China University of Petroleum (East  
China), China  
geboren te Shangqiu, Henan Province, China

This dissertation has been approved by the:

Promotor: Prof. dr. F. Kapteijn and Prof. dr. J. Gascon Sabate

Composition of the doctoral committee:

Rector Magnificus	Chairman
Prof. dr. F. Kapteijn	Delft University of Technology, promotor
Prof. dr. J. Gascon Sabate	Delft University of Technology and King Abdullah University of Science and Technology, promotor

Independent members:

Prof. dr. J. Coronas	University of Zaragoza
Prof. dr. rer. nat. J. Caro	Leibnitz University Hannover
Prof. dr. ir. I. Vankelecom	Catholic University Leuven
Prof. dr. ir. A. Nijmeijer	University of Twente
Prof. dr. S. J. Picken	Delft University of Technology
Prof. dr. ir. M.T. Kreutzer	Delft University of Technology, reserve member

The work described in this thesis was carried out in Catalysis Engineering section, Department of Chemical Engineering, Faculty of Applied Sciences, Delft University of Technology. The research was financed by China Scholarship Council (CSC).

ISBN/EAN: 978-94-6366-091-4

Cover designed by Yanchun Wei, <https://www.springwei.eu.com/en/>

Copyright © 2018 Meixia Shan

All rights reserved.

Printed

## ***To my family***

*Love is patient, love is kind. It does not envy, it does not boast, it is not proud. It does not dishonor others, it is not self-seeking, it is not easily angered, it keeps no record of wrongs. Love does not delight in evil but rejoices with the truth. It always protects, always trusts, always hopes, always perseveres.*

*Love never fails.*

**1 Corinthians 13:4-8**



## Contents

<b>INTRODUCTION</b>	1
1.1 INTRODUCTION	3
1.2 GENERAL PARAMETERS AND FUNDAMENTALS OF MEMBRANE-BASED CO <sub>2</sub> SEPARATION	4
1.3 PURE POF MEMBRANES	6
1.3.1 COF membranes	6
1.3.2 CTF membranes	8
1.3.3 CMP membranes	9
1.4 POF-BASED MMMs	10
1.5 THESIS OUTLINE	12
REFERENCES	13
<b>AZINE-LINKED COVALENT ORGANIC FRAMEWORK-BASED MIXED MATRIX MEMBRANES FOR CO<sub>2</sub>/CH<sub>4</sub> SEPARATION</b>	19
2.1. INTRODUCTION	21
2.2. EXPERIMENTAL	22
2.2.1. Materials	22
2.2.2 Synthesis of ACOF-1	23
2.2.3. Preparation of mixed-matrix membranes (MMMs)	23
2.2.4. Characterization techniques	24
2.2.5. Gas permeation experiments	26
2.3. RESULTS AND DISCUSSION	27
2.4. CONCLUSIONS	35
REFERENCES	36
<b>MIXED-MATRIX MEMBRANES CONTAINING AN AZINE-LINKED COVALENT ORGANIC FRAMEWORK: INFLUENCE OF THE POLYMERIC MATRIX ON POST-COMBUSTION CO<sub>2</sub>-CAPTURE</b>	47
3.1. INTRODUCTION	49
3.2. EXPERIMENTAL	52
3.2.1. Materials	52
3.2.2 Synthesis of ACOF-1	52
3.2.3. Preparation of mixed-matrix membranes (MMMs)	52
3.2.4. Characterization techniques	54
3.2.5. Gas permeation experiments	55
3.3. RESULTS AND DISCUSSION	55
3.3.1. Characterization of ACOF-1	55
3.3.2. Characterization of ACOF-1-based MMMs	55
3.3.3. Gas separation performance	60



4. CONCLUSIONS	63
REFERENCES	65
<b>BENZIMIDAZOLE LINKED POLYMERS (BILPS) IN MIXED-MATRIX MEMBRANES: INFLUENCE OF FILLER POROSITY ON THE CO<sub>2</sub>/N<sub>2</sub> SEPARATION PERFORMANCE</b>	75
4.1. INTRODUCTION	77
4.2. EXPERIMENTAL	79
4.2.1. Materials	79
4.2.2 Synthesis of BILP-101 and RT-BILP-101	79
4.2.3. Preparation of mixed-matrix membranes (MMMs)	80
4.2.4. BILP fillers and membrane characterization	81
4.2.5. Gas permeation experiments	83
4.3. RESULTS AND DISCUSSION	83
4.3.1. Characterization of BILP-101 and RT-BILP-101	83
4.3.2. Characterization of BILPs MMMs	86
4.3.3. Gas separation performance	89
4.4. CONCLUSIONS	94
REFERENCES	96
<b>ALUMINA SUPPORTED POROUS ORGANIC FRAMEWORK MEMBRANES FOR PRE-COMBUSTION CO<sub>2</sub> CAPTURE - MANUFACTURE AND PERFORMANCE</b>	115
5.1. INTRODUCTION	117
5.2. EXPERIMENTAL	118
5.2.1. Materials	118
5.2.2 Synthesis of supported BILP-101 membranes	118
5.2.3. Synthesis of BILP-101 film at the bulk liquid interface	120
5.2.4. Characterization techniques	120
5.2.5. Gas permeation experiments	122
5.3. RESULTS AND DISCUSSION	123
5.4. CONCLUSIONS	131
REFERENCES	133
<b>SUMMARY</b>	145
<b>SAMENVATTING</b>	149
<b>ACKNOWLEDGEMENTS</b>	153
<b>LIST OF PUBLICATIONS</b>	157
<b>CURRICULUM VITAE</b>	161

# Introduction

# 1

*The important thing is not to stop questioning. Curiosity has its own reason for existence. One cannot help but be in awe when he contemplates the mysteries of eternity, of life, of the marvelous structure of reality. It is enough if one tries merely to comprehend a little of this mystery each day.*

Albert Einstein

*Imagination is more important than knowledge. For knowledge is limited to all we now know and understand, while imagination embraces the entire world, and all there ever will be to know and understand.*

Albert Einstein



## 1.1 INTRODUCTION

The fast accumulation of CO<sub>2</sub> in the atmosphere in recent years is leading to serious global warming issues, such as abnormal climate change and rising of sea levels.<sup>1-3</sup> CO<sub>2</sub> emissions are mostly due to fossil fuels. CO<sub>2</sub> capture can be achieved mainly by pre-combustion capture (separation of H<sub>2</sub>/CO<sub>2</sub> mixture) or post-combustion capture (separation of CO<sub>2</sub>/N<sub>2</sub> mixture). On the other hand, the use of biogas as alternative fuel may also play a role in the direct capture of CO<sub>2</sub>. In that case, biogas upgrading would require the separation of CO<sub>2</sub>/CH<sub>4</sub>. Conventional technologies for CO<sub>2</sub> capture, such as cryogenic distillation or amine adsorption, are energy intensive and may bring environmental issues.<sup>4</sup> In this sense, membrane separation technology is more attractive owing to the advantages of energy efficiency, low cost, small footprint and environmental benefits. Membrane materials are the core part of the membrane technology. Polymers are the only membrane materials that could be produced in large-scale and have been successfully commercialized since the 1980s. Unfortunately, polymer membranes suffer from an undesirable “trade-off” relation between permeability (*P*) and selectivity (*S*), which is known as Robeson upper bound.<sup>5, 6</sup> The underlying reason accounting for this trade-off phenomena is the dense state or limited porosity of polymers.<sup>5, 7</sup> In this regard, the creation of nanopores by introducing microporous materials is a promising method for achieving a high membrane performance and surpass the Robeson bound. Thus, a wide variety of microporous materials, such as zeolites,<sup>8</sup> or metal-organic frameworks (MOFs),<sup>9</sup> among others, has been explored as membranes for CO<sub>2</sub> separation.

Porous organic frameworks (POFs) are a novel class of porous materials constructed exclusively from organic units. Different types of POFs (Fig. 1.1) have been synthesized, including crystalline covalent organic frameworks (COFs),<sup>10, 11</sup> semi-crystalline covalent trizine frameworks (CTFs),<sup>12</sup> amorphous porous aromatic frameworks (PAFs),<sup>13</sup> conjugated microporous polymers (CMPs) and benzimidazole linked-polymers (BILPs).<sup>14, 15</sup> Owing to their distinguishing features, such as inherent porosity, tunable pore size, high surface area, excellent thermochemical stability, low density and diverse functionality, POFs have gained tremendous attention in different fields, such as gas storage and separation,

## Porous Organic Frameworks

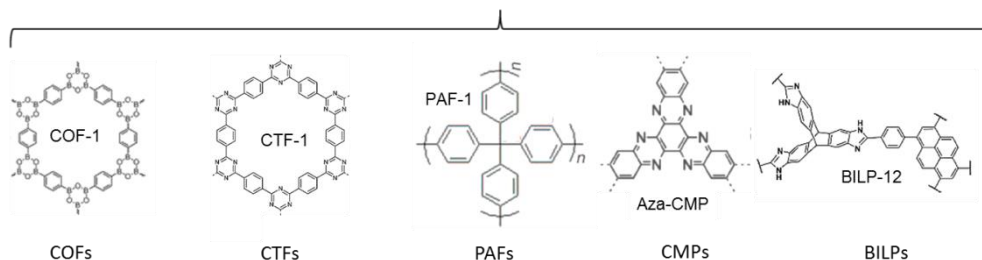


**Fig. 1.1.** Classification of POFs. COFs are crystalline porous networks.<sup>10</sup> CTFs are constructed by the trimerization reaction of carbonitriles and thus contains trizaine rings in the network.<sup>16</sup> PAFs possess a rigid aromatic open framework structure.<sup>17</sup> CMPs are  $\pi$ -conjugated three- dimensional (3D) networks.<sup>18</sup> BILPs are a class of POFs linked by the benzimidazole ring.<sup>19</sup>

catalysis, photovoltaics, chemical sensors and energy storage.<sup>20-24</sup> More information on POFs synthesis, properties and applications can be found in recent reviews.<sup>2, 25-28</sup> However, the use of POFs as membranes is still at the infancy stage.

This chapter reviews the latest advances in the formation of POF-based membranes. It starts with a brief introduction of the fundamentals of membrane separation, followed by the development of POF membranes. In particular, two main strategies to process POF membranes, including engineering of pure POFs membranes on substrates and the fabrication of mixed-matrix membranes (MMMs), have been reported and will be discussed in this chapter.

## 1.2 GENERAL PARAMETERS AND FUNDAMENTALS OF MEMBRANE-BASED CO<sub>2</sub> SEPARATION

In membrane-based gas separation, permeability ( $P$ ) and selectivity ( $S$ ) are key parameters used to evaluate the membrane separation performance. The gas permeability of an  $i$ -component ( $P_i$ ) is the permeance ( $Q_i$ ) normalized by the membrane thickness ( $l$ ) ( $P_i = Q_i \times l$ ), where the permeance is the mass, volume or molar flow rate across the membrane in unit area and pressure.  $P_i$  can be expressed as follows (Equation 1.1):

$$P_i = \frac{F_i \cdot l}{\Delta p_i \cdot A} \quad (1.1)$$

where  $F_i$  denotes the molar flow rate of compound  $i$  ( $\text{mol s}^{-1}$ ),  $l$  is the thickness of the membrane (m) and  $A$  is the membrane area ( $\text{m}^2$ ).  $\Delta p_i$  corresponds to the transmembrane pressure difference (or the partial pressure difference in the case of gas mixtures) of a component  $i$  across the membrane (Pa).

In a polymeric membrane, permeability depends on the gas solubility and diffusivity and is written as  $P_i = D_i \times S_i$ , where  $D_i$  and  $S_i$  are the gas component diffusivity and solubility coefficients in the polymer matrix, respectively. The gas selectivity of  $i$ -component over  $j$ -component is given by Equation 1.2:

$$\alpha_{i,j} = \left(\frac{D_i}{D_j}\right) \times \left(\frac{S_i}{S_j}\right) \quad (1.2)$$

where  $\frac{D_i}{D_j}$  and  $\frac{S_i}{S_j}$  are the diffusivity and solubility selectivities, respectively. The unit typically used for permeability is Barrer ( $1 \text{ Barrer} = 3.35 \times 10^{-16} \text{ mol} \cdot \text{s}^{-1} \cdot \text{m}^{-1} \cdot \text{Pa}^{-1}$ ), whereas the permeance unit is GPU ( $1 \text{ GPU} = 3.35 \times 10^{-10} \text{ mol} \cdot \text{s}^{-1} \cdot \text{m}^{-2} \cdot \text{Pa}^{-1}$ ).

Gas separation through a membrane may occur through three different mechanisms:<sup>29-31</sup>

(a) solution-diffusion, (b) molecular sieving and (c) Knudsen diffusion. For the solution-diffusion mechanism, there are no continuous pathways for gas transport, and the selectivity depends on the differences in species diffusivities and solubilities in the membrane. Solubility is governed by the gas condensability (function of the critical temperature) and the affinity between gas molecules and the membrane material. Diffusivity on the other hand depends on the free volume of the membrane, as well as the gas molecular size. In the case of the molecular sieving mechanism, the separation is mainly based on the difference of molecular size. Generally, membranes based on this mechanism possess small pores that could significantly constrict the diffusion of larger molecules when mixture gases are passing through the pores. In particular, small-pore membranes, such as some zeolites and MOFs, are good candidates for molecular sieving membranes that could achieve high selectivity.<sup>32-34</sup> As to the Knudsen diffusion, it is the dominant mechanism when the membrane pore size is smaller than the gas mean free path, but much larger than the molecular size. Molecules with low mass diffuse faster and show higher permeance. The selectivity of Knudsen diffusion is the inverse-square-root ratio of molecular mass of the gases, resulting in relatively low selectivities.

**Table 1.1.** Relevant physical properties of selected gases.<sup>7, 35</sup>

Gases	Kinetic diameter (Å)	Quadrupole moment ( $10^{-26}$ esu m <sup>2</sup> )	Condensability parameters	
			Boiling point (K)	Critical temperature (K)
H <sub>2</sub>	2.83-2.89	0.66	20.3	60
CO <sub>2</sub>	3.3	1.52	216.6	195
N <sub>2</sub>	3.64-3.80	4.30	77.4	71
CH <sub>4</sub>	3.76	0	111.7	149

In CO<sub>2</sub> separation processes, CO<sub>2</sub> is usually separated from CH<sub>4</sub>, N<sub>2</sub> and H<sub>2</sub>, which refers to natural gas purification, post- and pre-combustion CO<sub>2</sub> capture, respectively. Table 1.1 lists the relevant physical properties of these gas molecules. Compared to other gases, CO<sub>2</sub> has higher boiling and critical temperatures, resulting in a higher condensability and thus solubility in the membranes. Moreover, the larger quadrupole moment of CO<sub>2</sub> may favor its interaction with different functional groups in the membrane. The above characteristics of CO<sub>2</sub> result in the solubility selectivity over CH<sub>4</sub>, N<sub>2</sub> and H<sub>2</sub>. The diffusivity selectivity of CO<sub>2</sub>/CH<sub>4</sub>, CO<sub>2</sub>/N<sub>2</sub> on the other hand is higher than one due to the smaller kinetic diameter of CO<sub>2</sub>. Combining the higher solubility and diffusivity selectivities, CO<sub>2</sub> is easier to separate from CH<sub>4</sub> or N<sub>2</sub> than from H<sub>2</sub>. In the latter case, the separation is indeed more challenging given the smaller size of H<sub>2</sub> and higher condensability of CO<sub>2</sub>, resulting in an opposite trend in diffusivity and solubility selectivities.<sup>36</sup>

## 1.3 PURE POF MEMBRANES

### 1.3.1 COF membranes

Covalent organic frameworks (COFs) are a class of crystalline porous materials, constructed from light-weight elements linked by strong covalent bonds,<sup>26, 37</sup> resulting in different compounds with very low mass densities and extremely robust. Since the synthesis of the first COF was reported in 2005 by Yaghi and co-workers,<sup>10</sup> COFs have attracted tremendous interest due to their permanent porosity and high thermal and chemical stabilities, which prompt their application in different areas like gas storage,<sup>38</sup> catalysis<sup>20</sup> and photovoltaics.<sup>21</sup> Although there have been many reports on the design and synthesis of COFs and their application in gas storage or separation,<sup>22, 39, 40</sup> only a few

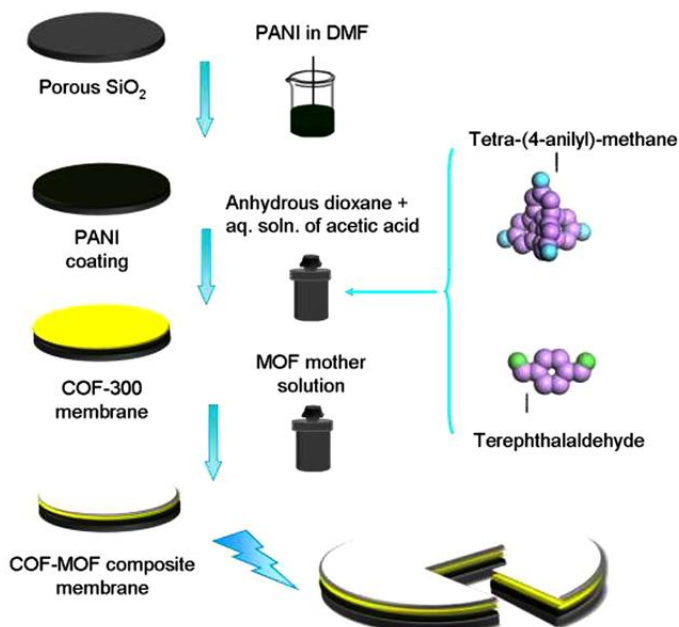


**Fig. 1.2.** Schematic representation of the fabrication of COF-MOF composite membranes.<sup>43</sup>

studies on the application of COFs as gas separation membranes can be found. Gao *et al.*<sup>41, 42</sup> first reported the growth of a COF membrane on a surface-modified  $\alpha$ -Al<sub>2</sub>O<sub>3</sub> ceramic support. However, the permeation performance towards different gases was mainly governed by Knudsen diffusion due to the large pores of the selected COF. Ben *et al.*<sup>43</sup> reported for the first time a MOF-COF composite membranes obtained through the growth of MOFs on top of a COF membrane (Fig. 1.2). The resulting hybrid membrane showed higher H<sub>2</sub>/CO<sub>2</sub> selectivity than the individual COF or MOF membranes, surpassing the 2008 Robeson upper bound of polymeric membranes for the H<sub>2</sub>/CO<sub>2</sub> gas pair. Tsuru *et al.*<sup>44</sup> successfully fabricated an ultrathin membrane via drop-coating of exfoliated COF-1 nanosheets on  $\alpha$ -Al<sub>2</sub>O<sub>3</sub> substrate. These ultrathin membranes resulted in high permeable composites, but the selectivity was however close to Knudsen diffusion. The above studies demonstrate the feasibility of preparing COF membranes for gas separation. However, it should be noted that the processing of COFs into defect-free membrane for gas separation remains a challenge and only few reports on the preparation of continuous COF



membranes on porous substrates, being used as nanofiltration membrane, have been reported.<sup>45, 46</sup>

### 1.3.2 CTF membranes

Covalent triazine frameworks (CTFs) are normally synthesized through ionothermal methods in which the cyclotrimerization of nitrile groups in molten Lewis acid (*e.g.*  $\text{ZnCl}_2$ ) under high pressure and high temperature affords crystalline or amorphous porous compounds.<sup>47-49</sup> Although the resultant CTFs exhibit excellent chemical and thermal stabilities, the conditions needed for their fabrication makes the preparation of CTF-based membranes quite challenging. Extensive efforts have been devoted to develop a more gentle method for the synthesis of CTFs.<sup>50, 51</sup> For instance, Dai *et al.*<sup>52</sup> used a super acid (*e.g.*  $\text{CF}_3\text{SO}_3\text{H}$ ) instead of the typically used molten salt  $\text{ZnCl}_2$ , to catalyze the cyclotrimerization of aromatic boronitriles into CTFs networks at relatively low temperatures ( $< 373$  K). Interestingly, the crosslinking reaction solution could be directly casted onto a glass to fabricate a continuous film. The synthesized porous triazine-framework-based membrane exhibited a good selectivity towards  $\text{CO}_2/\text{N}_2$  ( $29 \pm 2$ ) together with a  $\text{CO}_2$  permeability of  $518 \pm 25$  Barrer. However,  $\text{CF}_3\text{SO}_3\text{H}$  is a strong and corrosive acid, which is environmentally unfriendly. So as to circumvent this problem, Wang *et al.*<sup>53</sup> recently developed a new strategy to construct CTFs by polycondensation from a wide range of building units under mild conditions, using cesium carbonate as a base and DMSO as solvent at 373 K. The resulting CTFs display a layered structure, which can be exfoliated into nanosheets. Computational studies suggest that CTF-1 nanosheets can be restacked into few-layer ultra-thin membranes, providing selective interlayer flow passages, which results in enhanced inherent gas separation performance.<sup>54, 55</sup> Zhong *et al.*<sup>56</sup> first exfoliated CTF-1 into nanosheets using a ball milling method and then employ a graphene oxide (GO)-assisted vacuum filtration method for the preparation of ultrathin CTFs membranes on porous support (Fig. 1.3). The prepared membranes show a high  $\text{H}_2$  permeance together with a competitive  $\text{H}_2/\text{CO}_2$  selectivity ( $\sim 17$ ). This performance successfully surpassed the Robeson's 2008 upper bound, making these CTF-based membranes attractive for pre-combustion  $\text{CO}_2$  capture.

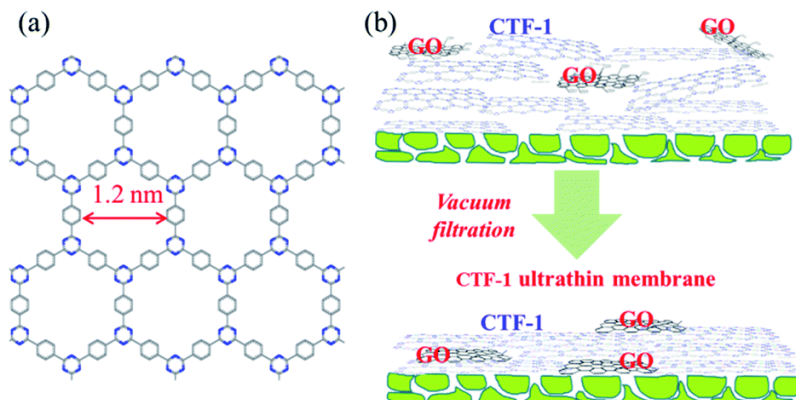


**Fig. 1.3.** Schematic representation of the fabrication of ultrathin CTF-1 membrane with the assistance of GO.<sup>56</sup>

### 1.3.3 CMP membranes

Conjugated microporous polymers (CMPs) refer to those porous frameworks that permit the connection of the building units in a  $\pi$ -conjugated manner. CMPs are usually synthesized by metal-catalyzed cross-coupling reactions resulting in insoluble powders, making it technically challenging to be processed into a defect-free membranes.<sup>18, 57</sup> Recently, Wu *et al.*<sup>58</sup> reported the synthesis of free-standing CMP nanofilms at an oil-water interface by an interfacial polymerization method, which has been proven as a very attractive approach to integrate CMP into membranes. The first CMP membrane for gas separation was reported by Tsotsalas' group,<sup>59</sup> and it was fabricated using a layer by layer growth method (Fig. 1.4a). Specifically, two different monomers with multiple copies of the same functional groups were employed as building units instead of one single monomer. The crucial strategy of their method was the use of a sacrificial substrate so that after the detachment of substrate a free-standing CMP membrane (Fig. 1.4b) could be transferred to a polydimethylsiloxane/polyacrylonitrile (PDMS/PAN) support. The resulting supported CMP film showed a  $\text{H}_2/\text{N}_2$  selectivity of 36 and  $\text{O}_2/\text{N}_2$  selectivity of 6, indicating the formation of a continuous defect-free CMP layer. Moreover, this fabrication method may allow for the synthesis of a variety of CMP films with different physical and chemical properties for other applications.

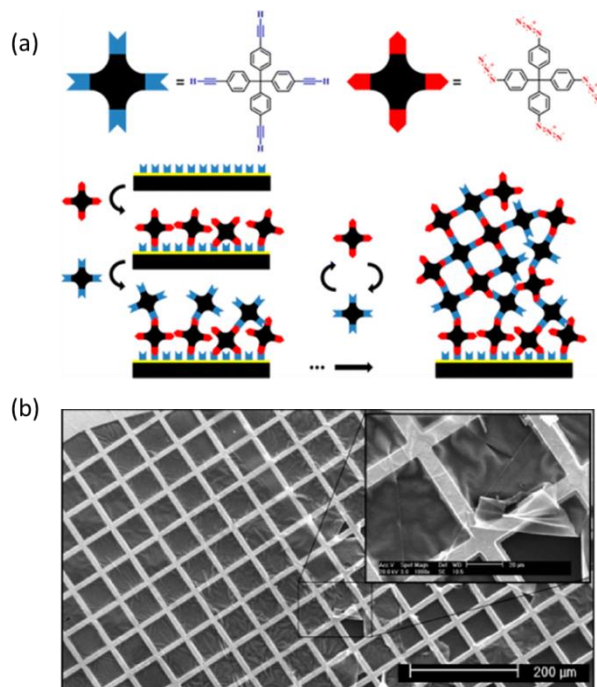


**Fig. 1.4.** (a) Molecular building units and schematic representation of the layer-by-layer synthesis of CMP systems on functionalized surfaces. (b) Scanning electron microscope (SEM) images of the freely floating CMP-membrane after its transfer to a TEM grid.<sup>59</sup>

#### 1.4 POF-BASED MMMs

Although some fabrication methods have been developed for the synthesis of continuous porous organic framework (POF) membranes (*vide supra*), POFs are typically obtained in the form of insoluble powders.<sup>60, 22, 39</sup> Considering their lack of processability, an alternative approach for the preparation of membranes is in the form of MMMs. This approach has been widely used for other porous materials, such as carbon molecular sieves,<sup>61</sup> zeolites,<sup>62</sup> MOFs<sup>63, 64</sup> and is especially appealing for POFs given their fully organic structure, which has been reported to result in good interaction with polymer matrix.<sup>65, 66</sup> POFs with pores in the micropore range are typically selected to prevent the penetration of the polymeric chains of the continuous matrices in the filler pores, which has been reported to result in a permeability loss of the final composite. Zhu *et al*<sup>67</sup> use spin-coating to incorporate a microporous POF (SNW-1) into polysulfone (PSF) to fabricate

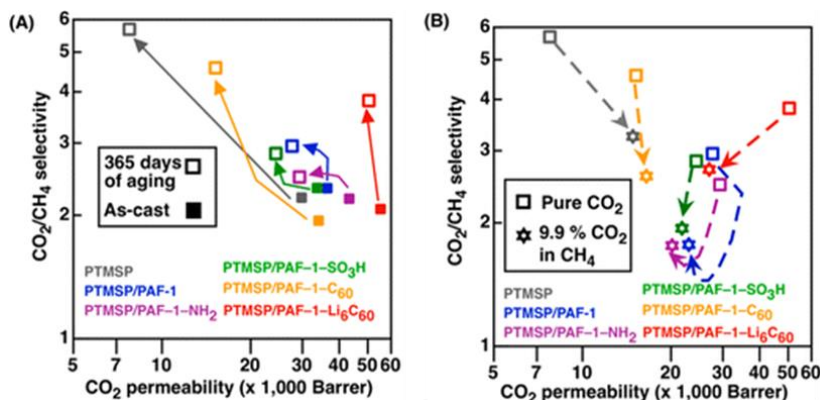


**Fig. 1.5.** (a) CO<sub>2</sub>/CH<sub>4</sub> pure gas selectivities of PAF-based membranes studied over 365 days of physical aging and (b) a comparison of mixed and pure gas permeabilities of these membranes.<sup>68</sup>

SNW-1/PSF membranes. The membranes prepared were applied to CO<sub>2</sub>/CH<sub>4</sub> and CO<sub>2</sub>/N<sub>2</sub> separations, resulting in a CO<sub>2</sub> permeability increase upon SNW-1 loading. Another solution-casting example is given by PAF-based MMMs. Hill *et al.*<sup>68</sup> employed a series PAFs, particularly PAF-1 and its derivatives, as fillers in poly(trimethylsilylpropyne) (PTMSP). The MMMs exhibited an exceptional increase in porosity, resulting in ultrafast CO<sub>2</sub> transport. CO<sub>2</sub> permeability of aged PAF-1 and PAF-1-Li<sub>60</sub>C<sub>60</sub> @PTMSP MMMs was as high as 28,400 and 50,600 Barrer, respectively, compared to 13600 Barrer of the aged bare membrane. Moreover, membrane aging was greatly reduced for PAF/PTMSP membrane with only 9% reduction in the CO<sub>2</sub> permeability after 1 year (Fig. 1.5). More impressively, their other works suggest that the loading of PAF-1 in PIM-1 could even enhance the gas separation performance after being aged.<sup>69, 70</sup> In addition to the highly-porous PAFs, crystalline COFs are also appealing fillers in MMMs. Recently, chemically-stable imine-linked COFs (particularly TpPa and TpBD) were incorporated into polybenzimidazole (PBI) to generate MMMs.<sup>71</sup> The filler loading could reach up to 50 wt.% and the resulting MMMs exhibited a sevenfold increase in the CO<sub>2</sub> permeability compared to the bare polymer with appreciable CO<sub>2</sub>/CH<sub>4</sub> (48.7) and CO<sub>2</sub>/N<sub>2</sub> (23) selectivities. Similarly, other POFs including NUS-2, NUS-3, COF-LZU1, ACOF-1 and BILP-101 have been also exploited as fillers in MMMs for CO<sub>2</sub> separation.<sup>66, 72-75</sup>

### 1.5 THESIS OUTLINE

This thesis consists of three parts. Part I (Chapter 1) gives an introduction on different types of POFs along with their application in membranes for gas separation, and some fundamentals on gas separation membranes. In the following parts of this thesis, we focus on the development of POF-based membranes for CO<sub>2</sub> separation. As shown in the previous paragraphs, POFs can be crystalline or amorphous in structure.

Thus, part II (Chapter 2 and 3) focuses on the development of crystalline POF-based mixed matrix membranes for CO<sub>2</sub> separation. An azine-linked COF (ACOF-1) is used as fillers to prepare MMMs. Chapter 2 presents the synthesis, characterization of ACOF-1 and ACOF-1@Matrimid® MMMs. The CO<sub>2</sub>/CH<sub>4</sub> separation performance of the prepared MMMs with different ACOF-1 loadings under different feed pressures was investigated. In Chapter 3, we extend this study to other polymers. MMMs are prepared with different loadings of ACOF-1 and three different non-structured non-porous polymers as continuous phase: the low flux-mid selectivity polymer Matrimid®, the mid flux-high selectivity polymer Polyactive™ and the high flux-low selectivity polymer 6FDA:DAM. The influence of the polymeric matrix on the MMMs performance for post-combustion CO<sub>2</sub> capture is discussed. Part III (Chapter 4 and 5) focuses on the development of amorphous BILP-101 membranes for CO<sub>2</sub> separation. In Chapter 4, BILP-101 particles with different porosities are synthesized controlling the initial polymerization temperature. The synthesized BILPs are further incorporated into Matrimid® to prepare MMMs and the influence of the filler porosity on the membrane separation performance towards CO<sub>2</sub>/N<sub>2</sub> is investigated. Chapter 5 describes the further engineering of BILP-101 into pure POF membranes. Using the interfacial polymerization method, BILP-101 free standing films are formed at the water-benzene interface and BILP-101 membranes are further prepared on top of  $\alpha$ -Al<sub>2</sub>O<sub>3</sub> substrates. The prepared membranes are explored for pre-combustion CO<sub>2</sub> capture, *i.e.* the H<sub>2</sub>/CO<sub>2</sub> separation. The influence of pressure, temperature and steam on the membrane performance is extensively studied.

Note that all chapters have been written as individual publications and can be read independently. As a result, some overlap may be present.

## REFERENCES

- 1 Y.-S. Bae and R. Q. Snurr, *Angewandte Chemie International Edition*, 2011, **50**, 11586.
- 2 L. Zou, Y. Sun, S. Che, X. Yang, X. Wang, M. Bosch, Q. Wang, H. Li, M. Smith, S. Yuan, Z. Perry and H.-C. Zhou, *Advanced Materials*, 2017, **29**, 1700229.
- 3 A. A. Olajire, *Energy*, 2010, **35**, 2610.
- 4 B. Seoane, J. Coronas, I. Gascon, M. E. Benavides, O. Karvan, J. Caro, F. Kapteijn and J. Gascon, *Chemical Society Reviews*, 2015, **44**, 2421.
- 5 L. M. Robeson, *Journal of Membrane Science*, 2008, **320**, 390.
- 6 H. B. Park, J. Kamcev, L. M. Robeson, M. Elimelech and B. D. Freeman, *Science*, 2017, **356**.
- 7 B. D. Freeman, *Macromolecules*, 1999, **32**, 375.
- 8 T.-H. Bae, J. Liu, J. S. Lee, W. J. Koros, C. W. Jones and S. Nair, *Journal of the American Chemical Society*, 2009, **131**, 14662.
- 9 S. R. Venna and M. A. Carreon, *Journal of the American Chemical Society*, 2010, **132**, 76.
- 10 A. P. Côté, A. I. Benin, N. W. Ockwig, M. O'Keeffe, A. J. Matzger and O. M. Yaghi, *Science*, 2005, **310**, 1166.
- 11 H. M. El-Kaderi, J. R. Hunt, J. L. Mendoza-Cortés, A. P. Côté, R. E. Taylor, M. O'Keeffe and O. M. Yaghi, *Science*, 2007, **316**, 268.
- 12 S. Hug, L. Stegbauer, H. Oh, M. Hirscher and B. V. Lotsch, *Chemistry of Materials*, 2015, **27**, 8001.
- 13 Y. Yuan, F. Sun, L. Li, P. Cui and G. Zhu, *Nature Communications*, 2014, **5**, 4260.
- 14 T. Islamoglu, S. Behera, Z. Kahveci, T.-D. Tessema, P. Jena and H. M. El-Kaderi, *ACS Applied Materials & Interfaces*, 2016, **8**, 14648.
- 15 M. G. Rabbani and H. M. El-Kaderi, *Chemistry of Materials*, 2012, **24**, 1511.
- 16 P. Kuhn, M. Antonietti and A. Thomas, *Angewandte Chemie International Edition*, 2008, **47**, 3450.
- 17 T. Ben, H. Ren, S. Ma, D. Cao, J. Lan, X. Jing, W. Wang, J. Xu, F. Deng, J. M. Simmons, S. Qiu and G. Zhu, *Angewandte Chemie International Edition*, 2009, **48**, 9457.
- 18 Y. Xu, S. Jin, H. Xu, A. Nagai and D. Jiang, *Chemical Society Reviews*, 2013, **42**, 8012.
- 19 A. K. Sekizkardes, T. Islamoglu, Z. Kahveci and H. M. El-Kaderi, *Journal of Materials Chemistry A*, 2014, **2**, 12492.

- 20 C. E. Chan-Thaw, A. Villa, P. Katekomol, D. Su, A. Thomas and L. Prati, *Nano Letters*, 2010, **10**, 537.
- 21 S. Jin, X. Ding, X. Feng, M. Supur, K. Furukawa, S. Takahashi, M. Addicoat, M. E. El-Khouly, T. Nakamura, S. Irle, S. Fukuzumi, A. Nagai and D. Jiang, *Angewandte Chemie International Edition*, 2013, **52**, 2017.
- 22 T. Ben, C. Pei, D. Zhang, J. Xu, F. Deng, X. Jing and S. Qiu, *Energy & Environmental Science*, 2011, **4**, 3991.
- 23 G. Das, B. P. Biswal, S. Kandambeth, V. Venkatesh, G. Kaur, M. Addicoat, T. Heine, S. Verma and R. Banerjee, *Chemical Science*, 2015, **6**, 3931.
- 24 N. Chaoui, M. Trunk, R. Dawson, J. Schmidt and A. Thomas, *Chemical Society Reviews*, 2017, **46**, 3302.
- 25 S.-Y. Ding and W. Wang, *Chemical Society Reviews*, 2013, **42**, 548.
- 26 X. Feng, X. Ding and D. Jiang, *Chemical Society Reviews*, 2012, **41**, 6010.
- 27 J.-X. Jiang and A. I. Cooper, in *Functional Metal-Organic Frameworks: Gas Storage, Separation and Catalysis*, ed. M. Schröder, Springer Berlin Heidelberg, Berlin, Heidelberg, 2010, pp. 1-33.
- 28 X. Zou and G. Zhu, *Advanced Materials*, 2018, **30**, 1700750.
- 29 W. J. Koros and G. K. Fleming, *Journal of Membrane Science*, 1993, **83**, 1.
- 30 L. Wang, M. S. H. Boutilier, P. R. Kidambi, D. Jang, N. G. Hadjicostantinou and R. Karnik, *Nature Nanotechnology*, 2017, **12**, 509.
- 31 G. Yu, H. Rong, X. Zou and G. Zhu, *Molecular Systems Design & Engineering*, 2017, **2**, 182.
- 32 Y. Peng, Y. Li, Y. Ban, H. Jin, W. Jiao, X. Liu and W. Yang, *Science*, 2014, **346**, 1356.
- 33 X. Wang, C. Chi, K. Zhang, Y. Qian, K. M. Gupta, Z. Kang, J. Jiang and D. Zhao, 2017, **8**, 14460.
- 34 N. Kosinov, J. Gascon, F. Kapteijn and E. J. M. Hensen, *Journal of Membrane Science*, 2016, **499**, 65.
- 35 C. Li, S. M. Meckler, Z. P. Smith, J. E. Bachman, L. Maserati, J. R. Long and B. A. Helms, *Advanced Materials*, 2018, **30**, 1704953.
- 36 S. Wang, X. Li, H. Wu, Z. Tian, Q. Xin, G. He, D. Peng, S. Chen, Y. Yin, Z. Jiang and M. D. Guiver, *Energy & Environmental Science*, 2016, **9**, 1863.
- 37 J. L. Mendoza-Cortes, W. A. Goddard, H. Furukawa and O. M. Yaghi, *The Journal of Physical Chemistry Letters*, 2012, **3**, 2671.

- 38 M. G. Rabbani, A. K. Sekizkardes, Z. Kahveci, T. E. Reich, R. Ding and H. M. El-Kaderi, *Chemistry – A European Journal*, 2013, **19**, 3324.
- 39 Y. Zhao, K. X. Yao, B. Teng, T. Zhang and Y. Han, *Energy & Environmental Science*, 2013, **6**, 3684.
- 40 X. Liu, H. Li, Y. Zhang, B. Xu, S. A. H. Xia and Y. Mu, *Polymer Chemistry*, 2013, **4**, 2445.
- 41 D. Hao, J. Zhang, H. Lu, W. Leng, R. Ge, X. Dai and Y. Gao, *Chemical Communications*, 2014, **50**, 1462.
- 42 H. Lu, C. Wang, J. Chen, R. Ge, W. Leng, B. Dong, J. Huang and Y. Gao, *Chemical Communications*, 2015, **51**, 15562.
- 43 J. Fu, S. Das, G. Xing, T. Ben, V. Valtchev and S. Qiu, *Journal of the American Chemical Society*, 2016, **138**, 7673.
- 44 G. Li, K. Zhang and T. Tsuru, *ACS Applied Materials & Interfaces*, 2017, **9**, 8433.
- 45 K. Dey, M. Pal, K. C. Rout, S. Kunjattu H, A. Das, R. Mukherjee, U. K. Kharul and R. Banerjee, *Journal of the American Chemical Society*, 2017, **139**, 13083.
- 46 S. Kandambeth, B. P. Biswal, H. D. Chaudhari, K. C. Rout, S. Kunjattu H, S. Mitra, S. Karak, A. Das, R. Mukherjee, U. K. Kharul and R. Banerjee, *Advanced Materials*, 2017, **29**, 1603945.
- 47 P. Kuhn, A. Forget, D. Su, A. Thomas and M. Antonietti, *Journal of the American Chemical Society*, 2008, **130**, 13333.
- 48 M. J. Bojdys, J. Jeromenok, A. Thomas and M. Antonietti, *Advanced Materials*, 2010, **22**, 2202.
- 49 A. Trewin and A. I. Cooper, *Angewandte Chemie International Edition*, 2010, **49**, 1533.
- 50 J. Liu, W. Zan, K. Li, Y. Yang, F. Bu and Y. Xu, *Journal of the American Chemical Society*, 2017, **139**, 11666.
- 51 E. Troschke, S. Grätz, T. Lübken and L. Borchardt, *Angewandte Chemie*, 2017, **129**, 6963.
- 52 X. Zhu, C. Tian, S. M. Mahurin, S.-H. Chai, C. Wang, S. Brown, G. M. Veith, H. Luo, H. Liu and S. Dai, *Journal of the American Chemical Society*, 2012, **134**, 10478.
- 53 K. Wang, L.-M. Yang, X. Wang, L. Guo, G. Cheng, C. Zhang, S. Jin, B. Tan and A. Cooper, *Angewandte Chemie*, 2017, **129**, 14337.
- 54 Y. Wang, J. Li, Q. Yang and C. Zhong, *ACS Applied Materials & Interfaces*, 2016, **8**, 8694.
- 55 M. Tong, Q. Yang, Q. Ma, D. Liu and C. Zhong, *Journal of Materials Chemistry A*, 2016, **4**, 124.



- 56 Y. Ying, D. Liu, J. Ma, M. Tong, W. Zhang, H. Huang, Q. Yang and C. Zhong, *Journal of Materials Chemistry A*, 2016, **4**, 13444.
- 57 J. Zhang, J. A. Schott, S. M. Mahurin and S. Dai, *Small Methods*, 2017, **1**, 1600051.
- 58 Z. Chen, M. Chen, Y. Yu and L. Wu, *Chemical Communications*, 2017, **53**, 1989.
- 59 P. Lindemann, M. Tsotsalas, S. Shishatskiy, V. Abetz, P. Krolla-Sidenstein, C. Azucena, L. Monnereau, A. Beyer, A. Götzhäuser, V. Mugnaini, H. Gliemann, S. Bräse and C. Wöll, *Chemistry of Materials*, 2014, **26**, 7189.
- 60 H. Ma, H. Ren, S. Meng, Z. Yan, H. Zhao, F. Sun and G. Zhu, *Chemical Communications*, 2013, **49**, 9773.
- 61 D. Q. Vu, W. J. Koros and S. J. Miller, *Journal of Membrane Science*, 2003, **211**, 311.
- 62 B. Zornoza, B. Seoane, J. M. Zamaro, C. Téllez and J. Coronas, *ChemPhysChem*, 2011, **12**, 2781.
- 63 X. Guo, H. Huang, Y. Ban, Q. Yang, Y. Xiao, Y. Li, W. Yang and C. Zhong, *Journal of Membrane Science*, 2015, **478**, 130.
- 64 Q. Song, S. K. Nataraj, M. V. Roussanova, J. C. Tan, D. J. Hughes, W. Li, P. Bourgoïn, M. A. Alam, A. K. Cheetham, S. A. Al-Muhtaseb and E. Sivaniah, *Energy & Environmental Science*, 2012, **5**, 8359.
- 65 X. Wu, Z. Tian, S. Wang, D. Peng, L. Yang, Y. Wu, Q. Xin, H. Wu and Z. Jiang, *Journal of Membrane Science*, 2017, **528**, 273.
- 66 M. Shan, B. Seoane, E. Andres-Garcia, F. Kapteijn and J. Gascon, *Journal of Membrane Science*, 2018, **549**, 377.
- 67 X. Gao, X. Zou, H. Ma, S. Meng and G. Zhu, *Advanced Materials*, 2014, **26**, 3644.
- 68 C. H. Lau, K. Konstas, C. M. Doherty, S. Kanehashi, B. Ozcelik, S. E. Kentish, A. J. Hill and M. R. Hill, *Chemistry of Materials*, 2015, **27**, 4756.
- 69 C. H. Lau, K. Konstas, A. W. Thornton, A. C. Y. Liu, S. Mudie, D. F. Kennedy, S. C. Howard, A. J. Hill and M. R. Hill, *Angewandte Chemie International Edition*, 2015, **54**, 2669.
- 70 C. H. Lau, P. T. Nguyen, M. R. Hill, A. W. Thornton, K. Konstas, C. M. Doherty, R. J. Mulder, L. Bourgeois, A. C. Y. Liu, D. J. Sprouster, J. P. Sullivan, T. J. Bastow, A. J. Hill, D. L. Gin and R. D. Noble, *Angewandte Chemie International Edition*, 2014, **53**, 5322.
- 71 U. K. Kharul, R. Banerjee, B. Biswal and H. D. Chaudhari, *Chemistry—A European Journal*, 2016, **22**, 4695.

- 72 Z. Kang, Y. Peng, Y. Qian, D. Yuan, M. A. Addicoat, T. Heine, Z. Hu, L. Tee, Z. Guo and D. Zhao, *Chemistry of Materials*, 2016, **28**, 1277.
- 73 X. Cao, Z. Qiao, Z. Wang, S. Zhao, P. Li, J. Wang and S. Wang, *International Journal of Hydrogen Energy*, 2016, **41**, 9167.
- 74 M. Shan, B. Seoane, E. Rozhko, A. Dikhtiarenko, G. Clet, F. Kapteijn and J. Gascon, *Chemistry-A European Journal*, 2016, **22**, 14467.
- 75 A. K. Sekizkardes, V. A. Kusuma, G. Dahe, E. A. Roth, L. J. Hill, A. Marti, M. Macala, S. R. Venna and D. Hopkinson, *Chemical Communications*, 2016, **52**, 11768.



# Azine-linked Covalent Organic Framework-based Mixed Matrix Membranes for CO<sub>2</sub>/CH<sub>4</sub> Separation

# 2



This chapter is based on the following publication:

M. Shan, B. Seoane, E. Rozhko, A. Dikhtiarenko, G. Clet, F. Kapteijn, J. Gascon, Azine-linked Covalent Organic Framework-based Mixed Matrix Membranes for CO<sub>2</sub>/CH<sub>4</sub> Separation, Chem. Eur. J., 22 (2016) 14467-14470.

---

**Abstract:** Mixed matrix membranes (MMMs) comprising Matrimid® and a microporous azine-linked covalent organic frameworks (ACOF-1) were prepared and tested in the separation of CO<sub>2</sub> from an equimolar CO<sub>2</sub>/CH<sub>4</sub> mixture. The COF-based MMMs show a more than doubling of the CO<sub>2</sub> permeability upon 16 wt.% ACOF-1 loading together with a slight increase in selectivity compared to the bare polymer. These results show the potential of COFs in the preparation of MMMs.

---

## 2.1. INTRODUCTION

The presence of CO<sub>2</sub> in different fuel gases, such as biogas and natural gas, leads to a decrease of their heating value and to pipeline corrosion. Thus, the removal of CO<sub>2</sub> from fuel gases through gas upgrading is often necessary. Traditional technologies for CO<sub>2</sub> removal, such as amine absorption, involve a phase transition, leading to a significant energy penalty. In this sense, membrane separation technology is a promising candidate for CO<sub>2</sub> separation, not only because it does not require a phase change but also because of its small footprint and ease of operation.<sup>1</sup> Polymeric membranes dominate the current market due to their good mechanical properties, good processability and low cost. However, polymeric membranes show little resistance towards high temperatures and aggressive chemical environments. Besides, the main issue of polymeric membranes is the trade-off relation between gas permeability and selectivity, which is widely referred to the Robeson upper bound.<sup>2,3</sup> One of the strategies proposed to overcome this limit is the preparation of mixed-matrix membranes (MMMs), consisting of selected fillers dispersed in a polymer matrix.<sup>4, 5, 6</sup>

A variety of fillers such as silica,<sup>7</sup> carbon molecular sieves (CMSs),<sup>8</sup> zeolites,<sup>9</sup> carbon nanotubes<sup>10</sup> and delaminated materials<sup>11</sup> and metal-organic frameworks (MOFs)<sup>12</sup> have been incorporated into different polymer matrices to prepare MMMs. However, poor filler-polymer compatibilities, filler aggregation and pore blocking by polymer chains are problems commonly encountered. In this sense, previous studies have shown that the use of fillers with at least partially organic nature, such as MOFs,<sup>13, 14</sup> metal-organic polyhedrons (MOPs)<sup>15, 16</sup> and porous aromatic frameworks (PAFs),<sup>17, 18</sup> results in a relatively good compatibility in the composite.

Covalent organic frameworks (COFs) are a class of porous organic polymers that have attracted tremendous interest in various fields such as gas adsorption and storage,<sup>19, 20</sup> catalysis,<sup>21</sup> sensing,<sup>22</sup> and photovoltaics.<sup>23</sup> They do not only exhibit exceptional properties (such as permanent porosity, high surface areas and easily-tunable frameworks) but also, their fully organic nature may result in an improved

filler–polymer interaction, avoiding the formation of non-selective defects upon MMM preparation.<sup>24</sup> Despite the fact that many reports on gas storage using COFs have been published,<sup>20a, 19, 25</sup> only a few reports on the application of COFs in membranes for gas separation can be found.<sup>26, 27, 24</sup> Recently, Zhao *et al.*<sup>28</sup> successfully incorporated two COFs (NUS-2 and NUS-3) into two different polymer matrices (Ultem® and polybenzimidazole, PBI) and applied the membranes in CO<sub>2</sub>/CH<sub>4</sub> and H<sub>2</sub>/CO<sub>2</sub> separation. Compared to the bare polymers, the NUS-2 and NUS-3 containing MMMs exhibited increased gas permeabilities together with slightly higher and constant selectivities, respectively. Interestingly, NUS-2@PBI showed an increase in the H<sub>2</sub>/CO<sub>2</sub> selectivity from 9 for the bare polymer up to 31 upon 20 wt.% COF loading, exceeding the upper bound reported by Robeson in 2008.

Herein, we report the synthesis of MMMs comprising a microporous azine-linked COF (ACOF-1) as filler and the commercial polymer Matrimid® 5218 as the polymer matrix. While ACOF-1 has been reported to possess high ideal adsorption selectivities for the separation of CO<sub>2</sub> from CH<sub>4</sub> and N<sub>2</sub>,<sup>29</sup> Matrimid® 5218 was chosen as polymer matrix due to its high selectivity, its high thermal and chemical resistance, and its commercial availability. The MMMs prepared were tested in the separation of CO<sub>2</sub> from equimolar mixtures of CO<sub>2</sub>/CH<sub>4</sub> and our study is particularly focused on evaluating the effect of the ACOF-1 loading and trans-membrane pressure difference on the membrane performance. With this approach the MMMs' permeability could be increased up to 130 % for 16 wt.% ACOF-1 loading with a slight enhancement in the membrane selectivity compared to the bare polymer.

## **2.2. EXPERIMENTAL**

### **2.2.1. Materials**

Benzene-1,3,5-tricarboxaldehyde (97 %), hydrazine hydrate (N<sub>2</sub>H<sub>4</sub> 50 % - 60 %), 1,4-dioxane (99.8 %), acetic acid, tetrahydrofuran (99.9 %), and acetone (99.9 %) were

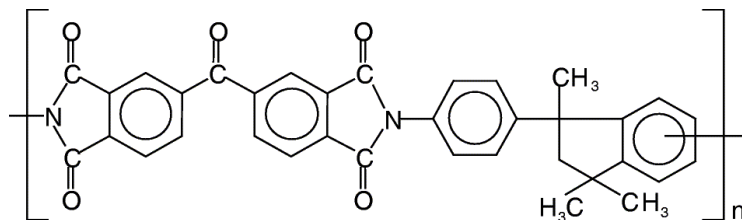


**Fig. 2.1.** Chemical structure of the polyimide Matrimid® 5218.

purchased from Sigma Aldrich. All these starting materials and solvents were used without further purification. Polymer Matrimid® 5218 ( $M_w = 123,000 \text{ g}\cdot\text{mol}^{-1}$ ,  $M_n \approx 11,000 \text{ g}\cdot\text{mol}^{-1}$ ) was kindly supplied by Huntsman Advanced Materials. The chemical structure of Matrimid® are shown in Fig. 2.1. To remove the adsorbed moisture, the polymer was degassed at 453 K for 48 h under vacuum before use.

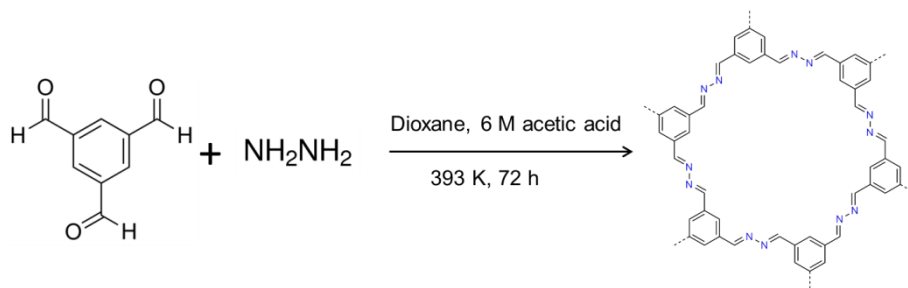
### 2.2.2 Synthesis of ACOF-1

The azine-linked covalent organic framework ACOF-1 was synthesized using a modified version of the procedure previously reported by Liu *et al.*<sup>29</sup> (see scheme 2.1). A 10 mL Pyrex tube 1 was charged with 1,3,5-triformylbenzene (60 mg, 0.37 mmol), dioxane (2 mL) and acetic acid (HAc, 0.2 mL, 6 M). Another 10 mL Pyrex tube 2 was charged with hydrazine hydrate. Both tubes were degassed under Ar for 1 h and then 32  $\mu\text{L}$  hydrazine hydrate was transferred from tube 2 to tube 1. Afterwards, tube 1 was tightly covered and the mixture was sonicated for 2 min and heated at 393 K for 72 h. The resulting powder was centrifuged at 5,000 rpm for 10 min, washed thoroughly with anhydrous dioxane, anhydrous tetrahydrofuran and anhydrous acetone and finally dried under vacuum at 373 K overnight.

### 2.2.3. Preparation of mixed-matrix membranes (MMMs)

For pure Matrimid® membrane fabrication, 0.4 g polymer was dissolved in 4.0 mL tetrahydrofuran (THF) to obtain a solution with a solvent / polymer weight ratio of 90/10. To prepare the MMMs, an extra step is needed in which the ACOF-1 particles were dispersed into THF, stirred for 2 h and sonicated for 30 min. To this suspension, 0.2 g





**Scheme 2.1.** Schematic procedure of the ACOF-1 synthesis.

Matrimid® was added and the casting suspension was further stirred for 24 h. The solvent / filler-polymer weight ratio was kept at 90/10 in all cases. The proportion of the ACOF-1 in the synthesis suspension was adjusted to achieve the desired final ACOF-1 loading of 8 wt.% and 16 wt. % in the resulting MMMs.

The prepared suspensions were then cast onto a clean glass plate with the help of a doctor blade knife. The cast membrane was then immediately covered with a small watch glass to prevent a too fast solvent evaporation. The glass plate was further covered with a square box with four small bottles of THF inside to create a saturated THF atmosphere. All these measures were taken to slow down the evaporation rate of THF and thereby preventing the formation of defects during drying. The membrane was left to dry overnight at room temperature. Then, the membrane was peeled off from the glass plate and dried under vacuum at 423 K for 24 h. The final thickness of the resulting membranes was evaluated using a digital micrometer and were in the range of 30 - 50  $\mu\text{m}$ .

#### 2.2.4. Characterization techniques

Diffuse reflectance infrared Fourier transform (DRIFT) spectra of ACOF-1 powder was acquired in a Nicolet 8700 FT-IR (Thermo Scientific) spectrometer equipped with a high temperature cell with  $\text{CaF}_2$  windows (Praying Mantis™). The samples were pretreated in a He flow at 393 K for 5 min and then collect the spectra.

The solid-state  $^{13}\text{C}$  cross-polarization magic-angle spinning (CP/MAS) NMR spectra were acquired at ambient temperature by a Bruker Advance 400 solid-state NMR spectrometer

at a MAS rate of 10 kHz. The chemical shift of dilute tetramethylsilane (TMS) in CDCl<sub>3</sub> (external) was used as reference. The operating frequency is 100.6 MHz.

Thermogravimetric analyses (TGA) were performed on a Mettler Toledo TGA/SDTA851e apparatus by measuring the mass loss of the sample while heating the sample (~ 5 mg) under N<sub>2</sub> (100 mL min<sup>-1</sup>) from room temperature to 1073 K at a heating rate of 10 K·min<sup>-1</sup>.

Powder X-ray diffraction (PXRD) patterns of the prepared COF powder and the membranes were recorded using a Bruker-D8 Advanced diffractometer with Co-K<sub>α</sub> radiation ( $\lambda = 1.78897 \text{ \AA}$ ). The samples were scanned in the  $2\theta$  range of 5 - 80° using a step size of 0.02° and a scan speed of 0.4 s per step in a continuous scanning mode.

N<sub>2</sub>-physisorption experiments were carried out at 77 K in a Quantachrome Autosorb-6B setup. Prior to the measurements, the samples were degassed at 393 K under N<sub>2</sub> flow for at least 16 h. The Brunauer-Emmet-Teller (BET) areas were calculated according to the criteria reported by Rouquerol *et al.*<sup>30</sup> and de Lange *et al.*<sup>31</sup>

CO<sub>2</sub> and CH<sub>4</sub> adsorption isotherms of ACOF-1 were recorded in a Tristar II 3020 (Micromeritics) at 273 K. Prior to the measurements, the samples were degassed at 393 K under N<sub>2</sub> flow for at least 16 h.

Scanning Electron Microscopy (SEM) micrographs were acquired using a JEOL JSM-6010LA InTouchScope microscope equipped with an integrated SDD EDS detector. ACOF-1 specimens were prepared by drop-casting a sonicated methanol ACOF-1 suspension directly on the sample holder and followed by gold sputtering for 20 s.

Transmission Electron Microscopy (TEM) analysis was performed in a JEOL JEM-1400-Plus microscope operated at 120 keV. The ACOF-1 samples were prepared by applying one drop of the ACOF-1 suspensions in methanol onto a copper grid.

Raman measurements were performed on the membranes with a Jobin Yvon Labram 300 confocal microscope equipped with a laser at 633 nm and an 1800 lines/mm grating. The homogeneity of the membranes for the dispersion of the ACOF-1 filler in the polymer was estimated from Raman intensities in the MMMs compared to the pure components. For this, *ca.* 25 measurements were done at several spots on both sides of the membrane. Acquisition conditions were modified in order to compare between the upper surface and

a somewhat larger portion of the surface (approximately between 0 and 3  $\mu\text{m}$ , named “deeper” in Fig. A3 and A4) to identify possible aggregation. As the MMMs spectra did not show any new peaks or shifts as compared to the pure components, all spectra of the MMMs were then modelled by combining the reference spectra of the pure ACOF-1 and Matrimid®. The spectroscopic contribution of the ACOF-1 filler in the membrane was calculated by a least-square minimization procedure of the reconstructed spectra in the 900 - 1830  $\text{cm}^{-1}$  range.

Differential scanning calorimetry (DSC) measurements were carried out using Perkin Elmer DSC 7 equipment to assess the glass transition temperature ( $T_g$ ) of the neat and MMMs. The scanning range was 298 K - 698 K at a heating rate of 10 K/min under nitrogen atmosphere. Two consecutive runs were performed. A first DSC cycle was performed to remove thermal history and adsorbed water from the samples. After cooling, a second cycle was performed following the same procedure. The glass transition temperature ( $T_g$ ) value was calculated as the middle point of the slope transition in the DSC curve.

#### **2.2.5. Gas permeation experiments**

Round membrane areas of 3.46  $\text{cm}^2$  were cut from the casted films, placed on a macroporous support and mounted in a flange between Viton® O-rings. This flange fits in a permeation module which was placed inside an oven in a permeation setup described elsewhere.<sup>32</sup> The  $\text{CO}_2/\text{CH}_4$  separation measurements were performed in a home-made setup employing an equimolar  $\text{CO}_2$  (50  $\text{ml}\cdot\text{min}^{-1}$ ) and  $\text{CH}_4$  (50  $\text{ml}\cdot\text{min}^{-1}$ ) mixture as gas feed. Helium (3.3  $\text{ml}\cdot\text{min}^{-1}$ ) was used as sweep gas at the permeate side. The absolute pressure of the feed stream was adjusted in a range of 4 - 10 bar using a back-pressure controller at the retentate side, keeping the permeate side atmospheric. The temperature in the permeation module was kept at 308 K. An on-line gas chromatograph (Interscience Compact GC) equipped with a packed Carboxen 1010 PLOT (30 m x 0.32 mm) column and TCD and FID detectors was used to periodically analyze the permeate stream. Each membrane was fabricated and measured at least two times to ensure reproducibility of reported data. In all cases, gas separation performance was evaluated after ensuring steady operation.

Gas separation performance was defined by the separation factor ( $\alpha$ ) and the gas permeability ( $P$ ) of the individual components. The permeability for the  $i$ -component ( $P_i$ ) was calculated as follows (Equation 2.1):

$$P_i = \frac{F_i \cdot l}{\Delta p_i \cdot A} \quad (2.1)$$

where flux  $F_i$  denotes the molar flow rate of compound  $i$ ,  $l$  is the thickness of the membrane,  $A$  is the membrane area.  $\Delta p_i$  is the partial pressure difference of component  $i$  across the membrane and it can be calculated according to Equation 2.2.

$$\Delta p_i = p_{feed} \times Y_{i,feed} - p_{perm} \times X_{i,permeate} \quad (2.2)$$

where  $p_{feed}$  and  $p_{permeate}$  represent the pressures at the feed and permeate sides and  $Y_{i,feed}$  and  $X_{i,permeate}$  are the molar fractions of component  $i$  in the feed and permeate gas streams, respectively.

The SI unit for the permeability is  $\text{mol} \cdot \text{s}^{-1} \cdot \text{m}^{-1} \cdot \text{Pa}^{-1}$ . However, gas permeabilities are reported in the widely used non-SI unit Barrer, where  $1 \text{ Barrer} = 3.35 \times 10^{-16} \text{ mol} \cdot \text{s}^{-1} \cdot \text{m}^{-1} \cdot \text{Pa}^{-1}$ .

The separation factor or mixed gas selectivity ( $\alpha$ ) was calculated as the ratio of the permeability of the more permeable compound (CO<sub>2</sub>) to the permeability of the less permeable compound (CH<sub>4</sub>) (equation 2.3).

$$\alpha = \frac{P_{CO_2}}{P_{CH_4}} \quad (2.3)$$

## 2.3. RESULTS AND DISCUSSION

ACOF-1 particles were synthesized modifying the method previously reported by Liu *et al.*,<sup>29</sup> and the powder recovered was characterized by diffuse reflectance infrared Fourier transform (DRIFT) and solid-state <sup>13</sup>C cross-polarization magic-angle spinning (CP/MAS) NMR spectroscopy. The DRIFT spectrum shows a band at 1631  $\text{cm}^{-1}$ , corresponding to the azine C=N stretching mode (Fig. 2.2a).<sup>33</sup> These observations were further corroborated by the <sup>13</sup>C CP-MAS NMR spectrum, which exhibits a peak at  $\delta = 164 \text{ ppm}$ , supporting the formation of the C=N bond (see Fig. 2.2b). Thermogravimetric analysis (TGA) under N<sub>2</sub> atmosphere was also performed in order to check the thermal stability of ACOF-1. The results show that ACOF-1 is

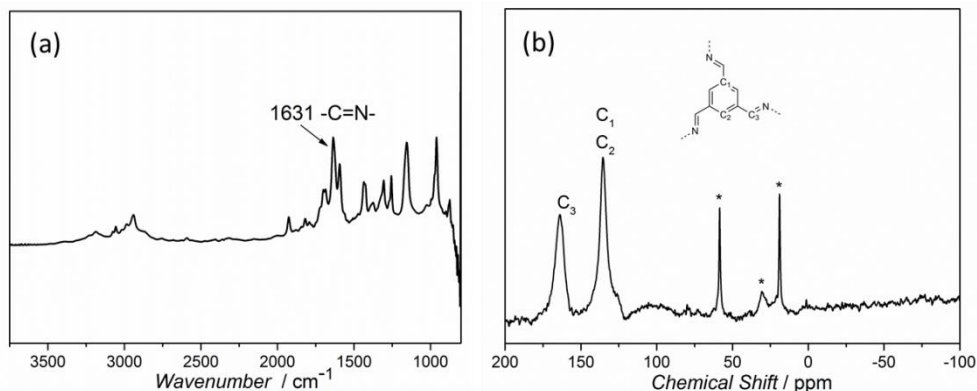


**Fig. 2. 2.** (a) DRIFT spectra of ACOF-1 at 393 K under He atmosphere and (b) <sup>13</sup>C CP/MAS solid-state NMR spectra of ACOF-1. \* Corresponding to spinning side bands.

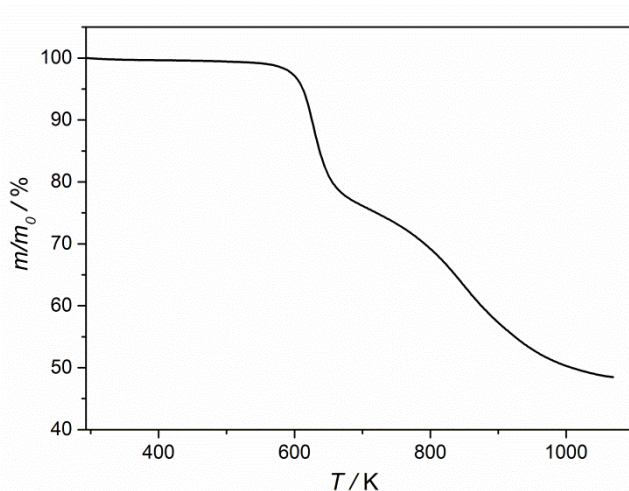


**Fig. 2. 3.** TGA curve of ACOF-1 and membranes under nitrogen flow at a heating rate of 10 K/min.

stable up to 573 K (see Fig. 2.3), where the degradation of the framework takes place, in agreement with the results previously reported by Liu *et al.*<sup>29</sup> Moreover, the slight weight loss taking place below 373 K can be attributed to the desorption of moisture and solvent trapped inside the COF.

The powder X-ray diffraction (PXRD) pattern of the synthesized ACOF-1 is shown in Fig. 2.4 together with the simulated pattern based on the crystallographic structure model (Fig. 2.4a and b, see Appendix A for the details) for comparison. ACOF-1

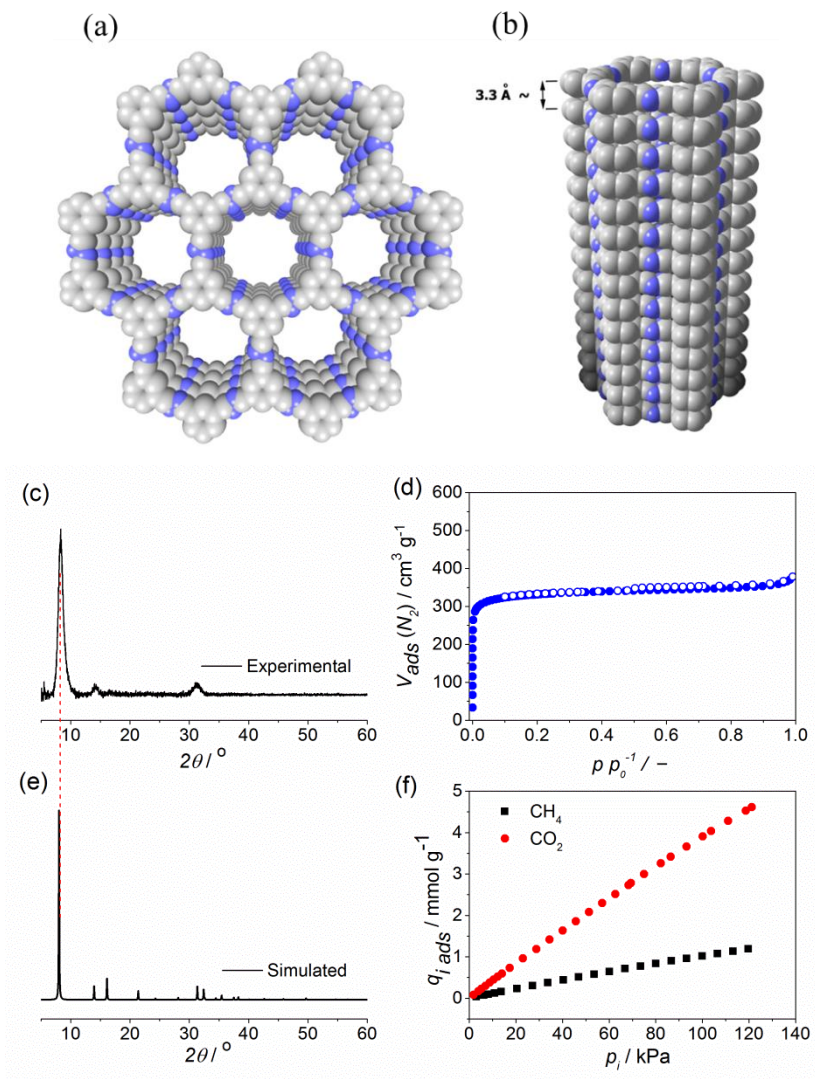


**Fig. 2.4.** Space-filling representation of ACOF-1 structure with hexagonal channels running along the [001] crystallographic direction. (b) Single hexagonal channel of ACOF-1 formed by  $\pi$ - $\pi$  stacking of 2D layers with 3.3 Å interplanar distances. X-ray diffraction patterns of (c) the synthesized and (e) the simulated ACOF-1, (d)  $N_2$  adsorption isotherm acquired at 77 K and (f)  $CO_2$  and  $CH_4$  adsorption isotherms of ACOF-1 acquired at 273 K. Closed symbols represent adsorption and open symbols desorption branch.

presents a similar diffraction pattern as reported in the literature,<sup>29</sup> confirming its successful preparation. In particular, the strong diffraction at  $8.34^{\circ}$  and the relatively weak diffractions at  $14.24^{\circ}$ ,  $16.50^{\circ}$ ,  $21.7^{\circ}$  can be assigned to the (100), (110), (200), and (120) crystallographic planes, respectively. Furthermore, a broad diffraction at  $31.56^{\circ}$  can be observed, which can be attributed to the  $\pi$ - $\pi$  stacking between the ACOF-1 layers. The broadening of all diffraction peaks is attributed to the small crystal size in the synthesized material. Scanning electron microscopy (SEM) (Fig. 2.5a) revealed that ACOF-1 is composed of homogeneous spherical-shaped sub-micron particles with a particle size of  $350 \pm 30$  nm calculated from TEM micrographs (Fig. 2.5c and d). In order to study the textural properties of ACOF-1, nitrogen adsorption isotherms were acquired at 77 K (see Fig. 2.4d). ACOF-1 exhibits a type I adsorption isotherm with a large  $N_2$  uptake at low relative pressures, which is typical for microporous materials. The calculated Brunauer-Emmett-Teller (BET) area of ACOF-1 was  $1310 \text{ m}^2 \cdot \text{g}^{-1}$ , slightly higher than previously reported values for this material.<sup>28-29, 34</sup> Moreover, Fig. 2.4f shows the  $CO_2$  and  $CH_4$  adsorption isotherms acquired for ACOF-1 at 273 K. At 1 bar (100 kPa) and 273 K, the  $CO_2$  uptake of ACOF-1,  $3.92 \text{ mmol} \cdot \text{g}^{-1}$ , is much higher than that of  $CH_4$ ,  $0.92 \text{ mmol} \cdot \text{g}^{-1}$ , which demonstrates its selectivity towards  $CO_2$  in line with the results reported by Liu *et al.*<sup>29</sup>

The as-synthesized ACOF-1 was used to prepare mixed-matrix membranes. Fig. A2 shows that the crystallinity of ACOF-1 is maintained during the membrane preparation procedure. To investigate the dispersion of ACOF-1 within the polymer matrix, SEM images of the cross-section of the 16 wt.% ACOF-1@Matrimid® MMM were acquired (see Fig.2.5b). The images show that ACOF-1 is uniformly distributed in the polymer matrix and no large clusters or aggregates of ACOF-1 could be found even at 16 wt.% ACOF-1 loading. Moreover, the homogeneity of the filler dispersion in the polymer matrix was further evaluated by Raman spectroscopy as previously described in our recent work.<sup>35</sup> Spectra of the individual components and MMMs are shown in Fig. 2.5e. No additional features can be observed in the MMMs compared to the pure components, indicating the absence of specific chemical

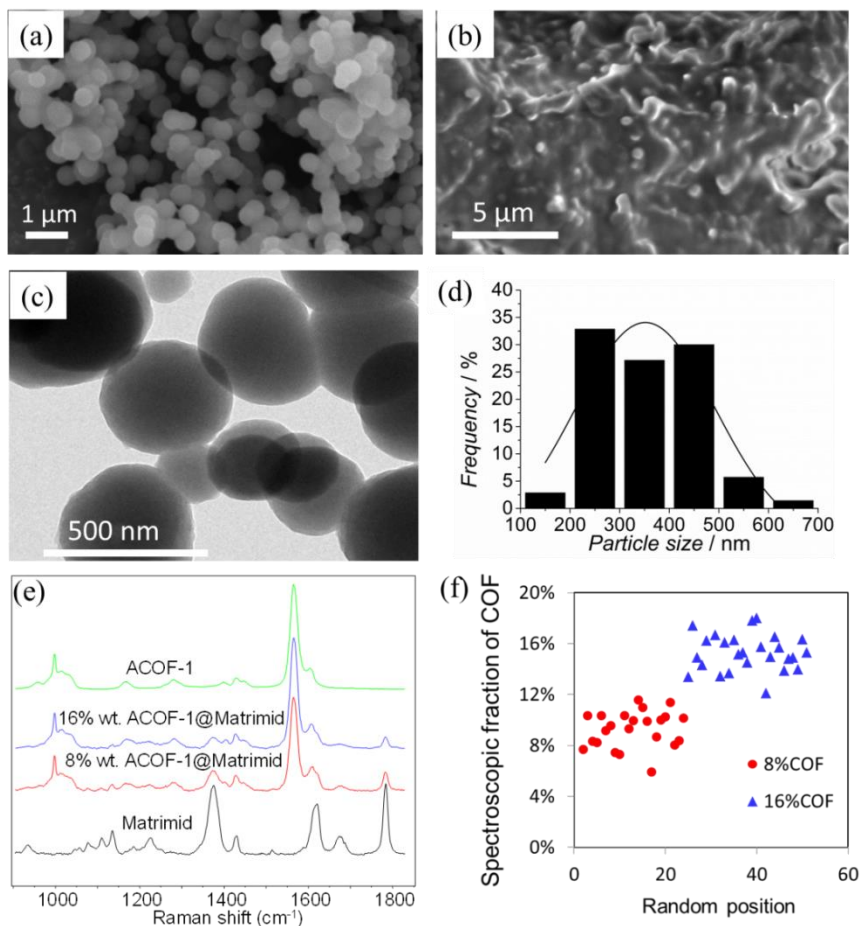


**Fig. 2.5.** SEM micrographs of (a) ACOF-1 and (b) the cross-section of a 16 wt.% ACOF-1@ Matrimid<sup>®</sup> MMMs. TEM images (c) and particle size distribution (d) of ACOF-1. (e) Raman spectra of the pure components and MMMs. (f) Spectroscopic fraction of COF calculated at random positions of two different MMMs (8 and 16 wt.% COF loading).

bonding between the ACOF-1 particles and Matrimid<sup>®</sup>. The spectra of the MMMs were modelled by combining the spectra of the pure components in order to evaluate the spectroscopic contribution of the ACOF-1 filler (see Appendix A for details). For each MMM, separate measurements performed at various positions on both sides of the membranes showed similar results (Fig. 2.5f), corroborating the good dispersion of ACOF-1 in the polymer matrix assessed by SEM. In addition, the



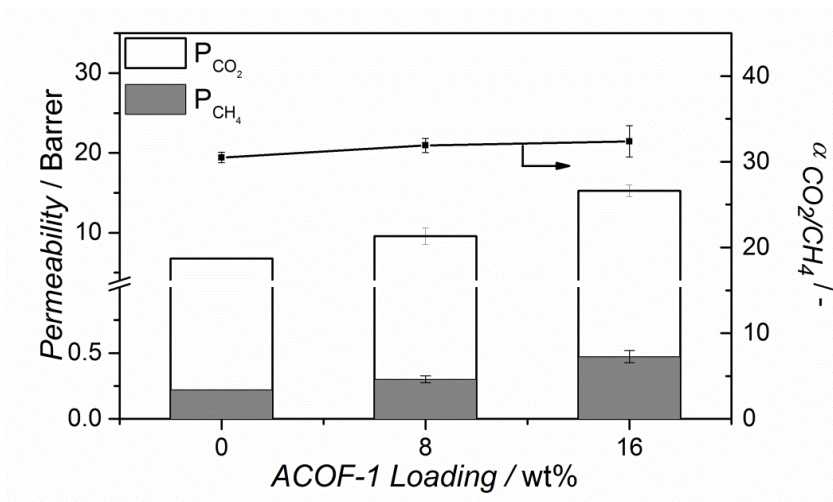


**Fig. 2.6.** Performance of MMMs with different ACOF-1 loadings in the separation of CO<sub>2</sub> from an equimolar CO<sub>2</sub>/CH<sub>4</sub> mixture at 308 K and a feed pressure of 4 bar. Error bars correspond to standard deviation.

glass transition temperatures ( $T_g$ ) of the MMMs are slightly higher than that of neat Matrimid® membrane (table A1), what could indicate the favourable compatibility between ACOF-1 filler and Matrimid®,<sup>36</sup> in agreement with the SEM micrographs. TGA analysis showed that the prepared membranes have a good thermal stability (Fig. A1) and that this stability is not reduced upon COF addition, conversely to what has been observed for some MOF-based MMMs.<sup>37</sup> Moreover, the filler weight loading of the MMMs calculated by TGA agreed with the nominal ACOF-1 content, the deviations being within 5 %.

To investigate the influence of ACOF-1 loading on the permeability and selectivity of the MMMs synthesized, pure Matrimid®, 8 wt.% and 16 wt.% ACOF-1 MMMs were tested in the separation of CO<sub>2</sub> from an equimolar CO<sub>2</sub>/CH<sub>4</sub> mixture at 308 K and a feed pressure of 4 bar. Upon increasing the ACOF-1 loading the permeability of both gases increases significantly together with a slight increase of the CO<sub>2</sub>/CH<sub>4</sub> mixed gas selectivity (Fig. 2.6). Particularly, for the 16 wt.% ACOF-1@ Matrimid® MMM, the CO<sub>2</sub> permeability increased by 130 % as compared to the neat polymer. The  $T_g$  of the MMMs barely changes (table A1), indicating that the properties of the

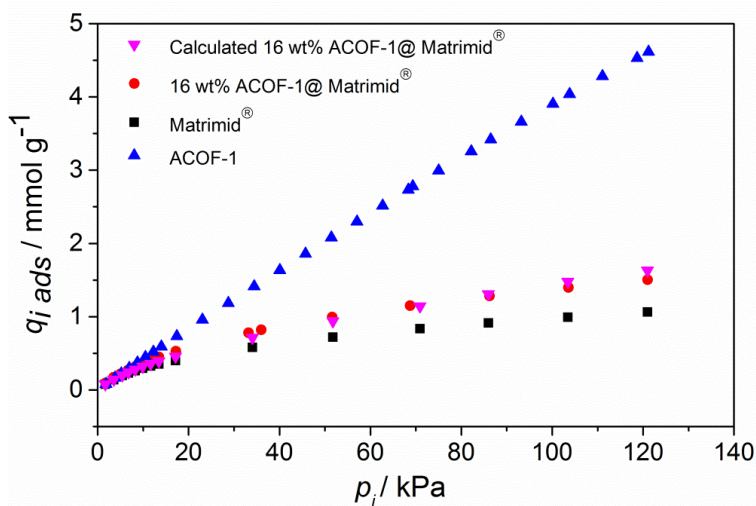


**Fig. 2.7.** CO<sub>2</sub> adsorption isotherms of the prepared membranes and ACOF-1 at 273 K.

Matrimid<sup>®</sup> polymer does not change much. Therefore, the significant increase in gas permeability is attributed to the additional gas transport pathways introduced by the porous ACOF-1 network. The slightly higher CO<sub>2</sub>/CH<sub>4</sub> separation factors measured for the MMMs can be rationalized by the selective adsorption of CO<sub>2</sub> over CH<sub>4</sub> in the N-rich ACOF-1 through dipole-quadrupole interactions.<sup>29</sup> Indeed, the CO<sub>2</sub> adsorption isotherms acquired for the 16 wt.% ACOF-1 MMMs (Fig. 2.7) show an increase in the CO<sub>2</sub> uptake upon ACOF-1 incorporation, mainly additive based on the individual isotherms.

Our previous research<sup>38</sup> demonstrated that the feed pressure has a significant effect on the gas separation performance of MOF-based MMMs. Here, the influence of the feed pressure on the gas separation performance was also studied for COF-based MMMs. The CO<sub>2</sub> and CH<sub>4</sub> permeabilities of the MMMs are both higher than those measured for bare Matrimid<sup>®</sup>, nearly independent of the partial pressure difference (Fig. 2.8a), indicating a permeation flux proportional with the partial pressure difference over the membrane  $\Delta P_i$ . The CO<sub>2</sub>/CH<sub>4</sub> separation factor (Fig. 2.8b) for the 8 wt.% ACOF-1@ Matrimid<sup>®</sup> MMMs shows a similar trend as that

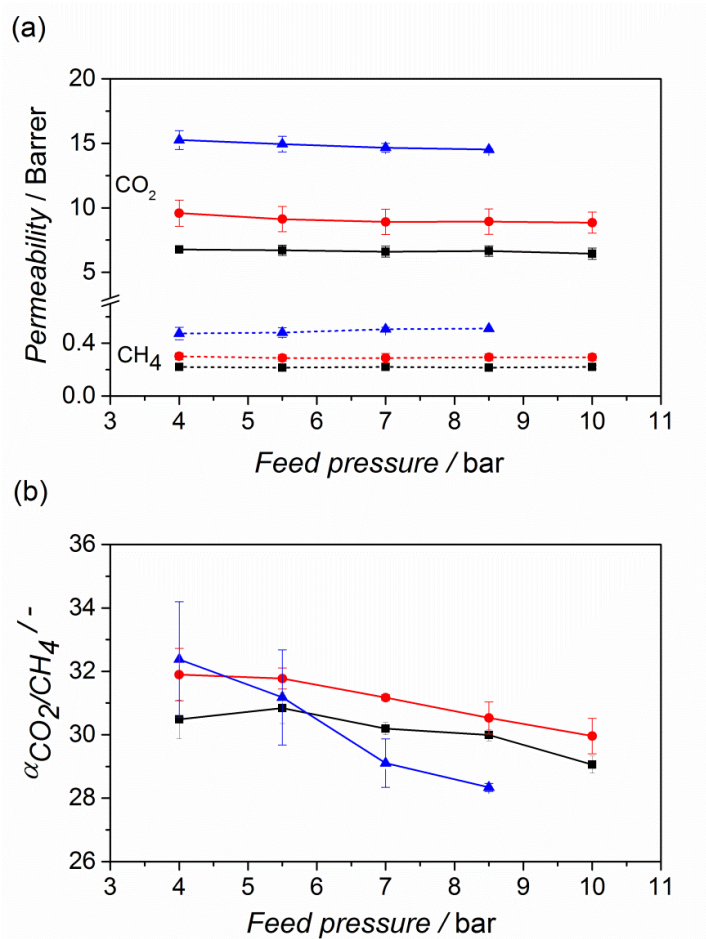


**Fig. 2.8.** Effect of the feed pressure on the (a) gas permeabilities and (b) CO<sub>2</sub>/CH<sub>4</sub> separation factor of different membranes obtained in the separation of CO<sub>2</sub> from an equimolar mixture of CO<sub>2</sub> and CH<sub>4</sub> at 308 K. Error bars correspond to standard deviation. ■ Pure Matrimid®, ● 8 wt.% ACOF-1@Matrimid®, ▲ 16 wt.% ACOF-1@Matrimid®.

observed for the pure polymer, showing a slight decrease when the feed pressure is increased.<sup>35, 39</sup> This behaviour can be ascribed to the saturation of Langmuir sites, leading to a decrease of the sorption coefficient with the transmembrane pressure difference. Moreover, a more pronounced decrease was observed for 16 wt.% ACOF-1@Matrimid®, for which the presence of small defects at higher COF loading, more important at higher pressures, may also play a role.

## **2.4. CONCLUSIONS**

In summary, microporous ACOF-1 particles with high BET areas were successfully synthesized and dispersed in Matrimid® to prepare MMMs. The resulting membranes also showed a good adhesion between the ACOF-1 particles and the polymer matrix, which was further corroborated by the improved MMMs separation performance over the polymer. Particularly, the MMMs were tested in the separation of CO<sub>2</sub> from an equimolar mixture of CO<sub>2</sub> and CH<sub>4</sub> at 308 K and different feed pressures. The ACOF-1 containing membranes show an increase of more than doubling of the CO<sub>2</sub> permeability for 16 wt.% COF loading relative to the bare Matrimid® membrane, together with slightly higher selectivities. These results render ACOF-1 an interesting candidate to prepare MMMs for gas separation.

### REFERENCES

- 1 D. M. D'Alessandro, B. Smit and J. R. Long, *Angewandte Chemie International Edition*, 2010, **49**, 6058.
- 2 L. M. Robeson, *Journal of Membrane Science*, 1991, **62**, 165.
- 3 *Journal of Membrane Science*, 2008, **320**, 390.
- 4 C. Zhang, Y. Dai, J. R. Johnson, O. Karvan and W. J. Koros, *Journal of Membrane Science*, 2012, **389**, 34.
- 5 B. Zornoza, O. Esekile, W. J. Koros, C. Téllez and J. Coronas, *Separation and Purification Technology*, 2011, **77**, 137.
- 6 B. Seoane, J. Coronas, I. Gascon, M. E. Benavides, O. Karvan, J. Caro, F. Kapteijn and J. Gascon, *Chemical Society Reviews*, 2015, **44**, 2421.
- 7 B. Zornoza, S. Irusta, C. Téllez and J. Coronas, *Langmuir*, 2009, **25**, 5903.
- 8 D. Q. Vu, W. J. Koros and S. J. Miller, *Journal of Membrane Science*, 2003, **211**, 311.
- 9 B. Zornoza, B. Seoane, J. M. Zamaro, C. Téllez and J. Coronas, *ChemPhysChem*, 2011, **12**, 2781.
- 10 M. M. Khan, V. Filiz, G. Bengtson, S. Shishatskiy, M. M. Rahman, J. Lillepaerg and V. Abetz, *Journal of Membrane Science*, 2013, **436**, 109.
- 11(a) T. Rodenas, I. Luz, G. Prieto, B. Seoane, H. Miro, A. Corma, F. Kapteijn, F. X. Llabrés i Xamena and J. Gascon, *Nat Mater*, 2015, **14**, 48; (b) B. Zornoza, P. Gorgojo, C. Casado, C. Téllez and J. Coronas, *Desalination and Water Treatment*, 2011, **27**, 42.
- 12 R. Lin, L. Ge, L. Hou, E. Strounina, V. Rudolph and Z. Zhu, *ACS applied materials & interfaces*, 2014, **6**, 5609.
- 13 L. Cao, K. Tao, A. Huang, C. Kong and L. Chen, *Chemical Communications*, 2013, **49**, 8513.
- 14 N. C. Su, D. T. Sun, C. M. Beavers, D. K. Britt, W. L. Queen and J. J. Urban, *Energy & Environmental Science*, 2016, **9**, 922.
- 15 J. Ma, Y. Ying, Q. Yang, Y. Ban, H. Huang, X. Guo, Y. Xiao, D. Liu, Y. Li, W. Yang and C. Zhong, *Chemical Communications*, 2015, **51**, 4249.
- 16 C. Zhao, N. Wang, L. Wang, H. Huang, R. Zhang, F. Yang, Y. Xie, S. Ji and J.-R. Li, *Chemical Communications*, 2014, **50**, 13921.
- 17 L. Meng, X. Zou, S. Guo, H. Ma, Y. Zhao and G. Zhu, *ACS Applied Materials & Interfaces*, 2015, **7**, 15561.

- 18 C. H. Lau, K. Konstas, A. W. Thornton, A. C. Y. Liu, S. Mudie, D. F. Kennedy, S. C. Howard, A. J. Hill and M. R. Hill, *Angewandte Chemie International Edition*, 2015, **54**, 2669.
- 19 H. Furukawa and O. M. Yaghi, *Journal of the American Chemical Society*, 2009, **131**, 8875.
- 20(a) C. J. Doonan, D. J. Tranchemontagne, T. G. Glover, J. R. Hunt and O. M. Yaghi, *Nat Chem*, 2010, **2**, 235; (b) A. Bhunia, I. Boldog, A. Moller and C. Janiak, *Journal of Materials Chemistry A*, 2013, **1**, 14990.
- 21 M. Rose, *ChemCatChem*, 2014, **6**, 1166.
- 22 D. Kaleeswaran, P. Vishnoi and R. Murugavel, *Journal of Materials Chemistry C*, 2015, **3**, 7159.
- 23 S. Jin, X. Ding, X. Feng, M. Supur, K. Furukawa, S. Takahashi, M. Addicoat, M. E. El-Khouly, T. Nakamura, S. Irle, S. Fukuzumi, A. Nagai and D. Jiang, *Angewandte Chemie International Edition*, 2013, **52**, 2017.
- 24 X. Cao, Z. Qiao, Z. Wang, S. Zhao, P. Li, J. Wang and S. Wang, *International Journal of Hydrogen Energy*, 2016, **21**, 9167.
- 25 M. G. Rabbani, A. K. Sekizkardes, Z. Kahveci, T. E. Reich, R. Ding and H. M. El-Kaderi, *Chemistry – A European Journal*, 2013, **19**, 3324.
- 26 H. Lu, C. Wang, J. Chen, R. Ge, W. Leng, B. Dong, J. Huang and Y. Gao, *Chemical Communications*, 2015, **51**, 15562.
- 27 D. Hao, J. Zhang, H. Lu, W. Leng, R. Ge, X. Dai and Y. Gao, *Chemical Communications*, 2014, **50**, 1462.
- 28 Z. Kang, Y. Peng, Y. Qian, D. Yuan, M. A. Addicoat, T. Heine, Z. Hu, L. Tee, Z. Guo and D. Zhao, *Chemistry of Materials*, 2016, **28**, 1277.
- 29 Z. Li, X. Feng, Y. Zou, Y. Zhang, H. Xia, X. Liu and Y. Mu, *Chemical Communications*, 2014, **50**, 13825.
- 30 J. Rouquerol, D. Avnir, C. Fairbridge, D. Everett, J. Haynes, N. Pernicone, J. Ramsay, K. Sing and K. Unger, *Pure and Applied Chemistry*, 1994, **66**, 1739.
- 31 M. F. De Lange, T. J. H. Vlught, J. Gascon and F. Kapteijn, *Microporous and Mesoporous Materials*, 2014, **200**, 199.
- 32 B. Zornoza, A. Martinez-Joaristi, P. Serra-Crespo, C. Tellez, J. Coronas, J. Gascon and F. Kapteijn, *Chemical Communications*, 2011, **47**, 9522.
- 33 L. D. Frederickson, *Analytical Chemistry*, 1964, **36**, 1349.

- 34 L. Stegbauer, M. W. Hahn, A. Jentys, G. Savasci, C. Ochsenfeld, J. A. Lercher and B. V. Lotsch, *Chemistry of Materials*, 2015, **27**, 7874.
- 35 A. Sabetghadam, B. Seoane, D. Keskin, N. Duim, T. Rodenas, S. Shahid, S. Sorribas, C. L. Guillouzer, G. Clet and C. Tellez, *Advanced Functional Materials*, 2016, **26**, 3154.
- 36 T.-S. Chung, S. S. Chan, R. Wang, Z. Lu and C. He, *Journal of Membrane Science*, 2003, **211**, 91.
- 37 F. Cacho-Bailo, C. Téllez and J. Coronas, *Chemistry – A European Journal*, 2016, **22**, 9533.
- 38 T. Rodenas, M. van Dalen, E. García-Pérez, P. Serra-Crespo, B. Zornoza, F. Kapteijn and J. Gascon, *Advanced Functional Materials*, 2014, **24**, 249.
- 39 J. E. Bachman and J. R. Long, *Energy & Environmental Science*, 2016, **9**, 2031.

## APPENDIX A

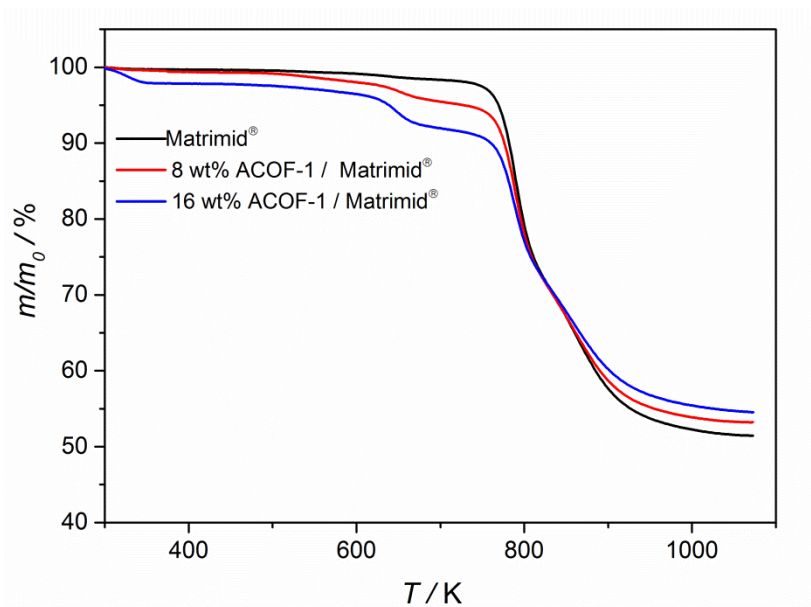


Fig. A1. TGA curve of the prepared membranes under nitrogen flow at a heating rate of 10 K/min.

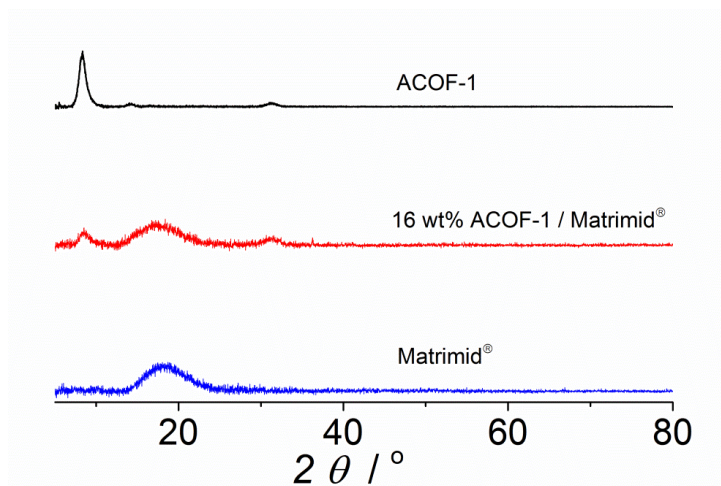
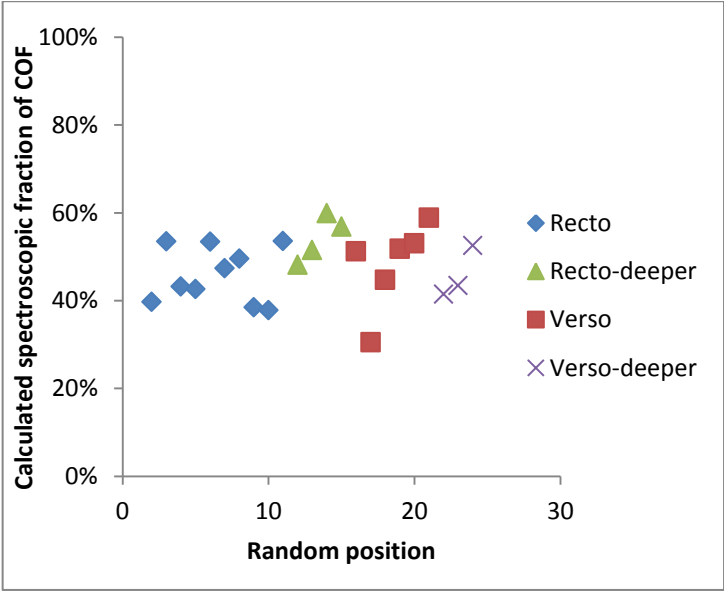
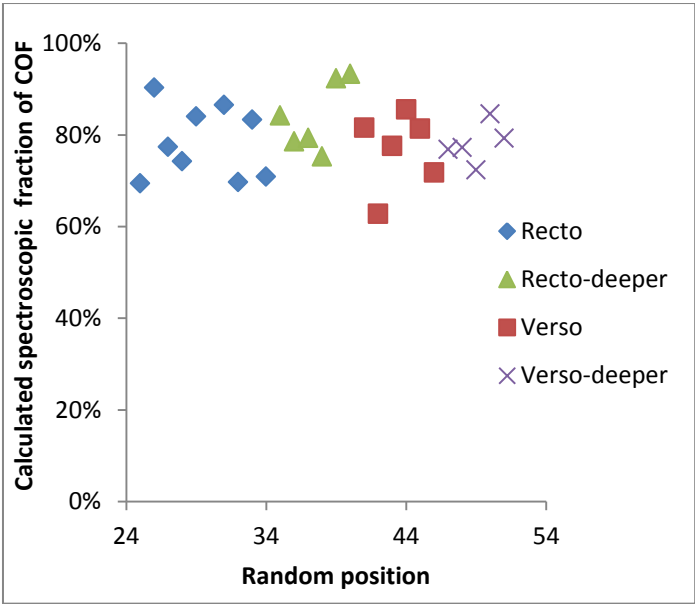


Fig. A2. PXRD patterns of ACOF-1 and the prepared membranes.





**Fig. A3.** ACOF-1 fractions calculated from the Raman spectra at various positions on the 8 wt.% ACOF-1@ Matrimid® MMM.



**Fig. A4.** ACOF-1 fractions calculated from the Raman spectra at various positions on the 16 wt.% ACOF-1@ Matrimid® MMM.

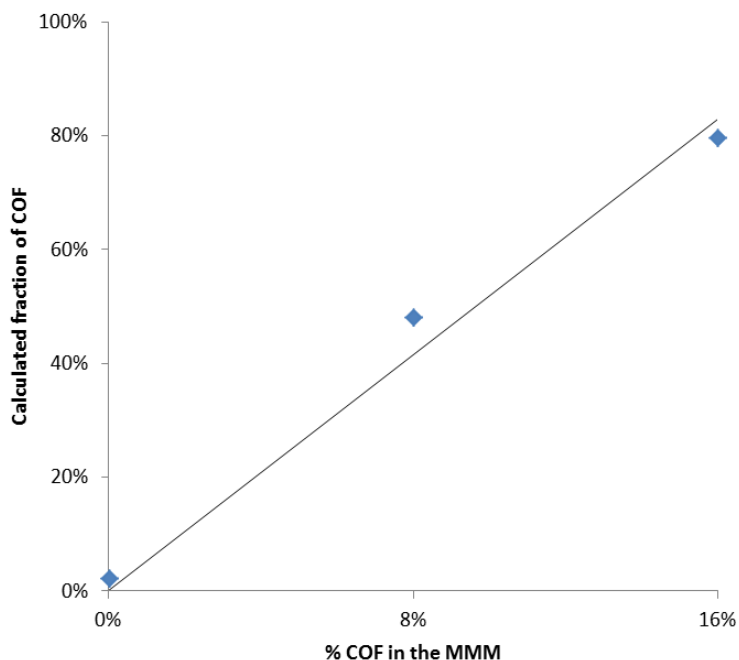


**Fig. A5.** Evolution of the average value of the calculated fractions of ACOF-1 with the effective ACOF-1 loading.

The limited scatter in the various measurements on the two membranes, independent of the membrane side and thickness probed (Fig. A3 and A4) show that the membranes are quite homogeneous and ACOF-1 is well dispersed at least for the depth (*ca.* 0-3  $\mu\text{m}$ ) that was possible to probe by the microscope.

The spectra of the MMMs were modelled by combining the spectra of the pure components in order to evaluate the spectroscopic contribution of the ACOF-1 filler. It should be noted that the numerical value calculated for the COF fractions depends on the intensity of the spectra of the pure components which in Raman depends on many aspects, and thus cannot be considered directly as meaningful. However, this calculated ratio appeared to evolve proportionally with the ACOF-1 loading (Fig. A5). Therefore, for comparison purposes, all the calculated values were divided by the slope of this curve to yield the spectroscopic COF fraction shown in Fig. 2. 5f. This overall proportionality also

**Table A1.** Glass transition temperature ( $T_g$ ) of different membranes.

Membrane	$T_g$ / K
Bare Matrimid®	594.0
8 wt.% ACOF-1@Matrimid®	596.0
16wt.% ACOF-1@Matrimid®	596.4

suggests that the volume scanned by the Raman microscope is representative of the whole membrane.

### Powder X-ray diffraction and structural identification of ACOF-1

The powder X-ray diffraction (PXRD) measurements were performed on a Bruker D8-Advance diffractometer equipped with a Co- $K\alpha$  irradiation source ( $\lambda_1 = 1.78897 \text{ \AA}$ ,  $\lambda_2 = 1.79285 \text{ \AA}$ ,  $\lambda_1/\lambda_2 = 0.5$ ) and operated in Bragg-Brentano geometry. The experimental XRD data were collected over an angle range from  $5^\circ$  -  $80^\circ$  with a step width of  $0.02^\circ$ .

The structural identification of ACOF-1 was performed by comparison of the experimental X-ray diffraction pattern with the theoretically expected.

The ACOF-1 identity was confirmed by Le Bail extraction and unit cell parameter refinement (Fig. A6) performed with EXPO2014.<sup>1</sup> In the first refinement step, zero offset, the scale factor, six background terms and profile parameters as a pseudo-Voigt function were refined. The initial unit cell for the refinement was constructed based on the unit cell values reported by Liu *et al.*<sup>2</sup> Triclinic P1 space group,  $a = b = 14.724 \text{ \AA}$ ,  $c = 3.31 \text{ \AA}$ ,  $\alpha = \beta = 90^\circ$ ,  $\gamma = 120^\circ$ . The atomic fractional coordinates for ACOF-1 model (Table A2) have been obtained by consideration of specific structural arrangement of 2D COF layers:  $\pi$ - $\pi$  staked parallel-laid covalent sheets with interplanar distance of  $\sim 3.3 \text{ \AA}$  between them.

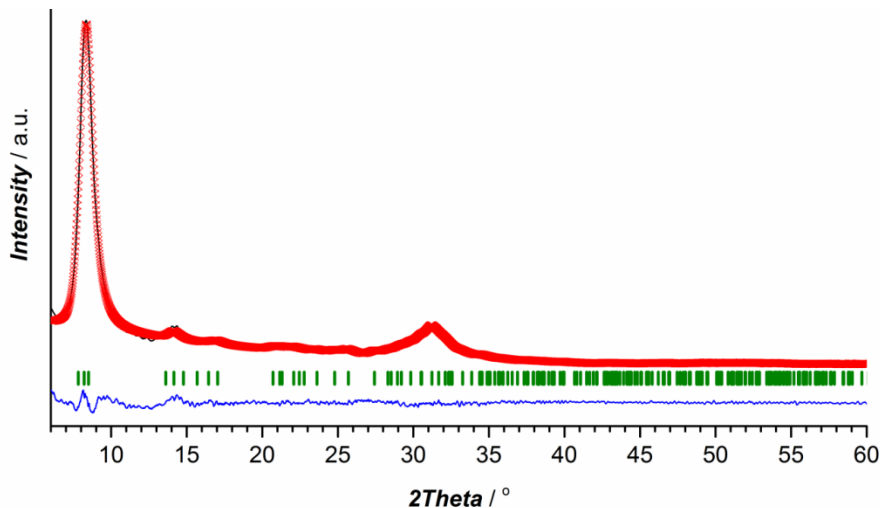


**Fig. A6.** The Le Bail fitting plot for ACOF-1 ( $R_p = 6.43\%$ ,  $R_{wp} = 10.1\%$ ,  $R_B = 3.92\%$ ). The experimental data is presented as black solid line, calculated one by red crosses and difference as blue solid line. The Bragg positions of the peaks are represented as green sticks.

**Table A2.** Atomic coordinates for ACOF-1 model structure.

Atom label	Atom symbol	x	y	z	occ
C1	C	0.441	0.8819	0.5027	1.00
C2	C	0.3859	0.7718	0.5027	1.00
C3	C	0.4421	0.7092	0.5027	1.00
C4	C	0.441	0.5354	0.5027	1.00
C5	C	0.0944	0.5354	0.5027	1.00
C6	C	0.3859	0.5904	0.5027	1.00
C7	C	0.2045	0.5905	0.5027	1.00
C8	C	0.2672	0.5343	0.5027	1.00
C9	C	0.2672	0.7092	0.5027	1.00
C10	C	0.5544	0.1089	0.5027	1.00
C11	C	0.6162	0.2325	0.5027	1.00
C12	C	0.9147	0.4692	0.5027	1.00
C13	C	0.5612	0.4624	0.5027	1.00
C14	C	0.7911	0.4074	0.5027	1.00
C15	C	0.6162	0.4074	0.5027	1.00
C16	C	0.7329	0.4657	0.5027	1.00
C17	C	0.7329	0.2908	0.5027	1.00
C18	C	0.558	0.2908	0.5027	1.00
N1	N	0.9754	0.4427	0.5027	1.00
N2	N	0.0371	0.5529	0.5027	1.00
N3	N	0.549	0.5278	0.5027	1.00
N4	N	0.4505	0.4701	0.5027	1.00
N5	N	0.5112	0.9715	0.5027	1.00

**Table A3.** Summary of membrane performance tested for the CO<sub>2</sub> separation of a CO<sub>2</sub>/CH<sub>4</sub> equimolar mixture at 308 K. The data were obtained for different membranes under several operation pressure conditions. Each type of membrane was fabricated at least 2 times. Error is given as the standard deviation from the independent tests of 3 different membranes. Permeate side at atmospheric pressure with helium as sweep gas.

Membrane		Matrimid®			
Membrane thickness		32 ± 1 µm			
Feed pressure [bar]	4	5.5	7	8.5	10
PCO <sub>2</sub> [Barrer]	6.8 ± 0.1	6.7 ± 0.4	6.6 ± 0.4	6.5 ± 0.4	6.5 ± 0.5
PCH <sub>4</sub> [Barrer]	0.22 ± 0.00	0.22 ± 0.01	0.22 ± 0.01	0.22 ± 0.01	0.22 ± 0.01
Selectivity [-]	30.5 ± 0.6	30.9 ± 0.5	30.2 ± 0.2	30.0 ± 0.2	29.1 ± 0.3

Membrane		8 wt % ACOF-1 / Matrimid®			
Membrane thickness		40 ± 1 µm			
Feed pressure [bar]	4	5.5	7	8.5	10
PCO <sub>2</sub> [Barrer]	9.6 ± 1.0	9.1 ± 1.0	8.9 ± 1.0	8.9 ± 0.8	8.8 ± 0.8
PCH <sub>4</sub> [Barrer]	0.30 ± 0.03	0.29 ± 0.02	0.29 ± 0.03	0.29 ± 0.03	0.29 ± 0.02
Selectivity [-]	31.9 ± 0.8	31.8 ± 0.3	31.2 ± 1.0	30.5 ± 0.5	30.0 ± 0.6

Membrane		16 wt % ACOF-1 / Matrimid®			
Membrane thickness		47 ± 1 µm			
Feed pressure [bar]	4	5.5	7	8.5	
PCO <sub>2</sub> [Barrer]	15.3 ± 0.7	14.9 ± 0.6	14.7 ± 0.3	14.5 ± 0.1	
PCH <sub>4</sub> [Barrer]	0.47 ± 0.04	0.48 ± 0.03	0.51 ± 0.01	0.51 ± 0.00	
Selectivity [-]	32.4 ± 1.8	31.2 ± 1.5	29.1 ± 0.7	28.3 ± 0.1	

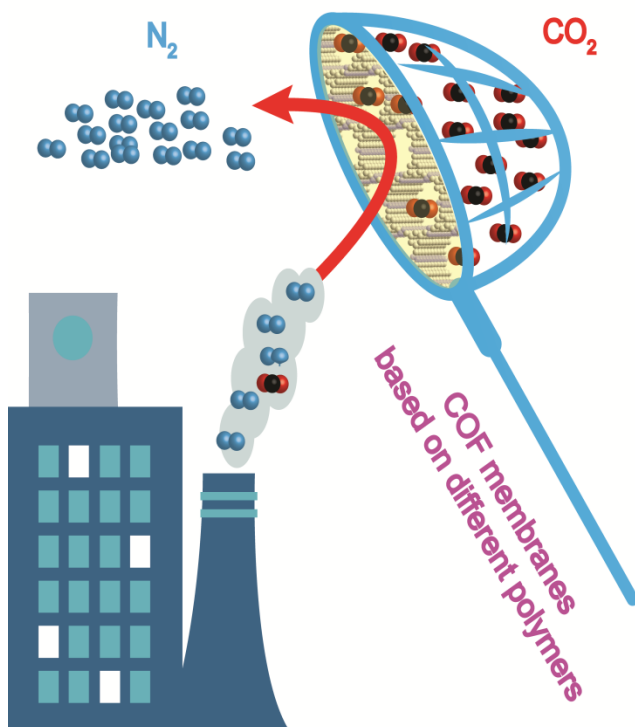
## References

- A1 A. Altomare, C. Cuocci, C. Giacobazzo, A. Moliterni, R. Rizzi, N. Corriero and A. Falcicchio, *Journal of Applied. Crystallagraphy*, 2013, **46**, 1231.
- A2 Z. Li, X. Feng, Y. Zou, Y. Zhang, H. Xia, X. Liu and Y. Mu, *Chemical Communication*, 2014, **50**, 13825.



# Mixed-Matrix Membranes containing an Azine-linked Covalent Organic Framework: Influence of the Polymeric Matrix on Post- Combustion CO<sub>2</sub>-Capture

# 3



This chapter is based on the following publication:

M. Shan, B. Seoane, E. Andres-Garcia, F. Kapteijn, J. Gascon, Mixed-Matrix Membranes containing an Azine-linked Covalent Organic Framework: Influence of the Polymeric Matrix on Post-Combustion CO<sub>2</sub>-Capture, J. Membr. Sci, 549 (2018) 377-384.



---

**Abstract:** The use of an azine-linked covalent organic framework (ACOF-1) as filler in mixed-matrix membranes (MMMs) has been studied for the separation of CO<sub>2</sub> from N<sub>2</sub>. To better understand the mechanisms that govern separation in complex composites, MMMs were prepared with different loadings of ACOF-1 and three different polymers as continuous phase: low flux-mid selectivity Matrimid®, mid flux-high selectivity Polyactive™ and high flux-low selectivity 6FDA:DAM. The homogeneous distribution of ACOF-1 together with the good adhesion between the ACOF-1 particles and the polymer matrices were confirmed by scanning electron microscopy. In mixed-gas CO<sub>2</sub>/N<sub>2</sub> separation, a clear influence of the polymer used was observed on the performance of the composite membranes. While for Matrimid® and 6FDA:DAM an overall enhancement of the polymer's separation properties could be achieved, in case of Polyactive™ penetration of the more flexible polymer into the COF porosity resulted in a decreased membrane permeability. The best improvement was obtained for Matrimid®-based MMMs, for which a selectivity increases from 29 to 35, together with an enhancement in permeability from 9.5 to 17.7 Barrer for 16 wt.% COF loading, was observed. Our results demonstrate that the combination of the filler-polymeric matrix pair chosen is crucial. For a given filler the polymer performance improvement strongly depends on the polymeric matrix selected, where a good match between the discontinuous and continuous phase, both in the terms of compatibility and gas separation properties, is necessary to optimize membrane performance.

---

### **3.1. INTRODUCTION**

Global warming has caused great public concern due to the fast increase of emissions of greenhouse gases, especially CO<sub>2</sub>. Capture of CO<sub>2</sub> from flue gas streams of fossil-fuelled power plants, which account for about 40 % of the total carbon emissions worldwide, will be instrumental in addressing measures against climate change.<sup>1,2</sup> Flue gas is composed of different gases such as CO<sub>2</sub>, N<sub>2</sub>, CO, O<sub>2</sub>, water vapour and sulphur oxide, where N<sub>2</sub> is the main component and the concentration of CO<sub>2</sub> (volume basis) is around 15 %.<sup>2,3</sup> Thus, the separation of CO<sub>2</sub> from CO<sub>2</sub>/N<sub>2</sub> mixtures is usually studied in the development of new separation technologies for post-combustion CO<sub>2</sub> capture.

Conventional technologies for gas separation, such as cryogenic distillation, condensation or amine absorption, are energy intensive and may pose environmental concerns. Membrane separation technology, on the other hand, has been greatly developed in recent years for CO<sub>2</sub> capture owing to its attractive features like inherent simplicity, easy operation, energy efficiency, and often smaller footprint. Among the different types of membranes<sup>4-6</sup> those based on polymers are the most widely used in the current market, mainly due to their good processability and low cost. However, polymeric membranes suffer from a well-known trade-off relationship between permeability and selectivity, as originally reported by Robeson in 1991.<sup>7,8</sup> Moreover, their limited thermal and chemical stability and the CO<sub>2</sub>-induced plasticization<sup>9,10</sup> also restrict their massive application. Better separation properties and chemical and thermal stabilities can be achieved with inorganic membranes, but they lack mechanical stability and suffer from processability and high cost issues.<sup>11</sup> In this sense, mixed-matrix membranes (MMMs), where selected fillers are dispersed in a continuous polymer matrix, were proposed to overcome the limitations of organic and inorganic membranes, aiming at the synthesis of processable membranes with a performance above the Robeson trade-off limit. Many different polymers, such as different polyimides<sup>12,13</sup> polysulfone (PSF)<sup>14</sup> and polybenzimidazole (PBI)<sup>15,16</sup>, have been used for the fabrication of MMMs, whereas zeolites,<sup>17</sup> carbon materials,<sup>8</sup> and metal-organic frameworks (MOFs)<sup>19,20</sup> are porous fillers commonly used. Among these fillers, MOFs have demonstrated great prospect in preparing MMMs for CO<sub>2</sub>

separation due to their high porosity, selectivity towards certain guest molecules and rich pre- and post-synthetic chemistry.<sup>21</sup> However, most MOFs show insufficient stabilities under humid conditions, which limit their application in real-life CO<sub>2</sub> capture.<sup>22</sup> Despite long-term stability of MOF-based MMMs with respect to moisture is of utmost importance, this issue remains largely unexplored and thus, still needs to be addressed.

As an alternative to MOFs, covalent organic frameworks (COFs) have recently emerged as potential candidates for the preparation of MMMs. COFs are a class of crystalline porous materials constructed from light-weight elements linked by strong covalent bonds.<sup>23, 24</sup> They have attracted tremendous interest due to their exceptional properties such as low densities, regular and permanent porosity, high surface areas and high thermal stabilities, appealing in different fields, like gas storage and separation,<sup>25</sup> catalysis<sup>26</sup> and photovoltaics.<sup>27</sup> Different MMMs have been reported in which COFs have been used as porous fillers.<sup>28-31</sup> Biswal *et al.*<sup>32</sup> dispersed two different chemically stable isorecticular COFs (TpPa-1 and TpBD) in PBI-Bul to prepare MMMs. The hybrid membranes (50 wt.% loading TpBD) exhibit H<sub>2</sub>, N<sub>2</sub>, CO<sub>2</sub>, CH<sub>4</sub> permeabilities up to seven times higher than those of bare PBI-Bul polymer with slightly decreased CO<sub>2</sub>/N<sub>2</sub> and CO<sub>2</sub>/CH<sub>4</sub> separation factors. Interestingly, the authors were able to increase the COF loading in PBI-Bul up to 50%, indicating the excellent compatibility of the COFs with the polymer matrix. Wang and co-workers<sup>33</sup> prepared highly compatible MMMs containing PVAm and COF for H<sub>2</sub>/CO<sub>2</sub> separation, and the resulting membranes showed a notable improved gas permeability together with slightly higher H<sub>2</sub>/CO<sub>2</sub> selectivities. Zhao *et al.*<sup>34</sup> successfully incorporated two COFs (NUS-2 and NUS-3) into two different polymer matrices (Ultem® and PBI) and applied the membranes to CO<sub>2</sub>/CH<sub>4</sub> and H<sub>2</sub>/CO<sub>2</sub> gas separation. The NUS-2@PBI membranes showed an increase in the H<sub>2</sub>/CO<sub>2</sub> selectivity from 9 for the bare polymer up to 31 upon 20 wt.% COF loading, exceeding the upper bound reported by Robeson in 2008. Recently, our group reported azine-linked COF (ACOF-1) @Matrimid® MMMs for CO<sub>2</sub>/CH<sub>4</sub> separation. A more than doubling of the CO<sub>2</sub> permeability together with slightly higher CO<sub>2</sub>/CH<sub>4</sub> separation factors were observed upon 16 wt.% ACOF-1 loading compared to the bare Matrimid® polymer.<sup>35</sup> These first examples illustrate the potential of COFs as fillers in the preparation of defect free MMMs. The fully-organic nature of COFs probably

accounts for this good adhesion between dispersed and continuous phases, in contrast to other traditional porous fillers, such as zeolites, for which their inorganic nature commonly leads to the formation of defects at the filler-polymer interface. However, choosing appropriate polymer and COF pairs for specific gas mixtures is of high importance to fully exploit the COF separation properties. Indeed, for a given COF, different polymers can be potentially used as the continuous polymeric matrix and *vice versa*, the proper combination of COF and polymer being key for the fabrication of promising MMMs for gas separation. Indeed, the importance of an appropriate selection of a polymer/filler pair has been recently highlighted by the work of Bae *et al.*<sup>36</sup> Using atomically detailed simulations and theoretical permeation models, Keskin and co-workers<sup>37, 38</sup> predicted the separation performance of several new MMMs composed of various polymers and MOFs, and the results provided some suggestions for selecting suitable polymer/MOF pairs to obtain improved separation results. However, despite the importance of such design predictions, no similar works have been reported for the preparation of COF-based MMMs.

Herein, three different polymers (6FDA:DAM, Polyactive™ and Matrimid®) with different CO<sub>2</sub> permeabilities and CO<sub>2</sub>/N<sub>2</sub> separation factors were used to investigate the influence of ACOF-1 on the separation performance of the different membranes. ACOF-1 was selected as filler since ACOF-1 has shown high CO<sub>2</sub> adsorption selectivity from N<sub>2</sub> in powder form together with a good stability.<sup>39</sup> Three different polymers with different separation properties, namely the low flux-mid selectivity Matrimid®, mid flux-high selectivity Polyactive™ and high flux-low selectivity 6FDA:DAM, were chosen as the continuous matrices. The resulting MMMs have been tested for CO<sub>2</sub>/N<sub>2</sub> separation. The best results were obtained for Matrimid®-based MMMs, for which no defects were observed at the filler/polymer interface and a good match between filler and polymer permeation properties allowed for the increase of the MMM permeability. Overall, our study provides some insight into the important topic of the selection of the filler/polymer pair in COF-based MMMs.

## **3.2. EXPERIMENTAL**

### **3.2.1. Materials**

Benzene-1,3,5-tricarboxaldehyde (97 %), hydrazine hydrate ( $\text{N}_2\text{H}_4$  50 % - 60 %), 1,4-dioxane (99.8 %), acetic acid, tetrahydrofuran (THF) (99.9 %), and acetone (99.9 %) were purchased from Sigma Aldrich. All these starting materials and solvents were used without further purification. Matrimid® 5218 ( $M_w = 123,000 \text{ g}\cdot\text{mol}^{-1}$ ,  $M_n \approx 11,000 \text{ g}\cdot\text{mol}^{-1}$ ) was kindly supplied by Huntsman Advanced Materials. 6FDA:DAM polyimide ( $M_w = 271,876 \text{ g}\cdot\text{mol}^{-1}$ ,  $M_n \approx 121,875 \text{ g}\cdot\text{mol}^{-1}$ ) and Polyactive™ ( $M_w = 35,000 \text{ g}\cdot\text{mol}^{-1}$ ) were purchased from Akron polymer systems and PolyVation, respectively. Fig. 3.1 shows the chemical structure of the different polymers used. All the polymers were dried prior to use to remove the adsorbed moisture under vacuum conditions for 48 h at 453 K, 433 K and 323 K for Matrimid®, 6FDA:DAM and Polyactive™, respectively.

### **3.2.2 Synthesis of ACOF-1**

ACOF-1 was synthesized following the same procedure as previously reported by Liu *et al.*<sup>39</sup> and Chapter 2 of this thesis.

### **3.2.3. Preparation of mixed-matrix membranes (MMMs)**

For Matrimid® and 6FDA:DAM MMMs fabrication, the required amount of ACOF-1 particles was first dispersed in THF and sonicated for 30 min. To this suspension, 0.2 g dried polymer were added and the casting suspension was further stirred for 24 h. The solvent/filler-polymer weight ratio was kept at 90/10 in all cases. The proportion of ACOF-1 in the casting suspension was adjusted to achieve the desired final ACOF-1 loadings of 8 wt.% and 16 wt.% in the resulting MMMs.

The prepared suspensions were then cast onto a clean glass plate with the help of a Doctor Blade knife. The cast membranes were then immediately covered with a small watch glass to prevent a too fast evaporation of the solvent. The glass plate was further covered with a square box with four small bottles of THF inside to create a saturated THF atmosphere. All these measures were taken to slow down the evaporation rate of THF and

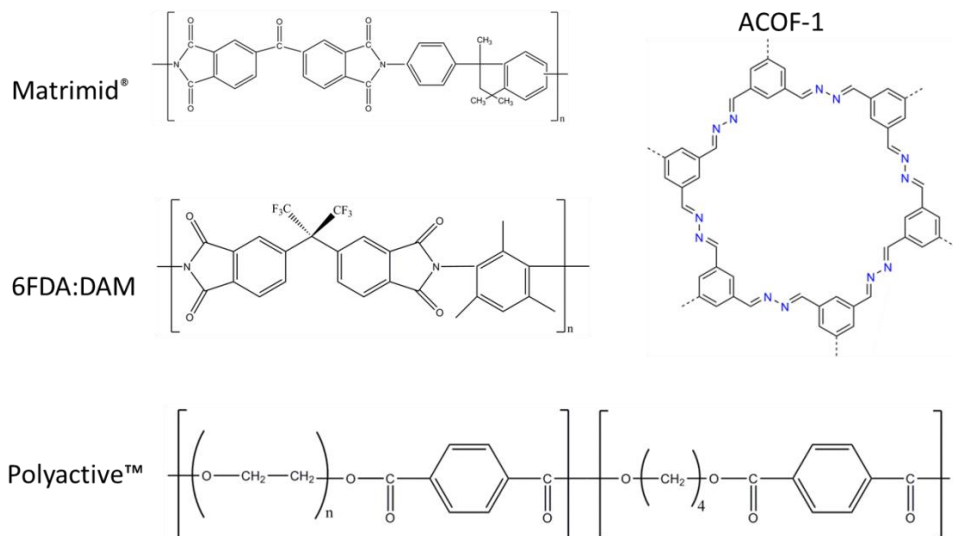


**Fig. 3.1.** Chemical structure of the polymers used together with that of ACOF-1 used as porous filler.

thereby preventing the formation of defects during drying. The membrane was first left to dry overnight at room temperature and then dried under vacuum for 24 h (423 K for Matrimid®-based and 433 K for 6FDA:DAM-based membranes).

For Polyactive™ MMMs preparation, the ACOF-1 particles were dispersed in THF and sonicated for 30 min. To this suspension, 0.2 g Polyactive™ was added and the casting suspension was further stirred for 24 h. Afterwards, the prepared solution was poured into a Teflon petri dish, which was covered with a square box with four small bottles of THF inside to create a saturated THF atmosphere. The membrane was first left to dry overnight and then dried under vacuum at 323 K for 24 h.

For the three polymers, the pure polymer membranes were prepared following the same procedure as for the MMMs, but without the extra step of dispersing ACOF-1 particles. The final thickness of the resulting membranes was individually evaluated using a digital micrometre.

**3.2.4. Characterization techniques**

Powder X-ray diffraction (PXRD) patterns of the prepared membranes were recorded using a Bruker-D8 Advanced diffractometer with Co- $K_{\alpha}$  radiation ( $\lambda = 1.78897 \text{ \AA}$ ). The samples were scanned in the  $2\theta$  range of  $5 - 80^{\circ}$  using a step size of  $0.02^{\circ}$  and a scan speed of  $0.4 \text{ s per step}$  in a continuous scanning mode.

Scanning Electron Microscopy (SEM) micrographs were acquired using a JEOL JSM-6010LA InTouchScope microscope equipped with an integrated SDD EDS detector. ACOF-1 specimens were prepared by drop-casting a sonicated methanol ACOF-1 suspension directly on the sample holder followed by gold sputtering for 20 s. Cross-section of the membranes were obtained by cryo-fracturing in liquid nitrogen.

$\text{N}_2$ -physisorption (77 K) and  $\text{CO}_2$  adsorption (273 K) isotherms of ACOF-1 and membranes were recorded in a Tristar II 3020 (Micromeritics). Prior to the gas adsorption measurements, the samples were degassed at 393 K under  $\text{N}_2$  flow for at least 16 h.

$\text{CO}_2$  and  $\text{N}_2$  high-pressure adsorption experiments were measured at 273 K, 298 K and 308 K with a volumetric apparatus from BEL Japan (Belsorp-HP). In all cases, around 0.1 g sample was outgassed overnight under vacuum conditions at 393 K.

Thermogravimetric analysis (TGA) was performed on a Mettler Toledo TGA/SDTA851e apparatus by measuring the mass loss of the sample while heating ACOF-1 and the prepared membranes under  $\text{N}_2$  ( $100 \text{ mL min}^{-1}$ ) from room temperature to 1073 K at a heating rate of  $10 \text{ K} \cdot \text{min}^{-1}$ .

Differential scanning calorimetry (DSC) measurements were carried out using a Perkin Elmer DSC 7 to assess the glass transition temperature ( $T_g$ ) of the neat membrane and MMMs. The scanning range was 298 K – 698 K at a heating rate of 10 K/min under nitrogen atmosphere for 6FDA:DAM and Matrimid<sup>®</sup> based membranes and 198 K – 348 K for Polyactive<sup>™</sup> membranes. Two consecutive runs were performed. A first DSC cycle was performed to remove thermal history and adsorbed water from the samples. After cooling, a second cycle was performed following the same procedure. The glass transition temperature ( $T_g$ ) value was determined as the point in the transition region where the step change in heat capacity ( $C_p$ ) attains half the value of the total step in the DSC curve<sup>40</sup>.

### **3.2.5. Gas permeation experiments**

The permeation test is the same as described in Chapter 2. The only difference is the different ratio of the gas mixtures. In here, the CO<sub>2</sub>/N<sub>2</sub> separation measurements were performed employing a 15:85 CO<sub>2</sub>:N<sub>2</sub> gas mixture (23 mL·min<sup>-1</sup> CO<sub>2</sub> and 130 mL·min<sup>-1</sup> of N<sub>2</sub>) as feed. Helium (4.6 mL·min<sup>-1</sup>) was used as sweep gas at the permeate side. The absolute pressure of the feed stream was adjusted in a range of 2 - 5 bar using a back-pressure controller at the retentate side, keeping the permeate side at atmospheric pressure. The temperature in the permeation module was kept at 308 K. Gas separation performance was defined by the separation factor ( $\alpha$ ) and the gas permeability ( $P$ ) of the individual components. See Chapter 2 for details.

## **3.3. RESULTS AND DISCUSSION**

### **3.3.1. Characterization of ACOF-1**

The synthesis and characterization of ACOF-1 particles were performed following the method as described in Chapter 2 and is not repeated here. Fig. 3.2. shows the CO<sub>2</sub> and N<sub>2</sub> adsorption isotherms acquired at 273 K, 298 K and 308 K for ACOF-1, with CO<sub>2</sub> uptakes at 5 bar of 6.1, 4.6 and 3.9 mmol g<sup>-1</sup> and N<sub>2</sub> uptakes of 1.2, 0.7 and 0.7 mmol g<sup>-1</sup> at 273, 298 and 308 K, respectively. The obtained CO<sub>2</sub> uptakes at 1 bar are in good agreement with the values previously reported by Stegbauer *et al.*<sup>41</sup> ACOF-1 shows a significant preference for CO<sub>2</sub> adsorption over N<sub>2</sub>, with ideal adsorption selectivities of 15, 13 and 14 based on the molar ratio of adsorbed amount of CO<sub>2</sub> and N<sub>2</sub> at 273 K, 298 K and 308 K, respectively, calculated at 1 bar. These results demonstrate that ACOF-1 is selective towards CO<sub>2</sub> over N<sub>2</sub>, rendering ACOF-1 an interesting candidate for the preparation of MMMs for post-combustion CO<sub>2</sub> capture.

### **3.3.2. Characterization of ACOF-1-based MMMs**

In order to study the influence of the polymeric matrix on membrane performance, MMMs containing ACOF-1 and 3 different polymers, namely, Matrimid®, Polyactive™ and 6FDA:DAM were prepared. Scanning electron microscopy (SEM) was used to assess the



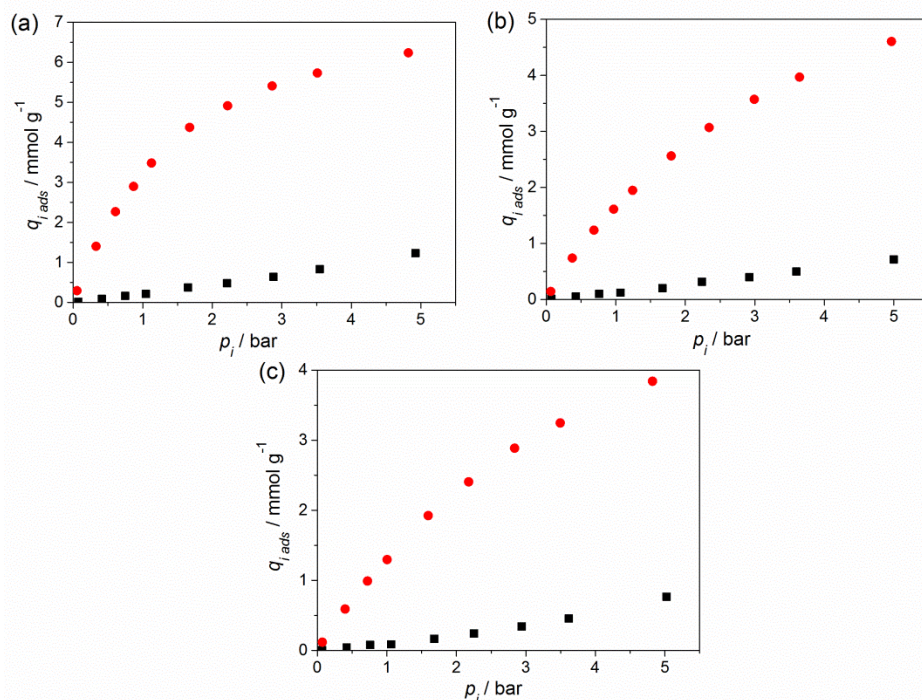


**Fig. 3.2.** CO<sub>2</sub> (red solid dots) and N<sub>2</sub> (black solid squares) adsorption isotherms (volumetric measurement) for ACOF-1 measured at 273 K.

dispersion of ACOF-1 at the cross-section of the different membranes. Fig. 3.3a shows that ACOF-1 particles show a spherical morphology. The average particle size is  $350 \pm 30$  nm calculated from transmission electron microscopy (TEM) images in Chapter 2. Fig. 3.3b-d demonstrate that ACOF-1 particles are homogeneously dispersed into the polymer matrices with no obvious interfacial voids at the filler-polymer interface. The good dispersion of the COF particles is in line with the homogenous distribution of ACOF-1 in Matrimid® previously observed by Raman spectroscopy.<sup>35</sup> Fig. 3.4 shows the thermogravimetric analyses acquired for the filler and bare polymeric membranes together with those obtained for the MMMs. The TGA of ACOF-1 shows that it is stable up to 573 K, temperature at which it starts decomposing. This temperature is higher for all three polymers, decomposing at around 740 K, 735 K and 610 K in the case of Matrimid®,

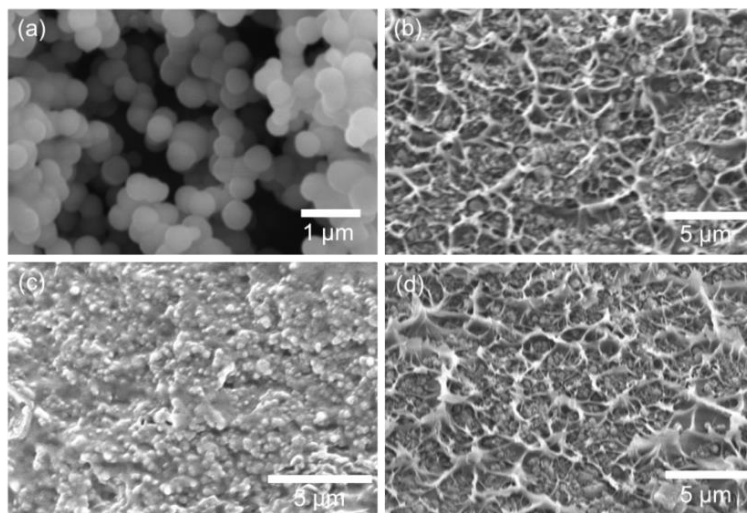


**Fig. 3.3.** SEM micrographs of (a) ACOF-1 and the cross-section of (b) 16 wt.% ACOF-1@Matrimid®, (c) 16 wt.% ACOF-1@Polyactive™ and (d) 16 wt.% ACOF-1@6FDA:DAM MMMs.

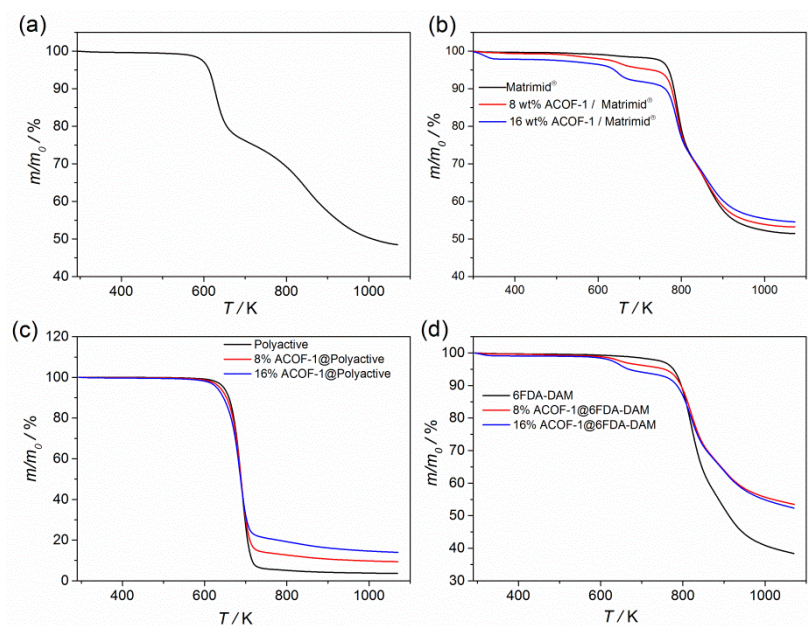


**Fig. 3.4.** TGA results for (a) ACOF-1, the bare polymers (b) Matrimid®, (c) Polyactive™, and (d) 6FDA:DAM and their mixed matrix membranes with ACOF-1 under nitrogen flow at a heating rate of 10 K/min.

6FDA:DAM and Polyactive™, respectively. Interestingly, for all three polymers the TGA curves remain flat up to the decomposition temperature, pointing to a complete removal of the solvent in the prepared membranes upon thermal treatment. As for the MMMs, the weight-loss observed between 620 K and 680 K for the Matrimid® and 6FDA:DAM containing membranes can be attributed to the decomposition of the COF. This allowed for the evaluation of the ACOF-1 loading, which is in agreement with the nominal filler content (accuracy within 5%). This is however not the case for Polyactive™-based MMMs, for which the decomposition temperature is closer to that of the COF<sup>42, 35, 39</sup> hindering such an estimation of the COF loading.

It is well accepted that pore blockage by the polymeric chains or polymer chain rigidification at the polymer-filler interface are commonly encountered in MMMs, which may lead to a decrease in the membrane gas permeability.<sup>43, 44</sup> Hence, in this study differential scanning calorimetry (DSC) and CO<sub>2</sub> adsorption were performed to gain insight into these possible non-ideal interface morphologies.<sup>45</sup> Fig. 3.5 shows the CO<sub>2</sub> adsorption isotherms acquired for ACOF-1, pure Matrimid®, Polyactive™ and 6FDA:DAM and the MMMs containing 16 wt.% COF loading. Furthermore, the estimated CO<sub>2</sub> uptake for the MMMs calculated as a linear combination of those uptakes for the pure components is also shown. While the calculated and experimentally obtained CO<sub>2</sub> uptakes coincide fairly well for Matrimid® and 6FDA:DAM-based MMMs, the experimental uptake obtained for Polyactive™-containing membranes is lower than that calculated. DSC measurements show that the  $T_g$  of the membranes is hardly affected by the presence of the COF, as shown in Table B1, only *ca* 2 K shift (from 594 to 596 K, from 662 to 659 K and from 222 to 221 K, for Matrimid®, 6FDA-DAM and Polyactive™ membranes, respectively) was observed for these three polymers at 16 wt.% COF loading, suggesting that significant rigidification of the polymeric chains surrounding the filler particles does not take place in the prepared COF MMMs. This is in contrast to some MOF-based MMMs, for which a significant increase in  $T_g$  was observed compare to the pure polymer.<sup>46-48</sup> Thus, the lower uptake observed for the Polyactive-based membranes can be ascribed to the partial pore blockage of ACOF-1 pores by the more flexible polymeric chains of Polyactive™. This is in

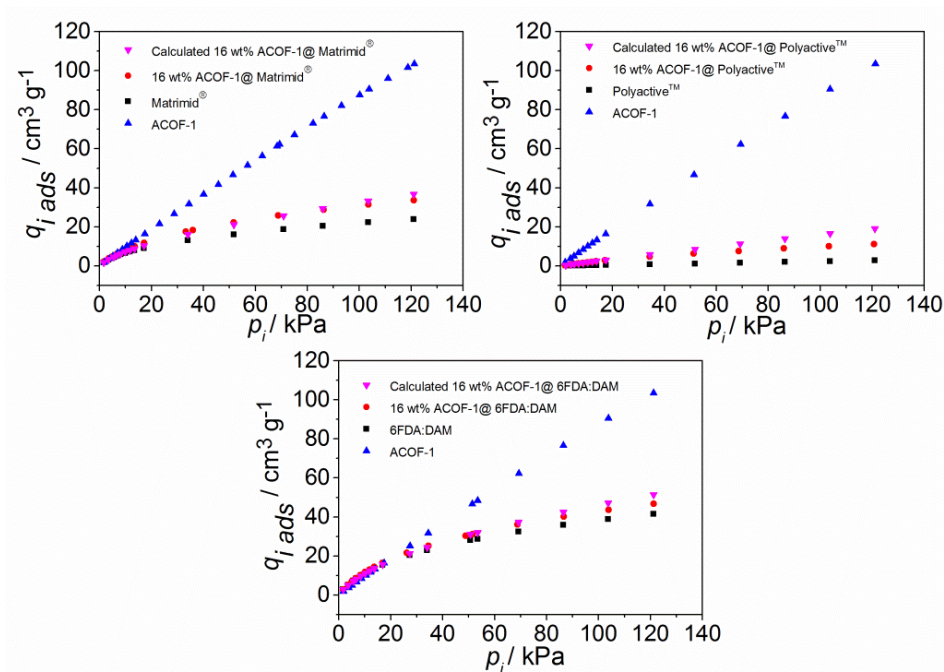


**Fig. 3.5.** CO<sub>2</sub> adsorption isotherms acquired at 273 K for the prepared membranes.

contrast to the polyimides Matrimid® and 6FDA:DAM, for which their higher glass transition temperature ( $T_g$ ) endow the polymeric chains with a higher rigidity, hampering their migration into the pores. Furthermore, the lower molecular weight of Polyactive™ may also play a role, where the shorter polymeric chains might facilitate the blockage of the COF pores. A further hint into the influence of the Polyactive™ on the ACOF-1 filler particles is given by XRD. Fig. B1 shows the XRD patterns of ACOF-1, the pure polymers and the composite membranes. For ACOF-1@Matrimid® and ACOF-1@6FDA:DAM MMMs, the reflection observed at  $8.3^\circ$ , corresponding to the COF, indicates that the ACOF-1 crystallinity is maintained upon membrane preparation. This is not the case for Polyactive™-based membranes, for which the absence of reflections related to ACOF-1 point to the loss of long range order.

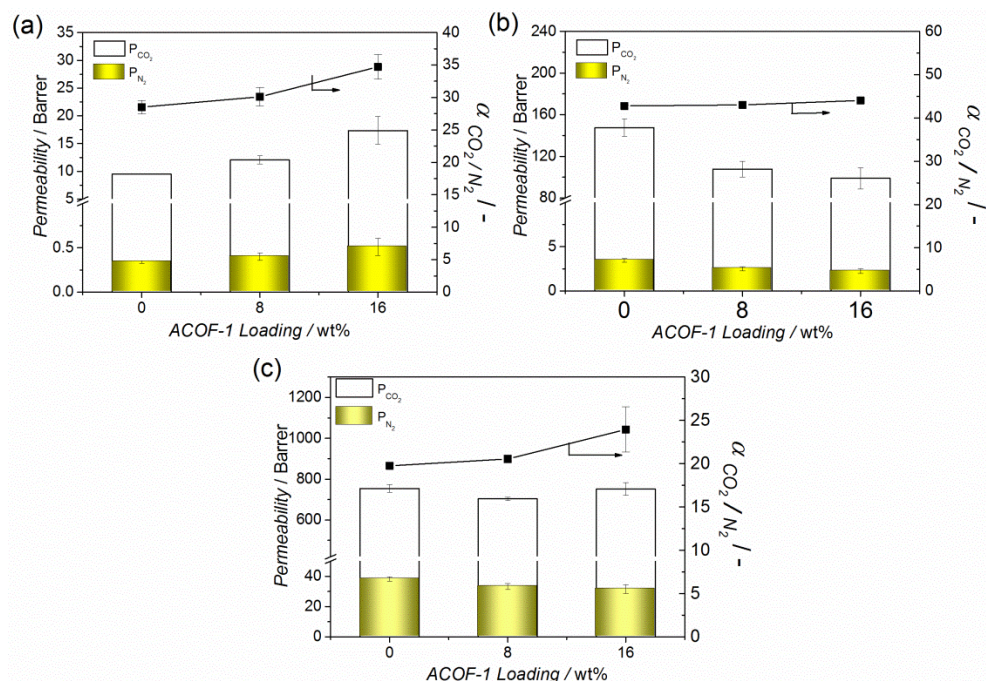


**Fig. 3.6.** Performance of MMMs based on (a) Matrimid®, (b) Polyactive™ and (c) 6FDA:DAM with different ACOF-1 loadings in the separation of CO<sub>2</sub> from a 15:85 CO<sub>2</sub>/N<sub>2</sub> mixture at 308 K and a feed pressure of 2 bar. Error bars correspond to standard deviation.

### 3.3.3. Gas separation performance

Membranes with three different loadings (0, 8 and 16 wt.%) were prepared for each polymeric matrix and tested in the separation of CO<sub>2</sub> from a 15:85 CO<sub>2</sub>:N<sub>2</sub> gas mixture at 308 K and different feed pressures (Fig. 3.6 and Table B2). Each membrane was fabricated and measured at least 3 times to ensure reliable results. Fig. 3.6 shows the different behavior of the MMMs depending on the polymeric matrix used, pointing to the importance of a good selection of the COF/polymer pair. MMMs synthesized with Matrimid® exhibited an increase in the CO<sub>2</sub> and N<sub>2</sub> permeabilities (P<sub>CO<sub>2</sub></sub> increases from 9.5 to 17.7 Barrer upon 16 wt.% COF loading) together with an increase in the CO<sub>2</sub>/N<sub>2</sub> separation factor from 29 to 35. This permeability and selectivity increase, being more pronounced at higher COF loadings, is in line with our previous results, where ACOF-1 @



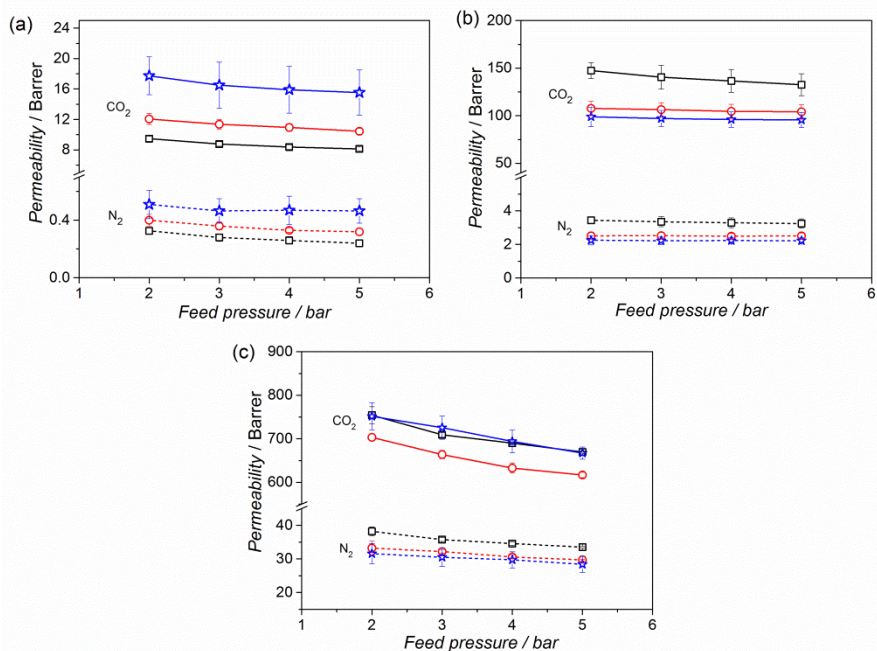


**Fig. 3.7.** Effect of the feed pressure on the gas separation performance of (a) Matrimid®, (b) Polyactive™ and (c) 6FDA:DAM containing membranes. Results obtained in the separation of CO<sub>2</sub> from a 15:85 CO<sub>2</sub>/N<sub>2</sub> mixture at 308 K. Error bars correspond to standard deviation. □ Pure polymer, ○ 8 wt.% ACOF-1 MMMs, ☆ 16 wt.% ACOF-1 MMMs

Matrimid® MMMs were studied in the separation of CO<sub>2</sub> from CH<sub>4</sub>. The additional transport pathways provided by the ACOF-1 are most likely behind the improvement of the membrane permeability, while the higher selectivity can be ascribed to the preferential adsorption of CO<sub>2</sub> over N<sub>2</sub> in the N-rich ACOF-1 framework.<sup>39</sup> In the case of Polyactive™-based MMMs however, a pronounced permeability decrease was observed at increasing filler loadings together with a rather constant CO<sub>2</sub>/N<sub>2</sub> selectivity. Pore blockage by Polyactive™ and crystallinity loss (*vide supra*) account for this observation. A slightly higher CO<sub>2</sub>/N<sub>2</sub> selectivity is observed for the 6FDA:DAM containing MMMs with a slight decrease in CO<sub>2</sub> permeability for 8 wt.% ACOF-1 MMMs. In this case, the absence of indications pointing to pore blockage and reduced framework crystallinity rule out the hypothesis of a lower gas accessibility to the ACOF-1. Therefore, the observed decrease in permeability can be probably attributed to the gas permeability of ACOF-1, which is lower

than the highly permeable 6FDA:DAM. This is in agreement with the calculated results reported in MOF-based MMMs, where a highly selective MOF can increase the selectivity of a highly permeable polymer but slightly decreases the MMM's CO<sub>2</sub> permeability.<sup>37</sup> At higher COF loadings (16 wt.% and 24 wt.%) however the membrane permeability increases together with a constant or decreased selectivity for 16 and 24 wt.% COF loading, respectively. This points to the formation of defects at the COF/polymer interface when the filler content is further increased.

The influence of feed pressure on the gas permeation performance of neat polymers and MMMs is shown in Fig. 3.7. The permeability of Matrimid® and 6FDA:DAM containing membranes shows a slight decrease with increasing feed pressure, what is attributed to the saturation of Langmuir adsorption sites following the well-known dual-mode sorption model.<sup>49</sup> Similar results have been reported for other MOF-based MMMs.<sup>44, 50</sup> For the case of rubbery Polyactive™, the gas solubility obeys Henry's law, where the solubility for each gas through the membrane is directly proportional to the applied pressure.<sup>51</sup> Therefore, the gas permeability of Polyactive™ membranes remained relatively constant over the whole pressure test range.

The results for the three neat polymers and the MMMs were put into perspective using the 2008 Robeson plot. Fig. 3.8 shows the CO<sub>2</sub> permeabilities together with CO<sub>2</sub>/N<sub>2</sub> selectivities for neat polymer membranes and the MMMs measured at 308 K and a feed pressure of 2 bar together with some relevant results for CO<sub>2</sub>/N<sub>2</sub> separation reported for MOF-based MMMs.<sup>21</sup> The results of the three bare polymer membranes from this work are in line with the previous literature. Although none of our results surpass the Robeson upper bound, the incorporation of ACOF-1 results in a clear improvement in the membranes containing Matrimid® and 6FDA:DAM. Specifically, the best results were observed for MMMs based on Matrimid®, which showed an enhancement in both CO<sub>2</sub> permeability and CO<sub>2</sub>/N<sub>2</sub> selectivity upon ACOF-1 loading. To gain further insight into the behavior of these best-performing membranes, one of the 16 wt.% ACOF-1@ Matrimid® MMMs was re-tested after one year (Table B3). Results show that the separation performance is maintained, pointing to a good stability of the prepared membranes. In

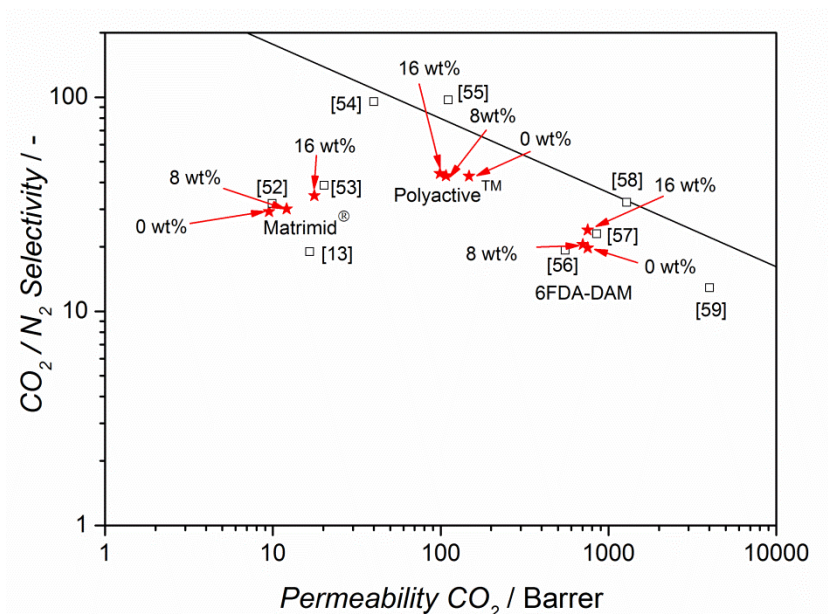


**Fig. 3.8.** Robeson plot for the separation of CO<sub>2</sub> from a 15:85 CO<sub>2</sub>/N<sub>2</sub> mixture at 308 K and a feed pressure of 2 bar, showing the gas separation performance of three pure polymers used in this study together with their MMMs (with 8 and 16 wt.% ACOF loading). Most relevant results<sup>13, 52-59</sup> reported in the literature for MOF-based MMMs have also been included for comparison (open squares). See detailed information in Table B4.

contrast to Matrimid-based MMM®, 6FDA:DAM and Polyactive™-containing MMMs exhibit a decrease in membrane permeability, which only in the case of 6FDA:DAM takes place together with an increase in membrane selectivity.

#### 4. CONCLUSION

MMMs comprising ACOF-1 were prepared with 2 different filler loadings and 3 different polymer matrices. Among the different polymers chosen, the best results were obtained for Matrimid® for which non-idealities were not observed at the filler-polymer interface and whose low permeability allows for an improvement in membrane permeability upon filler dispersion. In the case of Polyactive™ and 6FDA:DAM however, a decrease in membrane permeability was observed. In the former case, pore blockage by the more flexible polymeric chains together with a loss in long range order of the filler accounts for the poorer membrane performance. In the latter case, the additional transport pathways



provided by the COF are not sufficient to improve the permeability of the already highly permeable polymeric matrix, the composite membranes showing a higher selectivity in line with the still accessible filler pores.

Overall, our results demonstrate that the combination of the filler-polymeric matrix pair chosen is crucial. For a given filler, polymer performance improvement strongly depends on the polymeric matrix selected. A good match between the discontinuous and continuous phases, both in the terms of compatibility and gas separation properties, is necessary to optimize membrane performance.

## REFERENCES

- 1 R. T. Woodward, L. A. Stevens, R. Dawson, M. Vijayaraghavan, T. Hasell, I. P. Silverwood, A. V. Ewing, T. Ratvijitvech, J. D. Exley, S. Y. Chong, F. Blanc, D. J. Adams, S. G. Kazarian, C. E. Snape, T. C. Drage and A. I. Cooper, *Journal of the American Chemical Society*, 2014, **136**, 9028.
- 2 M.-S. Lee, M. Park, H. Y. Kim and S.-J. Park, *Scientific Reports*, 2016, **6**, 23224.
- 3 J. Wang and Q. Liu, *Nanoscale*, 2014, **6**, 4148.
- 4 P. Arab, E. Parrish, T. Islamoglu and H. M. El-Kaderi, *Journal of Materials Chemistry A*, 2015.
- 5 H. A. Patel, S. Hyun Je, J. Park, D. P. Chen, Y. Jung, C. T. Yavuz and A. Coskun, *Nature Communications*, 2013, **4**, 1357.
- 6 M. Shan, Q. Xue, N. Jing, C. Ling, T. Zhang, Z. Yan and J. Zheng, *Nanoscale*, 2012, **4**, 5477.
- 7 L. M. Robeson, *Journal of Membrane Science*, 1991, **62**, 165.
- 8 *Journal of Membrane Science*, 2008, **320**, 390.
- 9 A. Bos, I. G. M. Pünt, M. Wessling and H. Strathmann, *Journal of Membrane Science*, 1999, **155**, 67.
- 10 R. Swaidan, B. Ghanem, E. Litwiller and I. Pinnau, *Macromolecules*, 2015, **48**, 6553.
- 11 X. Wang, C. Chi, K. Zhang, Y. Qian, K. M. Gupta, Z. Kang, J. Jiang and D. Zhao, *Nature Communications*, 2017, **8**, 14460.
- 12 J. E. Bachman and J. R. Long, *Energy & Environmental Science*, 2016, **9**, 2031.
- 13 Q. Song, S. K. Nataraj, M. V. Roussanova, J. C. Tan, D. J. Hughes, W. Li, P. Bourgoïn, M. A. Alam, A. K. Cheetham, S. A. Al-Muhtaseb and E. Sivaniah, *Energy & Environmental Science*, 2012, **5**, 8359.
- 14 B. Zornoza, A. Martinez-Joaristi, P. Serra-Crespo, C. Tellez, J. Coronas, J. Gascon and F. Kapteijn, *Chemical Communications*, 2011, **47**, 9522.
- 15 J. Sánchez-Laínez, B. Zornoza, S. Friebe, J. Caro, S. Cao, A. Sabetghadam, B. Seoane, J. Gascon, F. Kapteijn, C. Le Guillouzer, G. Clet, M. Daturi, C. Téllez and J. Coronas, *Journal of Membrane Science*, 2016, **515**, 45.
- 16 J. Sanchez-Lainez, B. Zornoza, C. Tellez and J. Coronas, *Journal of Materials Chemistry A*, 2016, **4**, 14334.
- 17 I. Kiesow, D. Marczewski, L. Reinhardt, M. Mühlmann, M. Possiwan and W. A. Goedel, *Journal of the American Chemical Society*, 2013, **135**, 4380.

- 18 T.-S. Chung, S. S. Chan, R. Wang, Z. Lu and C. He, *Journal of Membrane Science*, 2003, **211**, 91.
- 19 T. Rodenas, M. van Dalen, E. García-Pérez, P. Serra-Crespo, B. Zornoza, F. Kapteijn and J. Gascon, *Advanced Functional Materials*, 2014, **24**, 249.
- 20 X. Liu, H. Jin, Y. Li, H. Bux, Z. Hu, Y. Ban and W. Yang, *Journal of Membrane Science*, 2013, **428**, 498.
- 21 B. Seoane, J. Coronas, I. Gascon, M. E. Benavides, O. Karvan, J. Caro, F. Kapteijn and J. Gascon, *Chemical Society Reviews*, 2015, **44**, 2421.
- 22 N. C. Burtch, H. Jasuja and K. S. Walton, *Chemical Reviews*, 2014, **114**, 10575.
- 23 X. Feng, X. Ding and D. Jiang, *Chemical Society Reviews*, 2012, **41**, 6010.
- 24 J. L. Mendoza-Cortes, W. A. Goddard, H. Furukawa and O. M. Yaghi, *The Journal of Physical Chemistry Letters*, 2012, **3**, 2671.
- 25 M. G. Rabbani, A. K. Sekizkardes, Z. Kahveci, T. E. Reich, R. Ding and H. M. El-Kaderi, *Chemistry – A European Journal*, 2013, **19**, 3324.
- 26 C. E. Chan-Thaw, A. Villa, P. Katekomol, D. Su, A. Thomas and L. Prati, *Nano Letters*, 2010, **10**, 537.
- 27 S. Jin, X. Ding, X. Feng, M. Supur, K. Furukawa, S. Takahashi, M. Addicoat, M. E. El-Khouly, T. Nakamura, S. Irle, S. Fukuzumi, A. Nagai and D. Jiang, *Angewandte Chemie International Edition*, 2013, **52**, 2017.
- 28 X. Wu, Z. Tian, S. Wang, D. Peng, L. Yang, Y. Wu, Q. Xin, H. Wu and Z. Jiang, *Journal of Membrane Science*, 2017, **528**, 273.
- 29 L. Xu, J. Xu, B. Shan, X. Wang and C. Gao, *Journal of Membrane Science*, 2017, **526**, 355.
- 30 J. Dechnik, J. Gascon, C. Doonan, C. Janiak and C. J. Sumby, *Angewandte Chemie International Edition*, 2017, **129**, 9420.
- 31 G. Yu, H. Rong, X. Zou and G. Zhu, *Molecular Systems Design & Engineering*, 2017, **2**, 182.
- 32 U. K. Kharul, R. Banerjee, B. Biswal and H. D. Chaudhari, *Chemistry–A European Journal*, 2016, **22**, 4695.
- 33 X. Cao, Z. Qiao, Z. Wang, S. Zhao, P. Li, J. Wang and S. Wang, *International Journal of Hydrogen Energy*, 2016, **41**, 9167.
- 34 Z. Kang, Y. Peng, Y. Qian, D. Yuan, M. A. Addicoat, T. Heine, Z. Hu, L. Tee, Z. Guo and D. Zhao, *Chemistry of Materials*, 2016, **28**, 1277.

- 35 M. Shan, B. Seoane, E. Rozhko, A. Dikhtiarenko, G. Clet, F. Kapteijn and J. Gascon, *Chemistry-A European Journal*, 2016, **22**, 14467.
- 36 T.-H. Bae, J. S. Lee, W. Qiu, W. J. Koros, C. W. Jones and S. Nair, *Angewandte Chemie International Edition*, 2010, **49**, 9863.
- 37 S. Keskin and D. S. Sholl, *Energy & Environmental Science*, 2010, **3**, 343.
- 38 G. Yilmaz and S. Keskin, *Journal of Membrane Science*, 2014, **454**, 407.
- 39 Z. Li, X. Feng, Y. Zou, Y. Zhang, H. Xia, X. Liu and Y. Mu, *Chemical Communications*, 2014, **50**, 13825.
- 40 P. Badrinarayanan, W. Zheng, Q. Li and S. L. Simon, *Journal of Non-Crystalline Solids*, 2007, **353**, 2603.
- 41 L. Stegbauer, M. W. Hahn, A. Jentys, G. Savasci, C. Ochsenfeld, J. A. Lercher and B. V. Lotsch, *Chemistry of Materials*, 2015, **27**, 7874.
- 42 A. Car, C. Stropnik, W. Yave and K.-V. Peinemann, *Advanced Functional Materials*, 2008, **18**, 2815.
- 43 Y. Li, T.-S. Chung, C. Cao and S. Kulprathipanja, *Journal of Membrane Science*, 2005, **260**, 45.
- 44 A. Sabetghadam, B. Seoane, D. Keskin, N. Duim, T. Rodenas, S. Shahid, S. Sorribas, C. L. Guillouzer, G. Clet and C. Tellez, *Advanced Functional Materials*, 2016, **26**, 3154.
- 45 T.-S. Chung, L. Y. Jiang, Y. Li and S. Kulprathipanja, *Progress in Polymer Science*, 2007, **32**, 483.
- 46 A. L. Khan, C. Klayson, A. Gahlaut, X. Li and I. F. J. Vankelecom, *Journal of Materials Chemistry*, 2012, **22**, 20057.
- 47 M. W. Anjum, F. Vermoortele, A. L. Khan, B. Bueken, D. E. De Vos and I. F. J. Vankelecom, *ACS Applied Materials & Interfaces*, 2015, **7**, 25193.
- 48 N. Tien-Binh, H. Vinh-Thang, X. Y. Chen, D. Rodrigue and S. Kaliaguine, *Journal of Materials Chemistry A*, 2015, **3**, 15202.
- 49 S. Kanehashi and K. Nagai, *Journal of Membrane Science*, 2005, **253**, 117.
- 50 S. Shahid and K. Nijmeijer, *Journal of Membrane Science*, 2014, **470**, 166.
- 51 V. Stannett, *Journal of Membrane Science*, 1978, **3**, 97.
- 52 Y. Zhang, I. H. Musselman, J. P. Ferraris and K. J. Balkus, *Journal of Membrane Science*, 2008, **313**, 170.
- 53 E. V. Perez, K. J. Balkus, J. P. Ferraris and I. H. Musselman, *Journal of Membrane Science*, 2009, **328**, 165.

- 54 J. O. Hsieh, K. J. Balkus, J. P. Ferraris and I. H. Musselman, *Microporous and Mesoporous Materials*, 2014, **196**, 165.
- 55 T. Li, Y. Pan, K.-V. Peinemann and Z. Lai, *Journal of Membrane Science*, 2013, **425–426**, 235.
- 56 R. P. Lively, M. E. Dose, L. Xu, J. T. Vaughn, J. R. Johnson, J. A. Thompson, K. Zhang, M. E. Lydon, J.-S. Lee, L. Liu, Z. Hu, O. Karvan, M. J. Realff and W. J. Koros, *Journal of Membrane Science*, 2012, **423–424**, 302.
- 57 T.-H. Bae and J. R. Long, *Energy & Environmental Science*, 2013, **6**, 3565.
- 58 V. Nafisi and M.-B. Hägg, *Journal of Membrane Science*, 2014, **459**, 244.
- 59 S. Japip, H. Wang, Y. Xiao and T. Shung Chung, *Journal of Membrane Science*, 2014, **467**, 162.

## APPENDIX B

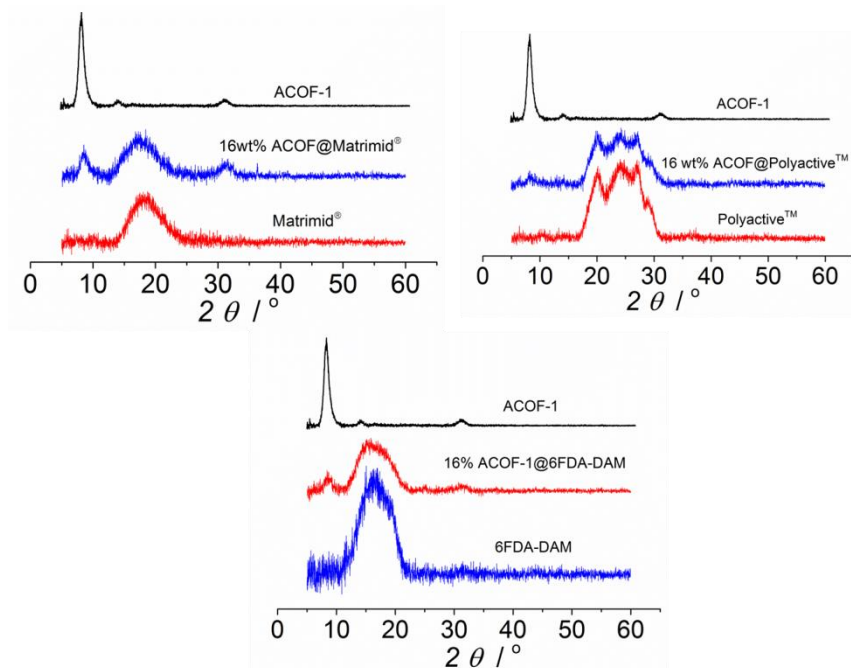


**Fig. B1.** PXRD patterns of ACOF-1, bare polymers and 16 wt.% ACOF-1 mixed-matrix membranes prepared with the three different polymers.

**Table B1.** Glass transition temperature ( $T_g$ ) of different membranes.

Membrane	$T_g$ / K
Bare Matrimid®	594.0
8 wt.% ACOF-1@Matrimid®	596.0
16 wt.% ACOF-1@Matrimid®	596.4
Bare 6FDA-DAM	661.7
8 wt.% ACOF-1@6FDA-DAM	659.0
16 wt.% ACOF-1@6FDA-DAM	658.6
Bare Polyactive™	222.0
8 wt.% ACOF-1@ Polyactive™	220.8
16 wt.% ACOF-1@ Polyactive™	221.4

**Table B2** Summary of membrane performance tested for the CO<sub>2</sub> separation of a 15:85 CO<sub>2</sub>/N<sub>2</sub> mixture at 308 K. The data were obtained for different membranes under several operation pressure conditions. Each type of membrane was fabricated at least 3 times. Error is given as the standard deviation from the independent tests of 3 different membranes. Permeate side at atmospheric pressure with helium as sweep gas.

Membrane	Matrimid®			
Membrane thickness	39 ± 5 µm			
Feed pressure [bar]	2	3	4	5
PCO <sub>2</sub> [Barrer]	9.5 ± 0.3	8.8 ± 0.3	8.4 ± 0.3	8.1 ± 0.2
PN <sub>2</sub> [Barrer]	0.33 ± 0.02	0.28 ± 0.03	0.26 ± 0.03	0.24 ± 0.03
Selectivity [-]	29.2 ± 1.5	31.7 ± 2.4	32.5 ± 2.7	33.6 ± 3.3

Membrane	8 wt. % ACOF-1 / Matrimid®			
Membrane thickness <sup>a</sup>	36 ± 4 µm			
Feed pressure [bar]	2	3	4	5
PCO <sub>2</sub> [Barrer] <sup>b</sup>	12.1 ± 0.7	11.4 ± 0.6	11.0 ± 0.5	10.4 ± 0.4
PN <sub>2</sub> [Barrer] <sup>b</sup>	0.40 ± 0.04	0.36 ± 0.03	0.33 ± 0.01	0.32 ± 0.00
Selectivity [-]	30.1 ± 1.4	31.6 ± 0.2	32.8 ± 0.2	32.9 ± 1.0

Membrane	16 wt. % ACOF-1 / Matrimid®			
Membrane thickness	46 ± 4 µm			
Feed pressure [bar]	2	3	4	5
PCO <sub>2</sub> [Barrer]	17.7 ± 2.4	16.5 ± 3.0	15.9 ± 3.0	15.5 ± 3.0
PN <sub>2</sub> [Barrer]	0.51 ± 0.09	0.46 ± 0.08	0.47 ± 0.10	0.47 ± 0.10
Selectivity [-]	34.7 ± 1.9	36.0 ± 0.3	34.2 ± 0.8	33.9 ± 1.2

### ***Azine-linked COF based MMMs for Post-Combustion CO<sub>2</sub> Capture***

Membrane	Polyactive™			
Membrane thickness	53 ± 1 µm			
Feed pressure [bar]	2	3	4	5
<i>PCO<sub>2</sub></i> [Barrer]	147.5 ± 8.4	140.5 ± 12.4	136.5 ± 11.9	132.6 ± 11.7
<i>PN<sub>2</sub></i> [Barrer]	3.44 ± 0.21	3.35 ± 0.31	3.29 ± 0.29	3.24 ± 0.28
Selectivity [-]	42.8 ± 0.2	41.9 ± 0.2	41.5 ± 0.5	40.8 ± 0.4

Membrane	8 wt.%ACOF-1@Polyactive™			
Membrane thickness	45 ± 10 µm			
Feed pressure [bar]	2	3	4	5
<i>PCO<sub>2</sub></i> [Barrer]	107.7 ± 7.6	106.4 ± 7.0	104.6 ± 7.4	104.2 ± 7.7
<i>PN<sub>2</sub></i> [Barrer]	2.51 ± 0.23	2.52 ± 0.18	2.49 ± 0.16	2.51 ± 0.17
Selectivity [-]	43.0 ± 0.82	42.3 ± 0.36	42.0 ± 0.33	41.5 ± 0.30

Membrane	16 wt.%ACOF-1@Polyactive™			
Membrane thickness	60 ± 1 µm			
Feed pressure [bar]	2	3	4	5
<i>PCO<sub>2</sub></i> [Barrer]	98.9 ± 10.2	97.1 ± 8.6	96.1 ± 8.1	95.6 ± 7.9
<i>PN<sub>2</sub></i> [Barrer]	2.25 ± 0.27	2.22 ± 0.22	2.23 ± 0.18	2.22 ± 0.18
Selectivity [-]	44.0 ± 0.62	43.8 ± 0.47	43.0 ± 0.08	43.2 ± 0.13



Membrane	6FDA-DAM			
Membrane thickness	56 ± 2 µm			
Feed pressure [bar]	2	3	4	5
$PCO_2$ [Barrer]	754.3 ± 19.4	709.2 ± 5.8	690.1 ± 2.6	669.7 ± 2.2
$PN_2$ [Barrer]	38.2 ± 1.4	35.8 ± 0.6	34.6 ± 0.6	33.5 ± 0.3
Selectivity [-]	19.8 ± 0.2	19.8 ± 0.2	20.0 ± 0.3	20.0 ± 0.1

Membrane	8 wt.%ACOF-1 @6FDA-DAM			
Membrane thickness	56 ± 1 µm			
Feed pressure [bar]	2	3	4	5
$PCO_2$ [Barrer]	703.3 ± 7.9	663.9 ± 9.6	632.8 ± 11.7	616.8±6.1
$PN_2$ [Barrer]	33.2 ± 2.0	32.2 ± 0.6	30.6 ± 0.5	29.7 ± 0.3
Selectivity [-]	20.5 ± 0.4	20.6 ± 0.1	20.7 ± 0.1	20.8 ± 0.2

Membrane	16 wt.%ACOF-1@6FDA-DAM			
Membrane thickness	46 ± 2 µm			
Feed pressure [bar]	2	3	4	5
$PCO_2$ [Barrer]	751.7 ± 31.1	725.7 ± 26.9	694.1 ± 25.9	667.3± 14.1
$PN_2$ [Barrer]	31.6 ± 3.0	30.5 ± 2.8	29.7 ± 2.4	28.4 ± 2.4
Selectivity [-]	24.0 ± 2.6	23.9 ± 2.4	23.4 ± 2.0	23.6 ± 1.9

Membrane	24 wt.% ACOF-1@6FDA-DAM			
Membrane thickness	44 ± 2 µm			
Feed pressure [bar]	2	3	4	5
$PCO_2$ [Barrer]	1282.7	1261.1	1219.0	1180.5
$PN_2$ [Barrer]	61.4	60.6	59.6	58.7
Selectivity [-]	20.9	20.8	20.5	20.1

**Table B3.** Long term stability test of 16 wt. % ACOF-1 / Matrimid® (tested after one year)

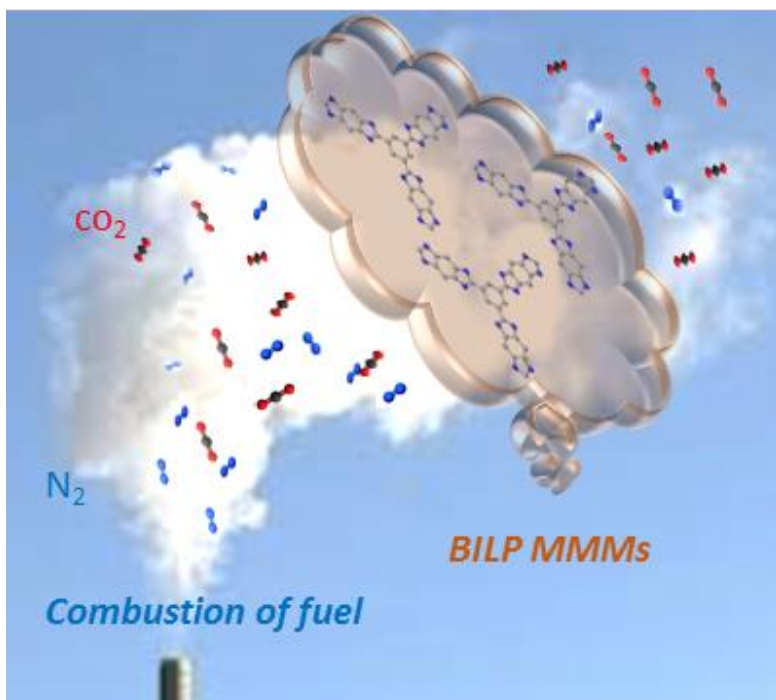
Membrane	16 wt. % ACOF-1 / Matrimid®			
Membrane thickness	39 ± 1 µm			
Feed pressure [bar]	2	3	4	5
$PCO_2$ [Barrer]	12.9 ± 0.2	11.9 ± 0.11	11.6 ± 0.03	11.5 ± 0.07
$PN_2$ [Barrer]	0.39 ± 0.01	0.34 ± 0.01	0.33 ± 0.01	0.33 ± 0.00
Selectivity [-]	33.4 ± 1.0	35.1 ± 0.9	35.1 ± 0.6	35.1 ± 0.4

**Table B4** Detailed information of the reference cited in Fig. 3.8.

MMMs			Performance		Operation conditions rate			Reference shown in Fig. 3.8
MOF	Polymer	wt.% loading	$P_{CO_2}$ (Barrer)	$CO_2/N_2$ selectivity (-)	Type of analysis	T (K)	P (bar)	
ZIF-8	Matrimid®	20	16.6	19.0	Single gas	22	4	[13]
Cu-4,4'-BPY-HFS	Matrimid®	20	9.9	31.9	Single gas	35	2	[52]
MOF-5	Matrimid®	30	20.2	38.8	Single gas	35	2	[53]
MIL-53(Al)-as	Matrimid®	37.5	40	95.2	Single gas	35	2	[54]
ZIF-7	Pebax®	22	111	97	Single gas	20	7.5 (3.75 for $CO_2$ )	[55]
ZIF-8	6FDA-DAM:DABA 4:1	20	553	19.3	Single gas	30	1.4	[56]
CPO-27(Mg)	6FDA-TMPDA	10	850	23	Single gas	25	2	[57]
ZIF-8	Pebax®	35	1287	32.2	Single gas	RT	2	[58]
ZIF-71	6FDA-durene	20	4006	12.8	Single gas	35	2	[59]

# Benzimidazole linked Polymers (BILPs) in Mixed-Matrix Membranes: Influence of Filler Porosity on the CO<sub>2</sub>/N<sub>2</sub> Separation Performance

# 4



This chapter is based on the following publication:

M. Shan, B. Seoane, A. Pustovarenko, X. Wang, X. Liu, I. Yarulina, E. Abou-Hamad, F. Kapteijn, and J. Gascon, Benzimidazole linked Polymers (BILPs) in Mixed-Matrix Membranes: Influence of Filler Porosity on the CO<sub>2</sub>/N<sub>2</sub> Separation Performance *J. Membr. Sci.*, 566 (2018) 213-222.

---

**Abstract:** The performance of mixed-matrix membranes (MMMs) based on Matrimid® and benzimidazole-linked polymers (BILPs) have been investigated for the separation of CO<sub>2</sub>/N<sub>2</sub> and the dependency on the filler porosity. BILPs with two different porosities (BILP-101 and RT-BILP-101) were synthesized through controlling the initial polymerization rate and further characterized by several techniques (DRIFTS, <sup>13</sup>C CP/MAS NMR, SEM, TEM, N<sub>2</sub> and CO<sub>2</sub> adsorption). To investigate the influence of porosity, the two types of fillers were incorporated into Matrimid® to prepare MMMs at different loadings (8, 16 and 24 wt.%). SEM confirmed the homogeneous dispersion of BILP-101 and RT-BILP-101, indicating their good compatibility with polymer matrix. The partial pore blockage of BILP fillers in the membrane was verified by CO<sub>2</sub> adsorption isotherms on the prepared membranes. In the separation of CO<sub>2</sub> from a 15:85 CO<sub>2</sub>:N<sub>2</sub> mixture at 308 K, the incorporation of both BILPs fillers resulted in an enhancement in gas permeability together at constant selectivity owing to the fast transport pathways introduced by the porous network. It was noteworthy that the initial porosity of the filler had a large impact on separation permeability. The best improvement was achieved by 24 wt.% RT-BILP-101 MMMs, for which the CO<sub>2</sub> permeability increased by up to 2.8 times (from 9.6 to 26.5 Barrer).

---

#### **4.1. INTRODUCTION**

The soaring increase in CO<sub>2</sub> emissions has caused great public concern due to its accompanying greenhouse effect. In this sense, the capture of CO<sub>2</sub> from flue gas has become necessary from the perspective of energy and the environment.<sup>1</sup> Traditional technologies using amines or solvents to absorb CO<sub>2</sub> are environmentally unfriendly and energy intensive. Membrane-based gas separation on the other hand is a promising alternative owing to its attractive features, such as smaller footprints, easy operation and energy efficiency. Although many novel membrane materials have been proposed, polymeric membranes still dominate the current membrane market given their good processability, mechanical stability and low price. Nevertheless, conventional polymeric membranes suffer from a universal ‘trade-off’ relation between permeability and selectivity, known as the Robeson upper bound.<sup>2,3</sup> Extensive efforts have been devoted to improve the gas separation performance (permeability and selectivity) of polymeric membranes, which include polymer blending,<sup>4</sup> post-treatment of the membranes via cross-linking<sup>5</sup> or thermal rearrangement<sup>6</sup> and the development of novel nanoporous polymers, such as polymers of intrinsic microporosity (PIMs).<sup>7,8</sup> In this line, one of the most promising approaches to overcome polymers’ gas separation performance is to use mixed-matrix membranes (MMMs), consisting of a blend of selected fillers dispersed in a continuous polymeric matrix. This strategy allows combining one membrane the better separation performance of the selected fillers with the good processability and low price of polymeric membranes. Numerous porous fillers such as zeolites<sup>9,10</sup> and metal-organic frameworks (MOFs)<sup>11,12</sup> have been successfully incorporated into different polymers to prepare MMMs, resulting in an improved separation performance compared to the bare polymer membranes.

Porous organic frameworks (POFs),<sup>13</sup> such as covalent organic frameworks (COFs),<sup>14,15</sup> conjugated microporous polymers (CMPs),<sup>16</sup> porous aromatic frameworks (PAFs)<sup>17</sup> and covalent triazine-based frameworks (CTFs),<sup>18</sup> are a relatively new category of porous materials constructed from covalent bonds. Given their diverse porosities, tunable chemical properties, inherent light weight and exceptional chemical and thermal

stabilities, POFs are promising candidates to be used as fillers in MMMs for CO<sub>2</sub> separation.<sup>19, 20</sup> For example, Jin *et al.*<sup>21</sup> studied the effect of dispersing COF nanosheets in polyether-block-amide (PEBA) and prepared PEBA-based MMMs, which show 56 % improvement in ideal selectivity towards CO<sub>2</sub>/N<sub>2</sub> compared to the pure PEBA membrane with only 1 wt.% COF loading. Zhu *et al.*<sup>22</sup> developed a new synthesis protocol to prepare self-supported PAF-56P@Polysulfone (PSF) composite hollow fibre membranes with a CO<sub>2</sub> over N<sub>2</sub> selectivity of 38.9 together with good thermal and mechanical stabilities. Recently, our group incorporated ACOF-1 in three different polymers to prepare MMMs for CO<sub>2</sub> separation.<sup>23</sup> The best improvement was observed for Matrimid®-based MMMs, for which a 20% and 87% increase in CO<sub>2</sub>/N<sub>2</sub> selectivity and CO<sub>2</sub> permeability was obtained for 16 wt.% COF loading, respectively. These examples underscore the good compatibility between POFs with different polymer matrices resulting in MMMs with improved performance when compared to the pure polymers. The fully organic nature of POFs has been reported to account for this good compatibility, in contrast to other inorganic fillers, such as silica and zeolites, for which a poor compatibility with the formation of voids at the filler-polymer interface has often been encountered.

Benzimidazole-linked polymers (BILPs) were first reported in 2011.<sup>24</sup> BILPs show high CO<sub>2</sub> uptakes (up to ~ 6 mmol·g<sup>-1</sup> at 273 K for BILP-19<sup>25</sup>) together with high CO<sub>2</sub>/N<sub>2</sub> and CO<sub>2</sub>/CH<sub>4</sub> selectivities.<sup>26</sup> This preference for CO<sub>2</sub> has been related to the presence of imidazole functionalities in the POF framework. Further, the excellent thermal and chemical stabilities of BILPs make them desirable for practical separations. Sekizkardes *et al.*<sup>27</sup> successfully incorporated BILP-101 nanoparticles into the high free volume PIM-1 matrix. The obtained MMMs achieved a 53% enhancement in the CO<sub>2</sub> permeability together with good stability under harsh conditions upon 30 wt.% POF loading, further proving the feasibility of using BILPs as fillers in the MMMs.

In terms of fillers, porosity is an important factor affecting CO<sub>2</sub> uptake and selectivity, playing a key role on the MMMs performance.<sup>28, 29</sup> Several studies have been devoted to the influence of the filler particle size and morphology<sup>12, 30-33</sup> as well as filler functionalities<sup>34</sup> on the membrane performance. However, the role of the fillers' porosity has remained largely unexplored. Therefore, the effect of filler porosity on the separation

performance of POFs-containing MMMs is studied for the first time. BILP-101 particles with two different porosities were synthesized by controlling the initial polymerization rate and used as fillers in the polyimide Matrimid® 5218. Matrimid® 5218 was chosen as polymer matrix due to its good CO<sub>2</sub> selectivity together with high thermal and chemical stabilities and commercial availability. The prepared membranes were tested for CO<sub>2</sub>/N<sub>2</sub> separation at 308 K and the effect of filler porosity, filler loading, and absolute feed pressure on membrane performance was assessed.

## **4.2. EXPERIMENTAL**

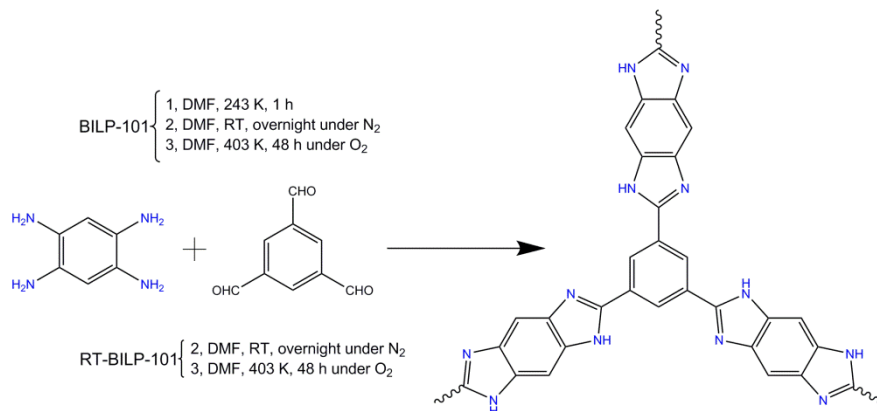
### **4.2.1. Materials**

Benzene-1,3,5-tricarboxaldehyde (97 %), 1,2,4,5-benzenetetramine tetrahydrochloride, hydrochloric acid (37 %), sodium hydroxide (99.99 % metals basis), acetone (99.9 %) and tetrahydrofuran (THF, 99.9 %) were purchased from Sigma Aldrich. N,N-Dimethylformamide (DMF, 99.8%, extra dry over molecular sieves) was purchased from Thermo Fisher. All these starting materials and solvents were used without further purification. Matrimid® 5218 ( $M_w \approx 123,000 \text{ g}\cdot\text{mol}^{-1}$ ,  $M_n \approx 11,000 \text{ g}\cdot\text{mol}^{-1}$ ) was kindly supplied by Huntsman Advanced Materials. Matrimid® was dried prior to use to remove the adsorbed moisture under vacuum at 453 K for 48 h.

### **4.2.2 Synthesis of BILP-101 and RT-BILP-101**

BILP-101 was synthesized following the same procedure as previously reported by Sekizkardes *et al.*<sup>35</sup> In a typical synthesis, a 100 mL round bottom flask was charged with 1,2,4,5-benzenetetramine tetrahydrochloride (100 mg, 0.35 mmol), 60 mL anhydrous DMF, and a stirring bar. The resultant homogeneous solution was degassed under N<sub>2</sub> for 1 h, cooled to approximately 243 K and treated drop-wise with a solution of 1,3,5-triformylbenzene (40 mg, 0.23 mmol) in anhydrous DMF (15 mL). The temperature was maintained at *ca.* 243 K for 1 h during which a dark-brown solid formed. The resultant slurry solution was then left to warm to room temperature overnight, flushed with air for 30 min, and further heated to 403 K in an oven, temperature at which the reaction mixture was kept for 2 days. The solid was then collected by centrifugation at 5,000 rpm





**Scheme 4.1.** Schematic of the procedure followed for the synthesis of BILP-101 and RT-BILP-101.

for 10 min for 2 cycles and subsequently washed with DMF, acetone, water, 1 M HCl, 1 M NaOH, water and acetone. Finally, the product was dried overnight at 393 K under vacuum. RT-BILP-101 was prepared following the same procedure as described for BILP-101, but without the low-temperature treatment, *i.e.*, 1,3,5-triformylbenzene was added to the 1,2,4,5-benzenetetramine tetrahydrochloride solution at room temperature (scheme 4.1).

#### 4.2.3. Preparation of mixed-matrix membranes (MMMs)

To prepare the MMMs, the required amount of BILP-101 (or RT-BILP-101) particles was first dispersed in THF and sonicated for 30 min. To this suspension, 0.2 g dried Matrimid® was added and the casting suspension was further stirred overnight. The solvent/filler-polymer weight ratio was kept at 90/10 in all cases. The amount of BILP-101 in the casting suspension was adjusted to achieve the desired final filler loading of 8 wt.%, 16 wt.% and 24 wt.% in the resulting MMMs.

The prepared suspensions were then casted onto a clean glass plate with the help of a Doctor Blade knife. The cast membranes were immediately covered with a small watch glass to prevent too fast evaporation of the solvent. The glass plate was further covered with a square box and four small vials containing THF to create a saturated THF atmosphere. All these measures were taken to slow down the evaporation rate of THF, thereby preventing the formation of defects during membrane drying. The membranes

were first left to dry overnight at room temperature and then dried under vacuum for 24 h at 423 K.

The pure polymer membranes were prepared following the same procedure as the MMMs, but without the extra step of dispersing BILP-101 or RT-BILP-101 particles. The final thickness of the resulting membranes was the average value of several measurements at various positions evaluated by a digital micrometer (Mitutoyo, IP54 Absolute Digimatic Micrometer, MDQ-30, range 0-30 mm, accuracy  $\pm 0.001$  mm).

#### **4.2.4. BILP fillers and membrane characterization**

Diffuse Reflectance Infrared Fourier transform (DRIFT) spectra of BILP-101 and RT-BILP-101 powder were acquired in a Nicolet 8700 FT-IR (Thermo Scientific) spectrometer equipped with a high-temperature cell with CaF<sub>2</sub> windows (Praying Mantis™). The samples were pretreated in a He flow at 393 K for 5 min prior to collecting the spectra.

One-dimensional <sup>13</sup>C CP/MAS solid state NMR spectra were recorded on a Bruker AVANCE III spectrometer operating at 600 MHz resonance frequencies for <sup>1</sup>H. Experiments at 600 MHz employed a conventional double-resonance 3.2 mm CP/MAS probe or a 2.5 mm double-resonance probe. Dry nitrogen gas was used for sample spinning to prevent degradation. NMR chemical shifts are reported with respect to the external references TMS and adamantane. For <sup>13</sup>C CP/MAS NMR experiments, the following sequence was used: 90° pulse on the proton (pulse length 2.4 s), then a cross-polarization step with contact time of typically 2 ms, and finally acquisition of the <sup>13</sup>C NMR signal under high-power proton decoupling. The delay between the scans was set to 5 s to allow the complete relaxation of the <sup>1</sup>H nuclei, and the number of scans ranged between 10,000 and 20,000. An exponential apodization function corresponding to a line broadening of 80 Hz was applied prior to Fourier transformation. The sample spinning frequency was 15 kHz and 20 KHz.

Powder X-Ray Diffraction (PXRD) patterns of BILP-101 and RT-BILP-101 were recorded using a Bruker-D8 Advanced diffractometer with Co-K<sub>α</sub> radiation ( $\lambda = 1.78897$  Å). The samples were scanned in the  $2\theta$  range of 5 – 80° using a step size of 0.02° and a scan speed of 0.4 s per step in a continuous scanning mode.

Scanning Electron Microscopy (SEM) micrographs were acquired using a JEOL JSM-6010LA InTouchScope microscope equipped with an integrated SDD EDS detector. BILP-101 and RT-BILP-101 particles were directly put on the sample holder and cross-section of the prepared membranes was obtained by cryo-fracturing in liquid nitrogen. All the samples were sputtered with gold for 60 s prior to acquiring SEM micrographs.

N<sub>2</sub> physisorption (77 K) and CO<sub>2</sub> adsorption isotherms (273 K) of BILP-101, RT-BILP-101 and the resulting MMMs were recorded in a Tristar II 3020 (Micromeritics). Argon adsorption isotherm was determined at 87 K (3Flex, Micromeritics). Prior to the gas adsorption measurements, the samples were degassed at 423 K under N<sub>2</sub> flow for 16 h to remove any solvent or moisture trapped in the polymer network. The pore size distribution (PSD) curves of the prepared BILPs fillers and corresponding MMMs were estimated by CO<sub>2</sub>-DFT (Density functional theory) model, using a non-negative regularization method with a factor of 0.03160. The standard deviation of the fit is 0.002057, 0.001954, 0.001904 and 0.002594 mmol·g<sup>-1</sup> for RT-BILP-101, BILP-101, 16 wt.% BILP-101 MMMs and 16 wt.% RT-BILP-101 MMMs, respectively. For the PSD calculation based on Ar adsorption, a Non Local DFT (NLDFT) model was employed with the assumption of cylindrical pores, using a non-negative regularization method with a factor of 0.03160. The standard deviation of the fit is 0.36770 and 0.52406 cm<sup>3</sup>(STP)·g<sup>-1</sup> for BILP-101 and RT-BILP-101, respectively.

Thermogravimetric analysis (TGA) were performed in a Mettler Toledo TGA/SDTA851e apparatus by measuring the mass loss of the sample while heating BILPs and the prepared membranes under air (100 mL·min<sup>-1</sup>) from room temperature to 1073 K at a heating rate of 5 K·min<sup>-1</sup>.

Differential Scanning Calorimetry (DSC) measurements were carried out using a Perkin Elmer DSC 7 equipment to assess the glass transition temperature ( $T_g$ ) of the neat membrane and the MMMs. The scanning range was 298 K – 698 K at a heating rate of 10 K·min<sup>-1</sup> under nitrogen atmosphere. Two consecutive runs were performed. A first DSC cycle was performed to remove thermal history and adsorbed water from the samples. After cooling, a second cycle was performed following the same procedure. The glass transition temperature ( $T_g$ ) value was determined as the middle point of the slope transition in the DSC curve.

#### 4.2.5. Gas permeation experiments

The permeation test is the same as described in Chapter 2 and 3 and was not repeated here. The performance of the membranes was tested for the CO<sub>2</sub> separation from a 15/85 CO<sub>2</sub>/N<sub>2</sub> gas mixture at 308 K. The effect of the absolute feed pressure was investigated between 2 and 5 bar. At least 2-3 membranes were tested for each BILP loading in order to provide reliable error estimations. The aged membranes were first tested at different feed pressures (up to 5 bar) and then at different temperatures, i.e. 308, 323 and 353 K, at 2 bar feed pressure.

### 4.3. RESULTS AND DISCUSSION

#### 4.3.1. Characterization of BILP-101 and RT-BILP-101

BILP-101 particles were synthesized by a condensation reaction following the synthetic route recently developed for BILP.<sup>26, 35, 36</sup> This approach requires the slow addition of aldehyde at low temperatures (243 K) during the initial polymerization stages to control the overall porosity of the final product (*vide supra*). In this work, we synthesized two different POFs: BILP-101 and RT-BILP-101. BILP-101 was obtained following the procedure previously reported by Sekizkardes *et al.*,<sup>35</sup> in which the 1,2,4,5-benzenetetramine tetrahydrochloride solution was cooled to 243 K prior to drop-wise adding the aldehyde-containing solution (see experimental section). Aiming at tuning the polymer porosity, RT-BILP-101 was prepared following the same procedure as described for BILP-101, but at room temperature (Scheme 4.1). This influences the early stages of the condensation reaction, affecting the initial polymerization rate and ultimately affects the porosity of the resulting product.

The DRIFT spectra acquired for BILP-101 and RT-BILP-101 (Fig. 4.1a) indicate the same chemical connectivity for these two polymers and confirmed the imidazole ring formation. Particularly, the bands at 1611 cm<sup>-1</sup> (-C=N-) and 1499 and 1440 cm<sup>-1</sup> (assigned to the skeleton vibration of the imidazole ring)<sup>26, 37</sup> point to the successful imidazole ring closure upon poly-condensation. These observations are further supported by the bands at 1362 cm<sup>-1</sup> (C-N stretching) and 1641 cm<sup>-1</sup> (N-H bending), which confirmed the formation of the

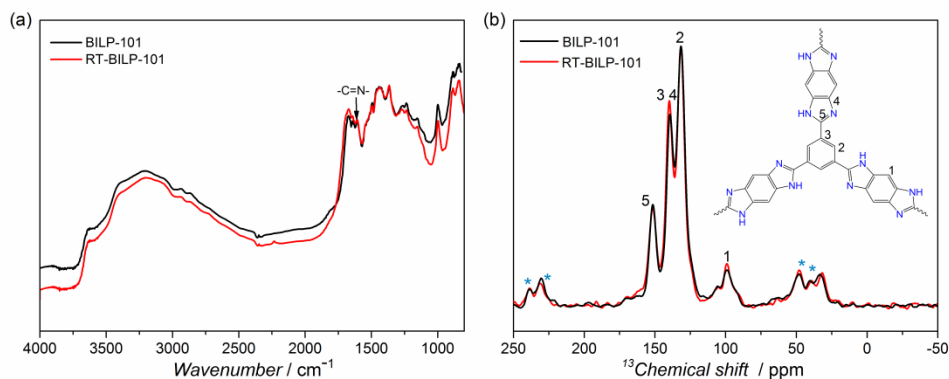


**Fig.4.1.** (a) DRIFT spectra of BILP-101 and RT-BILP-101 acquired at 393 K under He atmosphere and (b) assignments of the  $^{13}\text{C}$  CP-MAS NMR spectra obtained for BILP-101 and RT-BILP-101.

benzimidazole ring. Also, the absence of a band at  $1700\text{ cm}^{-1}$ , which could be ascribed to the residual  $\text{C=O}$  stretching of the aldehyde moieties, points to a complete consumption of the starting aldehyde functional groups. This was corroborated by  $^{13}\text{C}$  CP-MAS NMR spectroscopy. For both materials, BILP-101 and RT-BILP-101, the  $^{13}\text{C}$  CP-MAS NMR spectra show a peak at  $\delta = 151\text{ ppm}$  (Fig. 4.1b), corresponding to the  $\text{N=C-N}$  imidazole carbon.

The thermal stability of BILP-101 and RT-BILP-101 was supported by TGA under air atmosphere. BILP-101 and RT-BILP-101 are stable up to 635 K (Fig. C1), while the initial mass losses, below 373 K, can be attributed to the removal of the adsorbed moisture. Scanning electron microscopy (SEM) micrographs (Figs. 4.3 and 4.4a) reveal the formation of homogenous spherical-shaped particles for both BILP-101 and RT-BILP-101. In the case of RT-BILP-101, however, a decrease in the particle size can be observed compared to BILP-101 (from  $235 \pm 10\text{ nm}$  to  $310 \pm 10\text{ nm}$ , for the former and the latter case, respectively, Fig. 4.2c and d). We relate this to the higher initial reaction rate at room temperature than at 243 K, favouring nucleation and resulting in the observed decrease of particle size. As expected, both BILPs are amorphous as determined by powder X-ray diffraction (Fig. C2).

BILPs' porosity was investigated via  $\text{N}_2$  adsorption acquired at 77 K (Fig. 4.2e). The isotherms exhibit a steep uptake at low relative pressures ( $p/p_0 < 0.1$ ), indicating the microporous nature of the two prepared polymers. The calculated Brunauer-Emmett-

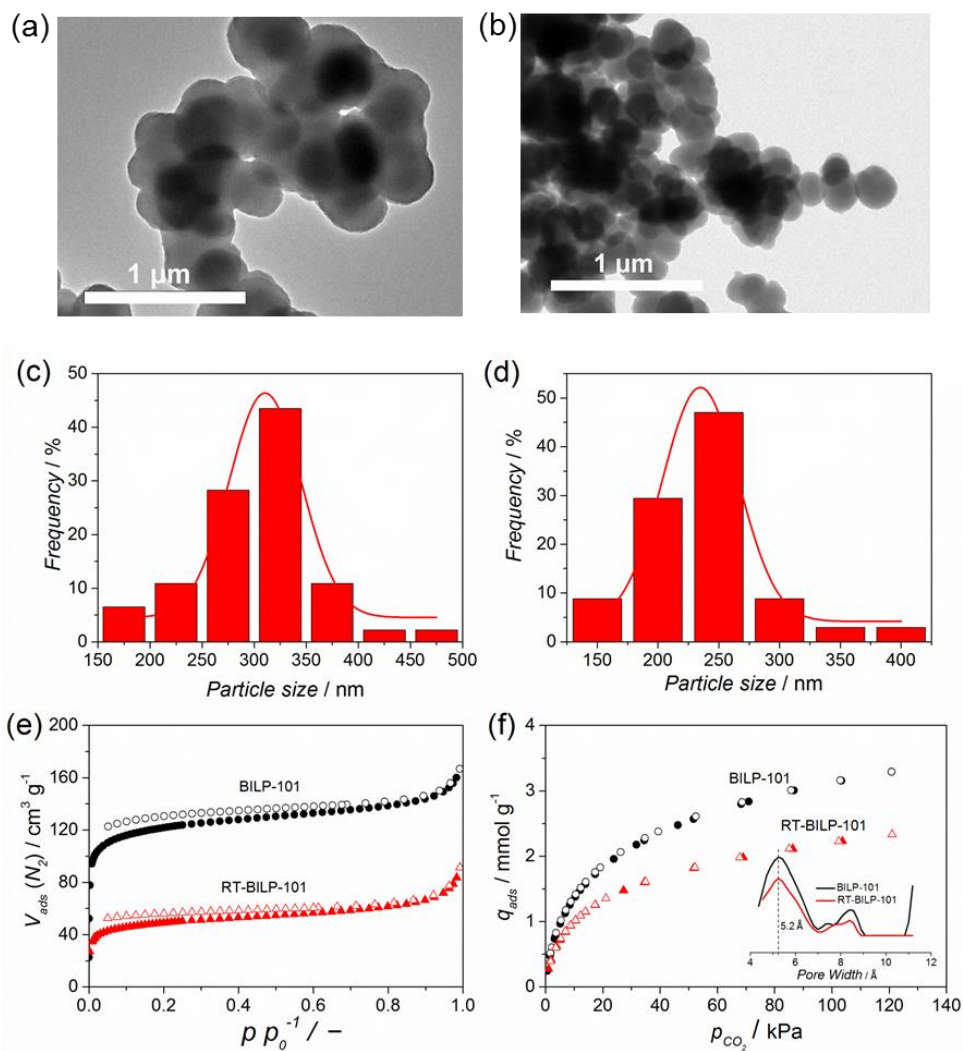


**Fig.4.2.** TEM micrographs (a and b), particle size distribution (c and d) and adsorption/desorption isotherms (e and f) of BILP-101 and RT-BILP-101, respectively. Closed symbols represent the adsorption and open symbols represent the desorption branches. Inset in (f) shows the pore size distribution (PSD) of BILP-101 and RT-BILP-101 calculated from the CO<sub>2</sub> adsorption isotherms.

Teller (BET) surface areas of BILP-101 and RT-BILP-101 are 460 and 180  $\text{m}^2 \cdot \text{g}^{-1}$ , respectively. As expected, BILP-101 possesses a higher BET surface area, which can indeed be ascribed to its slower initial formation rate (*vide supra*), preventing the premature precipitation of oligomers during the initial polymerization stages and allowing for a better

pore formation with an overall enhanced porosity.<sup>38</sup> Furthermore, Fig. 4.2f shows the low-pressure CO<sub>2</sub> adsorption isotherms acquired for BILP-101 and RT-BILP-101 acquired at 273 K. At 1 bar and 273 K, the CO<sub>2</sub> uptake observed for BILP-101 reach up to 3.2 mmol·g<sup>-1</sup>, which is comparable to other POFs<sup>39-42</sup> as well as to other BILPs.<sup>26, 43</sup> RT-BILP-101 on the other hand exhibits relatively lower CO<sub>2</sub> adsorption capacity (2.2 mmol·g<sup>-1</sup>), in line with the N<sub>2</sub> adsorption results. Inset in Fig.4.2f presents the pore size distribution (PSD) curves calculated using CO<sub>2</sub>-density functional theory (CO<sub>2</sub>-DFT) model. Both BILPs show a bimodal pore structure with pores centered around 5.2 Å and a broader range of pores between ca. 7 and 9 Å. BILP-101 presents more open pore volume than RT-BILP-101, being more prone to the penetration of the polymer chains, as discussed below.

Summarizing, two different BILPs were successfully synthesized with the same chemical connectivity, but with different textural properties. This was achieved by tuning the temperature during the early polymerization stages, influencing the initial reaction rate and allowing for a certain degree of control over the overall BILP porosity. In order to further evaluate the potential of these two BILPs for post-combustion CO<sub>2</sub> capture, the adsorption selectivities of CO<sub>2</sub>/N<sub>2</sub> were calculated using the initial slope method. Fig. C4 shows that BILP-101 and RT-BILP-101 have a CO<sub>2</sub>/N<sub>2</sub> selectivity of 89 and 60 at 273 K, respectively. These results are in line with reported values<sup>35</sup> and demonstrate that BILP-101 and RT-BILP-101 are promising fillers for the preparation of MMMs for CO<sub>2</sub>/N<sub>2</sub> separation.

#### **4.3.2. Characterization of BILPs MMMs**

In order to study the influence of the filler porosity on the performance of MMMs in gas separation, MMMs were prepared with both BILP-101 and RT-BILP-101 particles. SEM micrographs of the surface (Fig. C5) and cross-section of the prepared membranes were acquired (Figs. 4.3 and 4.4). The images show that both BILP-101 and RT-BILP-101 are randomly dispersed in the polymer matrix at low weight loading (8 wt.%) and began to undergo slightly aggregation at higher loadings. No evident interfacial voids or pinholes could be observed even at 24 wt.% BILP loading. In addition, both

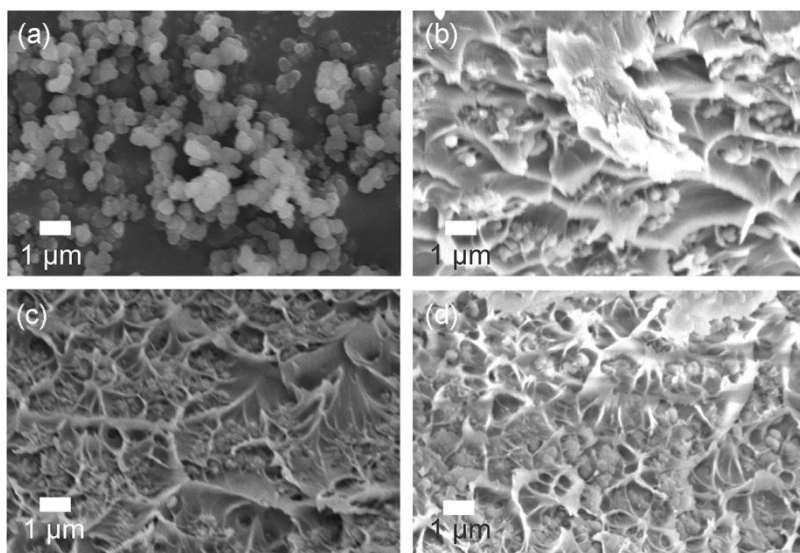


**Fig.4.3.** SEM micrographs of (a) BILP-101 and the cross-section of (b) 8 wt.% BILP-101@Matrimid®, (c) 16 wt.% BILP-101@Matrimid® and (d) 24 wt.% BILP-101@Matrimid®.

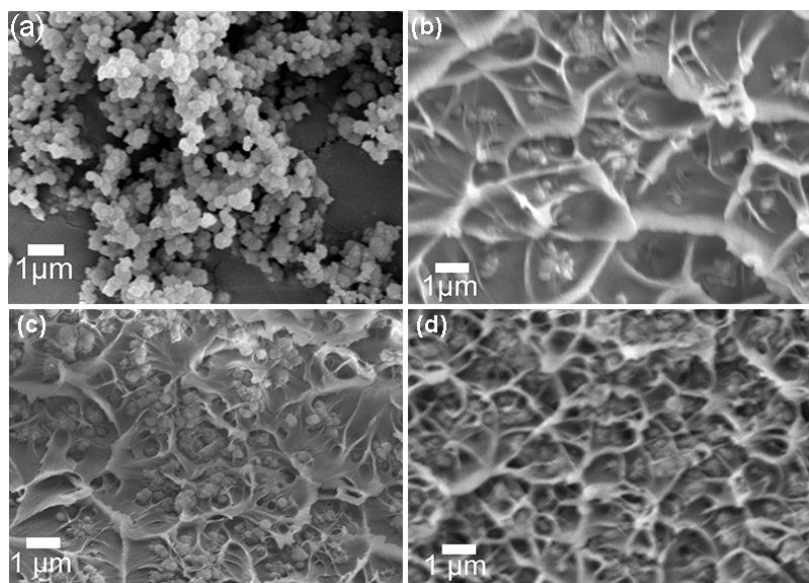


**Fig. 4.4.** SEM micrographs of (a) RT-BILP-101 and the cross-section of (b) 8 wt.% RT-BILP-101@Matrimid®, (c) 16 wt.% RT-BILP-101@Matrimid® and (d) 24 wt.% RT-BILP-101@Matrimid®.



fillers retain their spherical morphology upon membrane preparation. In comparison to BILP-101 MMMs, RT-BILP-101 MMMs exhibit better filler dispersion and a more integrated morphology, where the RT-BILP-101 particles are clearly well embedded in the polymeric matrix. Fig. C6 presents the thermogravimetric analyses acquired for the bare Matrimid® membranes together with those obtained for the BILP-101 and RT-BILP-101-based MMMs. The TGA results of BILP-101 and RT-BILP-101 were also included for comparison. As mentioned above, BILP-101 and RT-BILP-101 were stable up to 635 K, temperature at which it starts decomposing. This decomposition temperature is higher for the pure Matrimid® and the resulting MMMs for which decomposition starts at around 750 K. Further, the absence of weight loss at lower temperatures, for both MMMs and pure membranes, ensures the complete removal of solvents after the selected membrane drying procedure.

DSC and CO<sub>2</sub> adsorption measurements were performed on the MMMs to gain further insight into the filler-polymer interface. DSC results show that the  $T_g$  of all the MMMs are similar to that of bare Matrimid® (~ 594 K), suggesting that there is no significant rigidification of the polymeric chains around the BILP particles, like previously reported results on POF-MMMs.<sup>20, 44</sup> To check whether the BILP pores are still available in the MMMs. CO<sub>2</sub> adsorption isotherms were acquired at 273 K for both bare Matrimid® and the prepared MMMs. The incorporation of BILP-101 and RT-BILP-101 into the polymeric matrix results in an enhanced CO<sub>2</sub> uptake, achieving higher CO<sub>2</sub> uptakes compared to pure Matrimid® in all cases, increasing with filler loading (Fig. 4.5), indicating that the filler pores are still accessible to CO<sub>2</sub> once the BILP particles have been embedded in the polymeric matrix. In addition, the RT-BILP-101 MMMs can reach almost the same CO<sub>2</sub> uptake as BILP-101 MMMs at the same loading. The estimated CO<sub>2</sub> uptake for the 16 wt.% MMMs is calculated as a linear combination of relative uptakes for the pure components and shown in Fig. C7. together with the experimentally measured isotherms for that filler loading. The experimentally obtained CO<sub>2</sub> uptakes are somewhat lower than those calculated for both BILP-101 and RT-BILP-101 MMMs, pointing to a partial pore blockage of BILP-101 and RT-BILP-101 by the polymer chains.<sup>23, 44</sup> Moreover, the difference between the estimated and the experimental CO<sub>2</sub> uptake is larger for BILP-101 MMMs

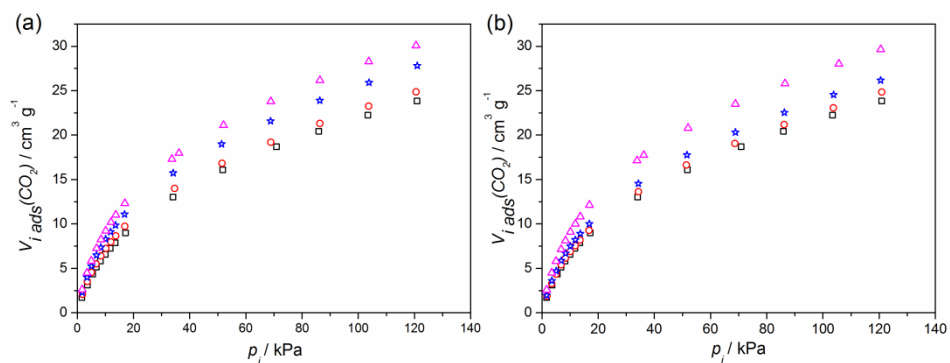


**Fig. 4.5.** CO<sub>2</sub> adsorption isotherms acquired at 273 K for the prepared membranes with (a) BILP-101 and (b) RT-BILP-101.  $\square$  Pure Matrimid<sup>®</sup> and  $\circ$  8 wt.%,  $\star$  16 wt.%, and  $\blacktriangle$  24 wt.% BILP-101 loading MMMs.

(33% porosity loss for BILP-101) than for RT-BILP-101 MMMs (26 % loss), suggesting that the probably bigger porosity of BILP-101 is more easily blocked by the polymer. This is further supported by the pore size distribution curves of the MMMs calculated from the adsorption branch of CO<sub>2</sub> isotherms (Fig. C8). Both, BILP-101 and RT-BILP-101-based MMMs showed a drastic reduction in the pore volume once the filler is embedded in Matrimid<sup>®</sup>, given the dense nature of the latter. Fig. C8b shows however a more pronounced reduction of the pore volume for BILP-101 than for RT-BILP-101 once incorporated in the polymeric matrix. We hypothesize that this, together with a reduction in the size of the bigger pores and in the expected CO<sub>2</sub> uptake (*vide supra*), this points to the partial blockage of the filler pores, which may take place together with a partial collapse of the BILP-101 porous polymer. As already observed for the CO<sub>2</sub> isotherms, this effect is more prominent for BILP-101.

### 4.3.3. Gas separation performance

The performance of Bare Matrimid<sup>®</sup> and MMMs containing different loadings (0, 8, 16 and 24 wt.%) of BILP-101 and RT-BILP-101 particles in the separation of CO<sub>2</sub> from a 15:85 CO<sub>2</sub>/N<sub>2</sub> gas mixture at 308 K and 2 bar absolute feed pressure is presented in Fig. 4.6. The error bars are the standard deviation for testing 2-3 membranes. All the prepared membranes can withstand the permeation test conditions, indicating a good mechanical

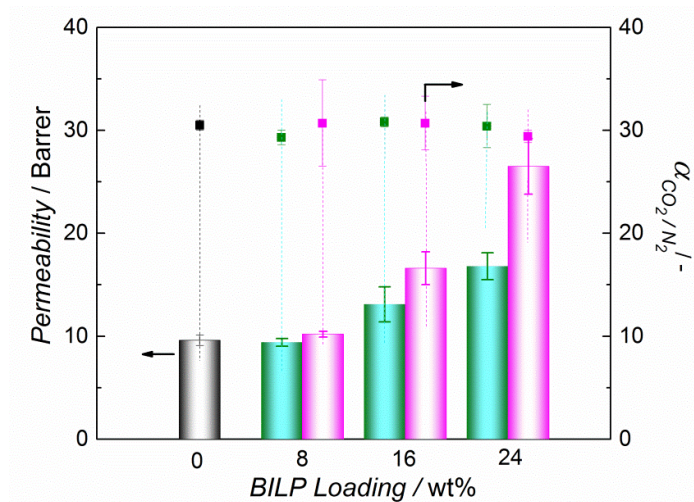


**Fig. 4.6.** Performance of MMMs with different BILP-101 and RT-BILP-101 loadings in the separation of  $CO_2$  from a 15:85  $CO_2/N_2$  mixture at 308 K and an absolute feed pressure of 2 bar. Grey, green and purple colour correspond to the pure Matrimid®, BILP-101 and RT-BILP-101 MMMs, respectively. Error bars correspond to the standard deviation of different membranes.

stability of the membranes under relevant conditions for post-combustion capture. Further, in line with the measured  $T_g$  values, the membranes remain flexible upon 24 % BILP-101 and RT-BILP-101 loading (Fig. C9). Upon addition of both BILP particles, the membranes showed an increase in the  $CO_2$  permeability preserving the original  $CO_2/N_2$  mixed gas selectivities (Fig. 4.6). In this situation, the enhanced  $CO_2$  permeability can be attributed to the incorporation of porous fillers into the polymeric matrix, providing additional transport pathways for the permeating gases.<sup>44</sup> Further, the  $CO_2$  adsorption isotherms of all the prepared membranes were fit on the dual-mode model (see Fig. C10 and Table C1). These results indicate that the incorporation of both BILP fillers lead to the increase of  $K_D$ ,  $C'_H$ , and  $b$  simultaneously. The increase in  $C'_H$  is more significant (~30% increase were achieved for 24 wt.% loading MMMs compared to pure Matrimid®), indicating a higher amount of free volume introduced by the BILP fillers.

It is noteworthy that MMMs fabricated with BILP-101, which possesses a higher BET surface area, showed a lower  $CO_2$  permeability than the RT-BILP-101 MMMs at the same loading. This may originate from the pore blocking by the polymer chains as indicated by

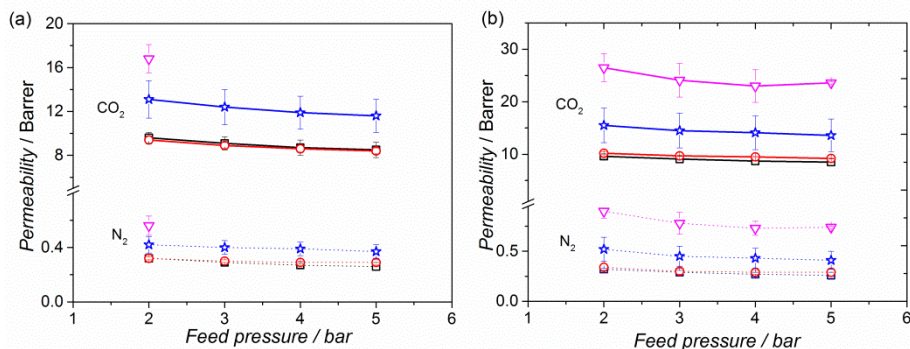


**Fig. 4.7.** Effect of the feed pressure on the gas permeation performance of the prepared (a) BILP-101 and (b) RT-BILP-101 membranes. Results obtained in the separation of CO<sub>2</sub> from a 15:85 CO<sub>2</sub>/N<sub>2</sub> mixture at 308 K. □ Pure Matrimid®, ○ 8 wt.% MMMs, ☆ 16 wt.% MMMs, and ▼ 24 wt.% MMMs.

CO<sub>2</sub> adsorption (Fig. 4.5), being more significant for BILP-101 than RT-BILP-101 due to the big porosity and more open pore volume.

The gas permeability increases with increasing BILP loading, for both BILP-101 and RT-BILP-101, attributed to the additional transport pathways introduced by the incorporation of the filler. Particularly, for the 24 wt.% RT-BILP-101 MMMs, the CO<sub>2</sub> permeability increased by a factor of 2.8 (from 9.6 to 26.5 Barrer) as compared to bare Matrimid® with constant CO<sub>2</sub>/N<sub>2</sub> selectivity.

Fig. 4.7 shows the influence of feed pressure on the gas permeation performance of the membrane. Both the CO<sub>2</sub> and N<sub>2</sub> permeability of the BILP MMMs are higher than the pure Matrimid® over the whole pressure range except for 8 wt.% loading, which performs similar as Matrimid®. The CO<sub>2</sub> permeability decreases with increasing feed pressure. This is a well-known for components adsorbing in the nonlinear pressure range. Saturation of Langmuir adsorption sites in zeolites<sup>45, 46</sup> and glassy polymers<sup>23, 44, 47</sup> at higher pressures results in a decrease in the membrane permeability. For the case of 24 wt.% loading BILP-101 MMMs (see Table C2 for the detailed value), only one low pressure data was included in Fig. 4.7a for clarity. This is due to the presence of small defects, which play a bigger role at high pressures, leading to the fast diffusion of N<sub>2</sub> and thereby decreasing the CO<sub>2</sub>/N<sub>2</sub> selectivity significantly.

To gain further insight into the long-term membrane performance, 16 wt.% loading MMMs (BILP-101 and RT-BILP-101) were re-tested after 4 months (Table C4), indicating that the separation performance was maintained. As expected, a slight decrease in the membrane permeability was observed, from 17 to 15 Barrer and from 13 to 11 Barrer for RT-BILP-101 and BILP-101-based MMMs, respectively, while keeping a relatively constant selectivity. This decrease in permeability is related to a decrease in the excess free volume of glassy polymers after physical aging.

Considering the practical post-combustion CO<sub>2</sub> capture process, the flue gas needs to be reheated to prevent corrosion problems caused by water vapour condensation in the stack<sup>48</sup>. Thus, the effect of temperature (308 – 358 K) on gas separation performance was further investigated to better understand the actual performance of BILP MMMs in real industrial applications. The gas permeability increases with increasing temperature while this is accompanied by a decrease in the CO<sub>2</sub>/N<sub>2</sub> selectivity for both BILP MMMs (Table C5). To better understand this, Arrhenius equation was applied to calculate the activation energy ( $E_p$ ) for permeation (Fig. 4.8).

$$P_i = P_{i,0} \exp\left(\frac{-E_{p,i}}{RT}\right) \quad (4)$$

Where  $E_{p,i}$ ,  $P_i$  and  $P_{i,0}$  represent the activation energy, the gas permeability and the pre-exponential factor of a gas component  $i$ , respectively,  $T$  is the absolute temperature and  $R$  is the ideal gas constant. Similarly to zeolite membranes<sup>49</sup>, the activation energy,  $E_p$ , is determined by two principle factors: the penetrants molecular size, which affects diffusivity, and the interaction with the polymer matrix, related to the penetrants' solubility and is given by the following equation:

$$E_p = E_d + \Delta H_s \quad (5)$$

Where  $E_d$  is the required energy for diffusion and increases with the penetrants' molecular size, being positive for a diffusion activated processes, and  $\Delta H_s$  is the heat of adsorption, being more negative for more soluble gases. An increase of temperature therefore results in two counteractive effects: on the one hand side, the gas solubility decreases, being this effect more pronounced for the more soluble gas, *i.e.* CO<sub>2</sub>; on the other hand, the diffusivity increases, being this enhancement larger for the penetrant with the higher

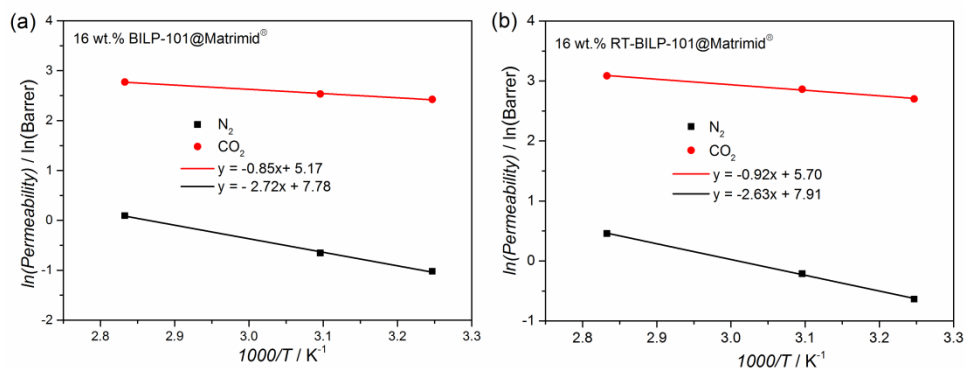


**Fig. 4.8.** Effect of operating temperature on CO<sub>2</sub> and N<sub>2</sub> permeability of aged (a) 16 wt% BILP-101 and (b) RT-BILP-101@Matrimid® at 2 feed bar pressure (solid lines represent the Arrhenius plot).

**Table 4.1.** Activation energies for the permeation of CO<sub>2</sub> and N<sub>2</sub> in aged 16 wt.% BILP MMMs at 2 bar feed pressure.

Membrane	$E_p$ (kJ mol <sup>-1</sup> )	
	CO <sub>2</sub>	N <sub>2</sub>
Aged 16 wt.% BILP-101 MMMs @ Matrimid®	7.1	22.6
Aged 16 wt.% RT-BILP-101 @ Matrimid®	7.7	21.9

molecular size, *i.e.* N<sub>2</sub>. This increase in diffusivity is related to a positive  $E_d$ , implying a diffusion activated processes, together with a higher mobility of the polymer segmental chains<sup>50, 51</sup>. Overall, the diffusivity increase dominates, resulting in an enhanced permeability for both, CO<sub>2</sub> and N<sub>2</sub>. This permeability increase is higher for N<sub>2</sub>, leading to a decrease in the resultant permselectivity (Table C5). This is in line with the calculated  $E_p$  activation energy values (Table 4.1): the positive values results into an increase of the gas permeability with temperature, this enhancement being larger for the penetrant with a higher  $E_p$ , *i.e.* N<sub>2</sub>.

Finally, the separation performance of BILP-101 and RT-BILP-101-based MMMs were compared with the Robeson upper bound together with the performance of other reported POF-containing MMMs (Fig. 4. 9 and Table C6). The performance of the MMMs prepared in this study is located in the same region as the membranes reported with other POF fillers, such as ACOF-1 or BILP-4. Although a significant increase in CO<sub>2</sub> permeability was achieved by incorporating RT-BILP-101 fillers in Matrimid®, the overall

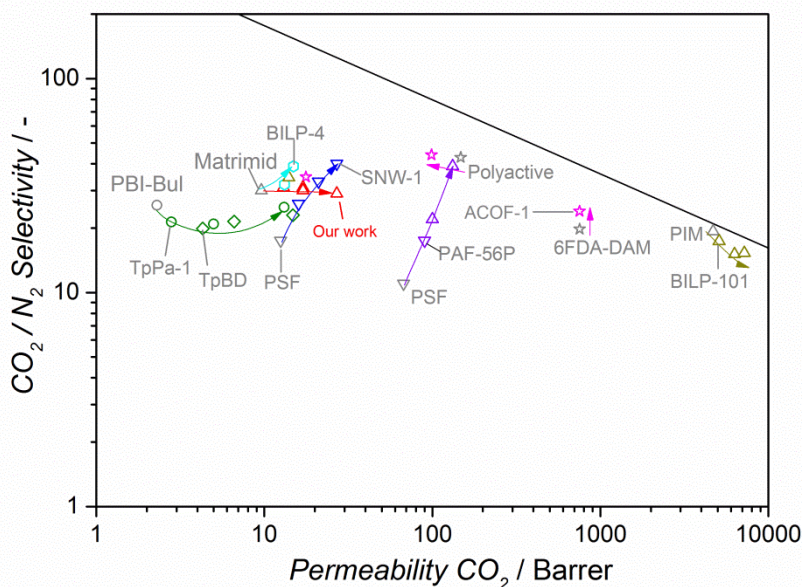


**Fig. 4.9.** Robeson plot for CO<sub>2</sub>/N<sub>2</sub> separation, showing the gas separation performance of the prepared BILPs-based MMMs (represented by red triangles and corresponding to 16 and 24 wt% filler loading). Most relevant results reported in literature for POF-based MMMs are also included for comparison. The black line corresponds to the 2008 Robeson bound line and the arrows indicate the trend of separation performance from pure polymer to POF based MMMs.

performance still stays below the upper bound limit due to the low permeability of pure Matrimid®. Our results are therefore in line with other POF-based MMMs prepared with low permeable polymers, for which by adding the filler the gas permeability can be typically increased while scarifying or maintaining the selectivity.

#### 4.4. CONCLUSIONS

Porous BILPs with different porosities (BILP-101 and RT-BILP-101) were prepared and dispersed in Matrimid® to prepare MMMs. Their structures and performance were compared in this study. Through controlling the initial polymerization rate, RT-BILP-101 with lower porosity than BILP-101 was synthesized. DRIFTS and <sup>13</sup>C CP-CMS NMR measurements confirms the same chemical connectivity of the two BILPs. In the MMMs, a good dispersion and adhesion between the fillers and the polymer matrix was obtained.

No rigidification was observed for the polymer chains after incorporating both BILPs. The incorporation of both BILPs into Matrimid® enhanced the gas permeability for both CO<sub>2</sub> and N<sub>2</sub>, while keeping the mixed gas selectivity constant. The permeability increases with increasing the filler loading attributed to the fast diffusion pathways introduced by the porous BILP network, while the polymer still controls the selectivity. Besides, MMMs fabricated with RT-BILP-101 exhibits higher gas permeability than BILP-101 MMMs at the same loading, due to the lower partial pore blockage of the filler porosity by the polymer in the MMMs.

Overall, our results demonstrate that the porosity of the filler has an impact on the MMM's permeation performance and should be helpful for the design of POF-based MMMs, especially considering the relatively large POF pores for gas separation.



### REFERENCES

- 1 Y.-S. Bae and R. Q. Snurr, *Angewandte Chemie International Edition*, 2011, **50**, 11586.
- 2 L. M. Robeson, *Journal of Membrane Science*, 2008, **320**, 390.
- 3 H. B. Park, J. Kamcev, L. M. Robeson, M. Elimelech and B. D. Freeman, *Science*, 2017, **356**, eaab0530.
- 4 A. Bos, I. Pünt, H. Strathmann and M. Wessling, *AIChE Journal*, 2001, **47**, 1088.
- 5 X. Y. Chen, V.-T. Hoang, D. Rodrigue and S. Kaliaguine, *RSC Advances*, 2013, **3**, 24266.
- 6 S. H. Han, J. E. Lee, K.-J. Lee, H. B. Park and Y. M. Lee, *Journal of Membrane Science*, 2010, **357**, 143.
- 7 P. Gorgojo, S. Karan, H. C. Wong, M. F. Jimenez-Solomon, J. T. Cabral and A. G. Livingston, *Advanced Functional Materials*, 2014, **24**, 4729.
- 8 M. Carta, R. Malpass-Evans, M. Croad, Y. Rogan, J. C. Jansen, P. Bernardo, F. Bazzarelli and N. B. McKeown, *Science*, 2013, **339**, 303.
- 9 I. Kiesow, D. Marczewski, L. Reinhardt, M. Mühlmann, M. Possiwan and W. A. Goedel, *Journal of the American Chemical Society*, 2013, **135**, 4380.
- 10 T. W. Pechar, S. Kim, B. Vaughan, E. Marand, M. Tsapatsis, H. K. Jeong and C. J. Cornelius, *Journal of Membrane Science*, 2006, **277**, 195.
- 11 T. Rodenas, M. van Dalen, E. García-Pérez, P. Serra-Crespo, B. Zornoza, F. Kapteijn and J. Gascon, *Advanced Functional Materials*, 2014, **24**, 249.
- 12 T. Rodenas, I. Luz, G. Prieto, B. Seoane, H. Miro, A. Corma, F. Kapteijn, F. X. Llabrés i Xamena and J. Gascon, *Nature Materials*, 2015, **14**, 48.
- 13 L. Zou, Y. Sun, S. Che, X. Yang, X. Wang, M. Bosch, Q. Wang, H. Li, M. Smith, S. Yuan, Z. Perry and H. C. Zhou, *Advanced Materials*, 2017, **29**, 1700229.
- 14 X. Feng, X. Ding and D. Jiang, *Chemical Society Reviews*, 2012, **41**, 6010.
- 15 S.-Y. Ding and W. Wang, *Chemical Society Reviews*, 2013, **42**, 548.
- 16 Y. Xu, S. Jin, H. Xu, A. Nagai and D. Jiang, *Chemical Society Reviews*, 2013, **42**, 8012.
- 17 H. Ma, H. Ren, X. Zou, S. Meng, F. Sun and G. Zhu, *Polymer Chemistry*, 2014, **5**, 144.
- 18 A. Bhunia, I. Boldog, A. Moller and C. Janiak, *Journal of Materials Chemistry A*, 2013, **1**, 14990.
- 19 X. Wu, Z. Tian, S. Wang, D. Peng, L. Yang, Y. Wu, Q. Xin, H. Wu and Z. Jiang, *Journal of Membrane Science*, 2017, **528**, 273.
- 20 T. D. M. Tessema, S. R. Venna, G. Dahe, D. P. Hopkinson, H. M. El-Kaderi and A. K. Sekizkardes, *Journal of Membrane Science*, 2018, **554**, 90.

- 21 C. Zou, Q. Li, Y. Hua, B. Zhou, J. Duan and W. Jin, *ACS Applied Materials & Interfaces*, 2017, **9**, 29093.
- 22 L. Meng, X. Zou, S. Guo, H. Ma, Y. Zhao and G. Zhu, *ACS Applied Materials & Interfaces*, 2015, **7**, 15561-15569.
- 23 M. Shan, B. Seoane, E. Rozhko, A. Dikhtiarenko, G. Clet, F. Kapteijn and J. Gascon, *Chemistry-A European Journal*, 2016, **22**, 14467.
- 24 M. G. Rabbani and H. M. El-Kaderi, *Chemistry of Materials*, 2011, **23**, 1650.
- 25 C. Klumpen, F. Radakovitsch, A. Jess and J. Senker, *Molecules*, 2017, **22**, 1343.
- 26 M. G. Rabbani and H. M. El-Kaderi, *Chemistry of Materials*, 2012, **24**, 1511.
- 27 A. K. Sekizkardes, V. A. Kusuma, G. Dahe, E. A. Roth, L. J. Hill, A. Marti, M. Macala, S. R. Venna and D. Hopkinson, *Chemical Communications*, 2016, **52**, 11768.
- 28 L. Zou, Y. Sun, S. Che, X. Yang, X. Wang, M. Bosch, Q. Wang, H. Li, M. Smith, S. Yuan, Z. Perry and H.-C. Zhou, *Advanced Materials*, 2017, **29**, 1700229.
- 29 X. Zou and G. Zhu, *Advanced Materials*, 2018, **30**, 1700750.
- 30 L. Ge, W. Zhou, V. Rudolph and Z. Zhu, *Journal of Materials Chemistry A*, 2013, **1**, 6350.
- 31 J. Dechnik, J. Gascon, C. Doonan, C. Janiak and C. J. Sumby, *Angewandte Chemie International Edition*, 2017, **129**, 9420.
- 32 J. Sánchez-Laínez, B. Zornoza, S. Friebe, J. Caro, S. Cao, A. Sabetghadam, B. Seoane, J. Gascon, F. Kapteijn, C. Le Guillouzer, G. Clet, M. Daturi, C. Téllez and J. Coronas, *Journal of Membrane Science*, 2016, **515**, 45.
- 33 A. Sabetghadam, B. Seoane, D. Keskin, N. Duim, T. Rodenas, S. Shahid, S. Sorribas, C. L. Guillouzer, G. Clet and C. Tellez, *Advanced Functional Materials*, 2016, **26**, 3154.
- 34 M. W. Anjum, F. Vermoortele, A. L. Khan, B. Bueken, D. E. De Vos and I. F. J. Vankelecom, *ACS Applied Materials & Interfaces*, 2015, **7**, 25193.
- 35 A. K. Sekizkardes, J. T. Culp, T. Islamoglu, A. Marti, D. Hopkinson, C. Myers, H. M. El-Kaderi and H. B. Nulwala, *Chemical Communications*, 2015, **51**, 13393.
- 36 S. Altarawneh, T. İslamoğlu, A. K. Sekizkardes and H. M. El-Kaderi, *Environmental Science & Technology*, 2015, **49**, 4715.
- 37 P. Totsatitpaisan, S. P. Nunes, K. Tashiro and S. Chirachanchai, *Solid State Ionics*, 2009, **180**, 738.
- 38 P. Pandey, A. P. Katsoulidis, I. Eryazici, Y. Wu, M. G. Kanatzidis and S. T. Nguyen, *Chemistry of Materials*, 2010, **22**, 4974.

- 39 H. Furukawa and O. M. Yaghi, *Journal of the American Chemical Society*, 2009, **131**, 8875.
- 40 M. Zhang, Z. Perry, J. Park and H.-C. Zhou, *Polymer*, 2014, **55**, 335.
- 41 T. Ben, C. Pei, D. Zhang, J. Xu, F. Deng, X. Jing and S. Qiu, *Energy & Environmental Science*, 2011, **4**, 3991.
- 42 R. Dawson, D. J. Adams and A. I. Cooper, *Chemical Science*, 2011, **2**, 1173.
- 43 A. K. Sekizkardes, T. Islamoglu, Z. Kahveci and H. M. El-Kaderi, *Journal of Materials Chemistry A*, 2014, **2**, 12492.
- 44 M. Shan, B. Seoane, E. Andres-Garcia, F. Kapteijn and J. Gascon, *Journal of Membrane Science*, 2018, **549**, 377.
- 45 J. M. van de Graaf, F. Kapteijn and J. A. Moulijn, *Journal of Membrane Science*, 1998, **144**, 87.
- 46 J.M.v.d. Graaf, F. Kapteijn, J.A. Moulijn, in: J. A. Moulijn, A. Cybulski (Eds.), *Structured catalysts and reactors*, Marcel Dekker, New York, 1998, pp. 543–574.
- 47 T. Li, Y. Pan, K.-V. Peinemann and Z. Lai, *Journal of Membrane Science*, 2013, **425–426**, 235.
- 48 H. Z. Chen, Z. Thong, P. Li and T.-S. Chung, *International Journal of Hydrogen Energy*, 2014, **39**, 5043.
- 49 K. Freek, v. d. G. J. M. and M. J. A., *AIChE Journal*, 2000, **46**, 1096.
- 50 A. L. Khan, X. Li and I. F. J. Vankelecom, *Journal of Membrane Science*, 2011, **380**, 55.
- 51 A. Ebadi Amooghin, M. Omidkhah and A. Kargari, *RSC Advances*, 2015, **5**, 8552.

## APPENDIX C

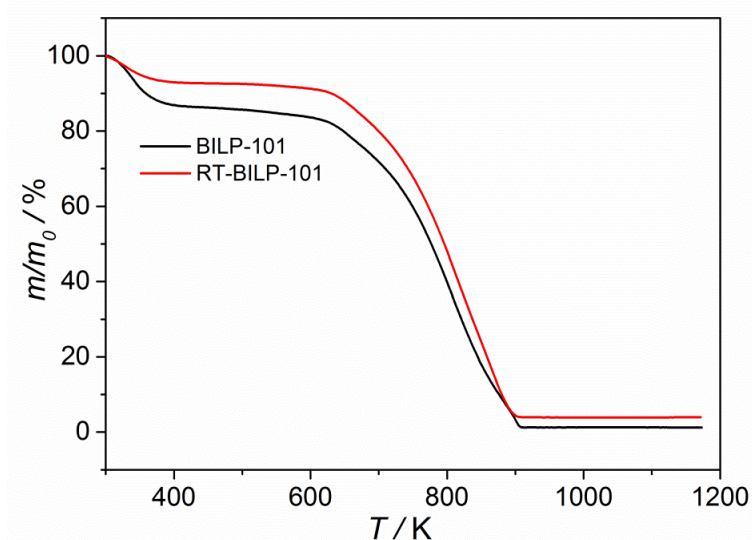


Fig. C1. TGA results of BILP-101 and RT-BILP-101 under air flow obtained at a heating rate of 5 K·min<sup>-1</sup>.

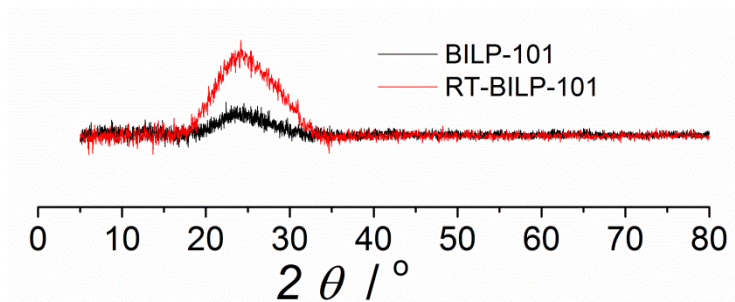
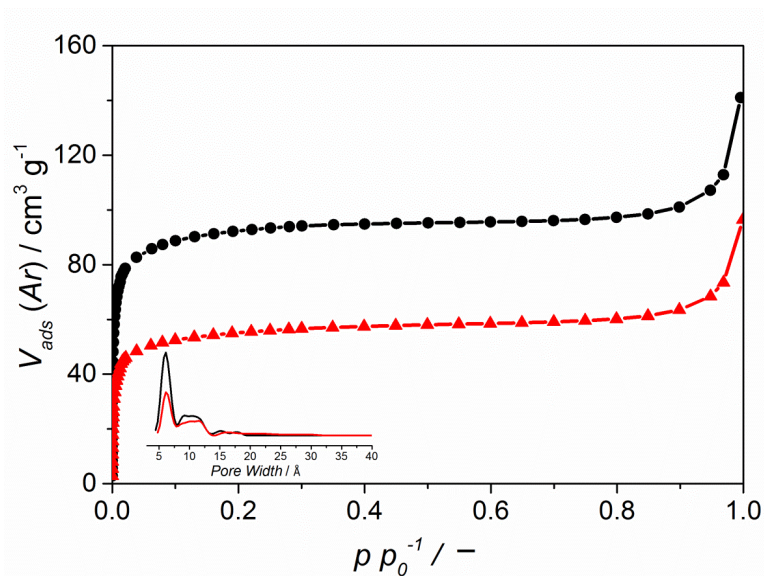
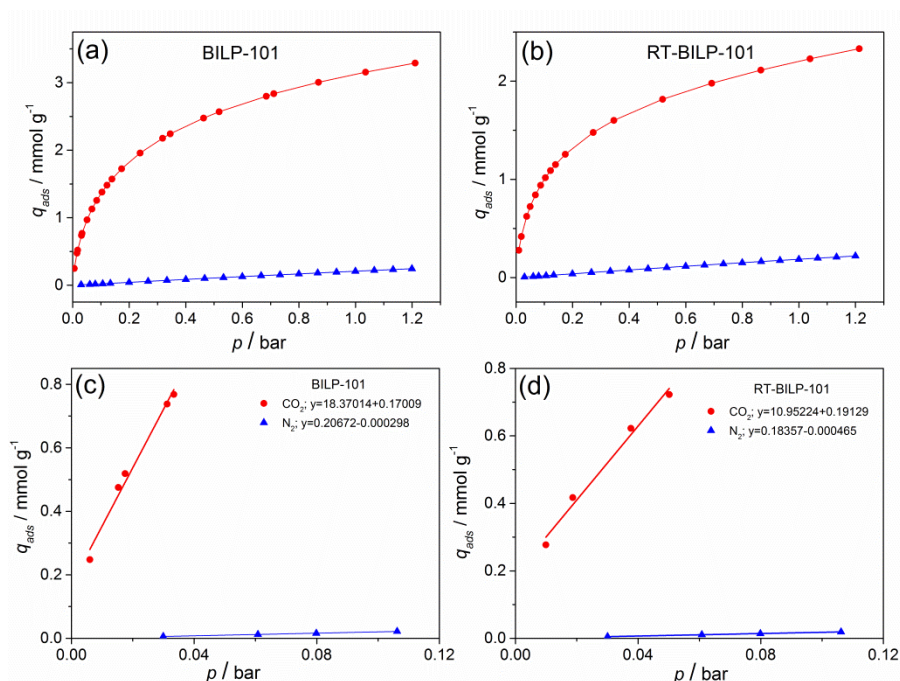


Fig. C2. PXRD patterns of BILP-101 and RT-BILP-101.



**Fig. C3.** Ar adsorption isotherms of BILP-101 (*black*) and RT-BILP-101 (*red*) at 87 K. Inset shows the corresponding PSD curves calculated from the adsorption branch.

Fig. C3 shows the pore size distribution curves calculated from Ar isotherms acquired at 87 K to further validate the pore structure calculated from  $\text{CO}_2$ . The non-polar nature of Ar hampers possible interactions with the porous framework and thus, may provide a more accurate calculation of the PSD curves. As it can be seen, the pore structure shows a similar qualitative trend, with a bimodal pore size distribution possessing a relatively narrow distribution of ultra-micropores and a broader range of bigger pores (8 – 12.5 Å).



**Fig. C4.** CO<sub>2</sub> and N<sub>2</sub> adsorption isotherms of BILP fillers and the corresponding CO<sub>2</sub>/N<sub>2</sub> adsorption selectivity using initial slope calculation method.

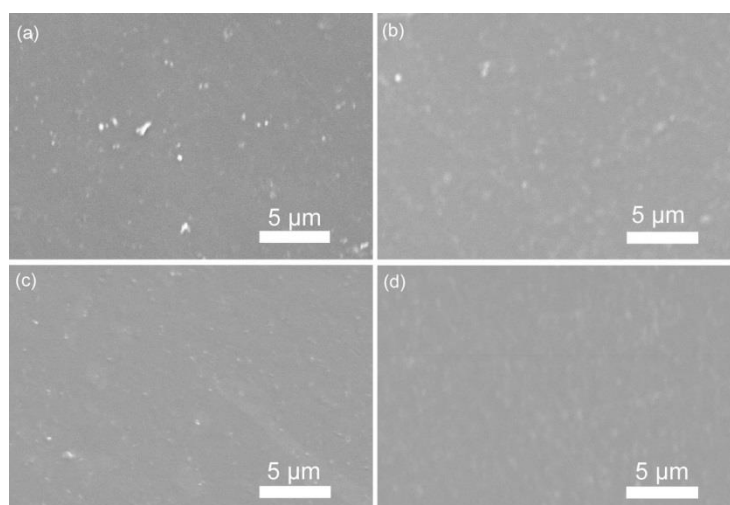


**Fig. C5.** SEM micrographs of the surface of (a) 16 wt.% BILP-101@Matrimid®, (b) 16 wt.% BILP-RT-101@Matrimid®, (c) 24 wt.% BILP-101@Matrimid® and (d) 24 wt.% BILP-RT-101@Matrimid®.

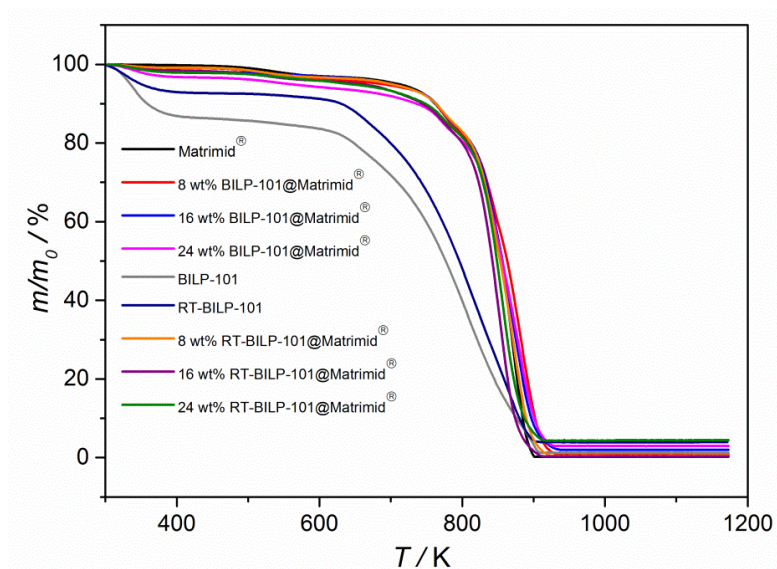


**Fig. C6.** TGA results for BILP and BILP-based MMMs under air flow at a heating rate of 5 K·min<sup>-1</sup>.

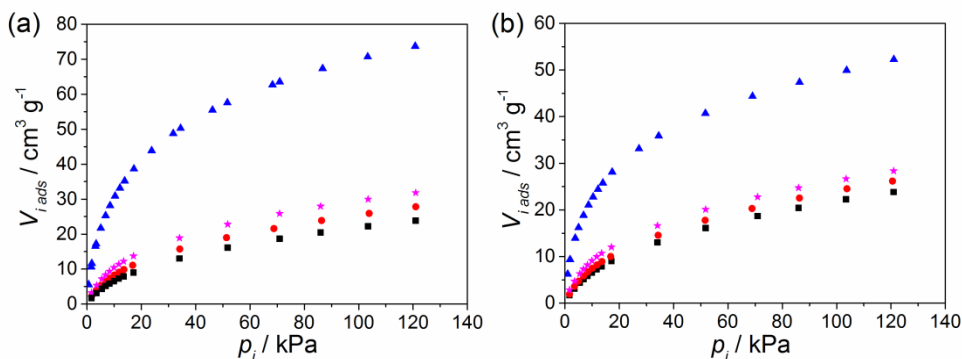


**Fig. C7.** CO<sub>2</sub> adsorption isotherms acquired for (a) BILP-101 and (b) RT-BILP-101 and the prepared membranes at 273 K. ★ Calculated 16 wt.% BILP@MMMs, ● Experimental 16 wt.% BILP@MMMs, ▲ BILP fillers and ■ Matrimid®. The calculated value was obtained by a linear combination of those uptakes for the pure components.

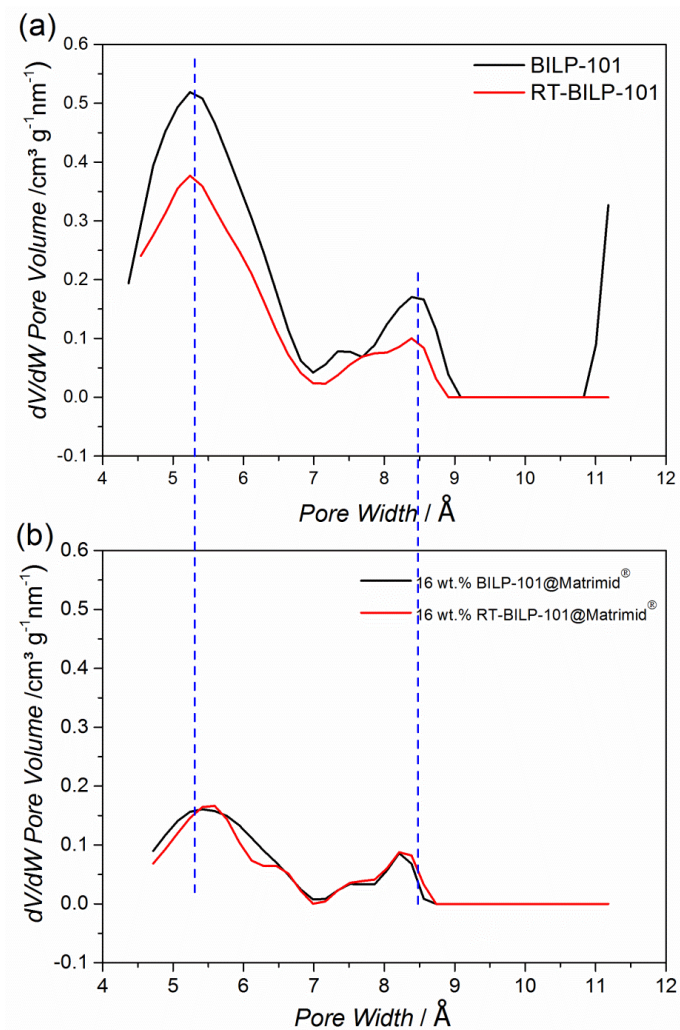


**Fig. C8.** Pore size distribution (PSD) curve of (a) BILP fillers and (b) 16 wt.% loading MMMs calculated from their CO<sub>2</sub> adsorption isotherms at 273 K.



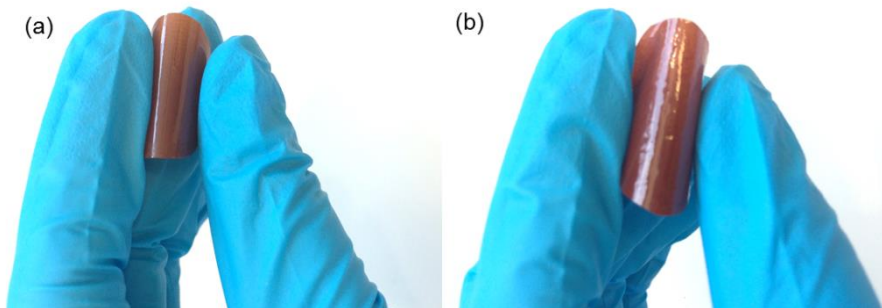


**Fig. C9.** Flexible (a) 24 wt.% BILP-101@Matrimid® and (b) 24 wt.% RT-BILP-101@Matrimid® membranes with a thickness of *ca.* 40  $\mu\text{m}$ .

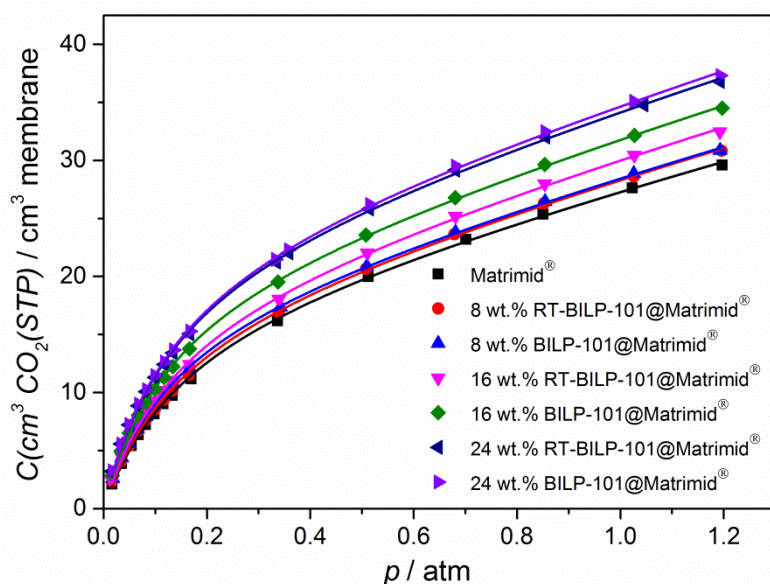


**Fig. C10.**  $\text{CO}_2$  adsorption isotherms acquired at 273 K for the prepared membranes. Solid lines correspond to the fit dual-model sorption model.

The  $\text{CO}_2$  adsorption isotherms of the prepared membranes were fit on the dual-mode model, as described in the following equation.

$$C = K_D p + \frac{C'_H b p}{(1 + b p)}$$

Where  $K_D$  is the Henry's law coefficient indicating the ability of gas molecules to be dissolved in the polymer matrix at equilibrium,  $C'_H$  is the Langmuir capacity constant, which is usually used to evaluate the non-equilibrium excess free volume in the glassy

state and  $b$  is the Langmuir affinity constant, representing the sorption ability for a particular gas-polymer<sup>1, 2</sup>. Table C1 summarizes the dual-model sorption coefficients.

**Table C1.** Dual-model sorption coefficients of the prepared membranes.

Membrane	$K_D$ (cm <sup>3</sup> (STP)/cm <sup>3</sup> · atm)	$C'_H$ (cm <sup>3</sup> (STP)/cm <sup>3</sup> )	$b$ (atm <sup>-1</sup> )
Matrimid®	11.3	18.5	6.3
8 wt.% RT-BILP-101@Matrimid®	12.1	18.6	6.6
8 wt.% BILP-101@Matrimid®	12.0	18.7	7.2
16 wt.% RT-BILP-101@Matrimid®	12.5	20.1	6.8
16 wt.% BILP-101@Matrimid®	12.9	21.4	7.4
24wt.% RT-BILP-101@Matrimid®	13.0	24.0	7.3
24wt.% BILP-101@Matrimid®	13.2	24.4	7.2

**Table C2.** Glass transition temperature ( $T_g$ ) of different membranes.

Membrane	$T_g$ / K
Bare Matrimid®	594
8 wt.% BILP-101@Matrimid®	593.3
16 wt.% BILP-101@Matrimid®	594.7
24 wt.% BILP-101@Matrimid®	594.2
8 wt.% RT-BILP-101@Matrimid®	593.5
16 wt.% RT-BILP-101@Matrimid®	594.0
24 wt.% RT-BILP-101@Matrimid®	593.9

**Table C3** Summary of the membrane performance data for the CO<sub>2</sub> separation from a 15:85 CO<sub>2</sub>/N<sub>2</sub> mixture at 308 K. The data were obtained for different membranes under several operation pressure conditions. Each loading of the membrane was measured at least 2-3 times. Error is given as the standard deviation from the independent tests of different membranes. Permeate side at atmospheric pressure with helium as sweep gas.

Membrane		Matrimid®			
Membrane thickness		39 ± 5 µm			
Feed pressure [bar]	2	3	4	5	
$PCO_2$ [Barrer]	9.6 ± 0.5	9.1 ± 0.6	8.7 ± 0.7	8.5 ± 0.7	
$PN_2$ [Barrer]	0.32 ± 0.01	0.29 ± 0.02	0.27 ± 0.02	0.26 ± 0.03	
Selectivity [-]	30 ± 1	31 ± 2	32 ± 2	33 ± 2	

Membrane		8 wt.% RT-BILP-101 / Matrimid®			
Membrane thickness		45 ± 5 µm			
Feed pressure [bar]	2	3	4	5	
$PCO_2$ [Barrer]	10 ± 0.3	9.7 ± 0.07	9.5 ± 0.07	9.2 ± 0.07	
$PN_2$ [Barrer]	0.34 ± 0.06	0.30 ± 0.03	0.29 ± 0.02	0.29 ± 0.04	
Selectivity [-]	31 ± 4	33 ± 3	33 ± 3	33 ± 4	

## Chapter 4

Membrane	16 wt.% RT-BILP-101 / Matrimid®			
Membrane thickness	42 ± 7 µm			
Feed pressure [bar]	2	3	4	5
$PCO_2$ [Barrer]	17 ± 2	16 ± 2	15 ± 2	15 ± 2
$PN_2$ [Barrer]	0.55 ± 0.09	0.48 ± 0.07	0.46 ± 0.06	0.44 ± 0.06
Selectivity [-]	31 ± 3	33 ± 3	33 ± 2	33 ± 3

Membrane	24 wt.% RT-BILP-101 / Matrimid®			
Membrane thickness	53 ± 3 µm			
Feed pressure [bar]	2	3	4	5
$PCO_2$ [Barrer]	27 ± 3	24 ± 3	23 ± 3	23.6 ± 0.2
$PN_2$ [Barrer]	0.90 ± 0.07	0.78 ± 0.1	0.73 ± 0.07	0.74 ± 0.01
Selectivity [-]	29 ± 0.6	31 ± 0.6	32 ± 1	32 ± 0.6

Membrane	8 wt.% BILP-101 / Matrimid®			
Membrane thickness	35 ± 3 µm			
Feed pressure [bar]	2	3	4	5
$PCO_2$ [Barrer]	9.4 ± 0.4	8.9 ± 0.3	8.6 ± 0.4	8.4 ± 0.3
$PN_2$ [Barrer]	0.32 ± 0.01	0.3 ± 0.01	0.29 ± 0.01	0.29 ± 0.02
Selectivity [-]	29 ± 0.7	30 ± 0.3	31 ± 0.2	30 ± 0.07

Membrane	16 wt.% BILP-101 / Matrimid®			
Membrane thickness	40 ± 2 µm			
Feed pressure [bar]	2	3	4	5
PCO <sub>2</sub> [Barrer]	13 ± 2	12 ± 2	12 ± 2	12 ± 2
PN <sub>2</sub> [Barrer]	0.42 ± 0.06	0.4 ± 0.05	0.39 ± 0.05	0.37 ± 0.05
Selectivity [-]	31 ± 0.5	31 ± 0.7	31 ± 0.3	32 ± 0.4

Membrane	24 wt.% BILP-101 / Matrimid®			
Membrane thickness	46 ± 3 µm			
Feed pressure [bar]	2	3	4	5
PCO <sub>2</sub> [Barrer]	17 ± 1	17 ± 0.4	17 ± 0.7	17 ± 1
PN <sub>2</sub> [Barrer]	0.56 ± 0.07	1.3 ± 1	2.0 ± 1	2.4 ± 2
Selectivity [-]	30 ± 2	19 ± 13	16 ± 14	15 ± 15

Table C4. Membrane performance of a 4 month-aged 16 wt.% BILP-101 and RT-BILP-101@Matrimid<sup>®</sup> MMMs. Membranes were tested for the CO<sub>2</sub> separation from a 15:85 CO<sub>2</sub>/N<sub>2</sub> mixture at 308 K. Error is given as the standard deviation from the 7 independent measurements of GC.

Membrane	Aged 16 wt.% RT-BILP-101@Matrimid <sup>®</sup>			
Membrane thickness	42 ± 0.3 μm			
Feed pressure [bar]	2	3	4	5
PCO <sub>2</sub> [Barrer]	15 ± 0.3	14 ± 0.1	14 ± 0.1	13 ± 0.07
PN <sub>2</sub> [Barrer]	0.53 ± 0.01	0.47 ± 0.01	0.46 ± 0.01	0.46 ± 0.01
Selectivity [-]	28 ± 0.7	30 ± 0.5	30 ± 0.7	29 ± 0.5

Membrane	Aged 16 wt.% BILP-101@Matrimid <sup>®</sup>			
Membrane thickness	40 ± 0.7 μm			
Feed pressure [bar]	2	3	4	5
PCO <sub>2</sub> [Barrer]	11 ± 0.2	11 ± 0.05	10 ± 0.05	10 ± 0.1
PN <sub>2</sub> [Barrer]	0.36 ± 0.01	0.34 ± 0.01	0.33 ± 0.01	0.32 ± 0.00
Selectivity [-]	31 ± 0.7	31 ± 0.4	32 ± 0.7	32 ± 0.6

**Table C5.** Membrane performance of the 4 month-aged 16 wt.% BILP-101 and RT-BILP-101@Matrimid® MMMs. Membranes were tested for the CO<sub>2</sub> separation from a 15:85 CO<sub>2</sub>/N<sub>2</sub> mixture under different temperatures and at a feed pressure of 2 bar. Error is given as the standard deviation from the 7 independent measurements of GC.

Membrane	Aged 16 wt.% RT-BILP-101@Matrimid®		
Membrane thickness	42 ± 0.3 µm		
Temperature [K]	308	323	353
<i>PCO<sub>2</sub></i> [Barrer]	15 ± 0.3	18 ± 0.2	22 ± 0.2
<i>PN<sub>2</sub></i> [Barrer]	0.53 ± 0.03	0.81 ± 0.01	1.58 ± 0.01
Selectivity [-]	28 ± 0.7	22 ± 0.4	14 ± 0.3

Membrane	Aged 16 wt.% BILP-101@Matrimid®		
Membrane thickness	40 ± 0.7 µm		
Temperature [K]	308	323	353
<i>PCO<sub>2</sub></i> [Barrer]	11.3 ± 0.1	12.6 ± 0.1	16.0 ± 0.2
<i>PN<sub>2</sub></i> [Barrer]	0.36 ± 0.01	0.52 ± 0.01	1.1 ± 0.01
Selectivity [-]	31.2 ± 0.7	24.3 ± 0.4	14.5 ± 0.3



**Table C6.** Detailed information of the reference cited in Fig. 4.9.

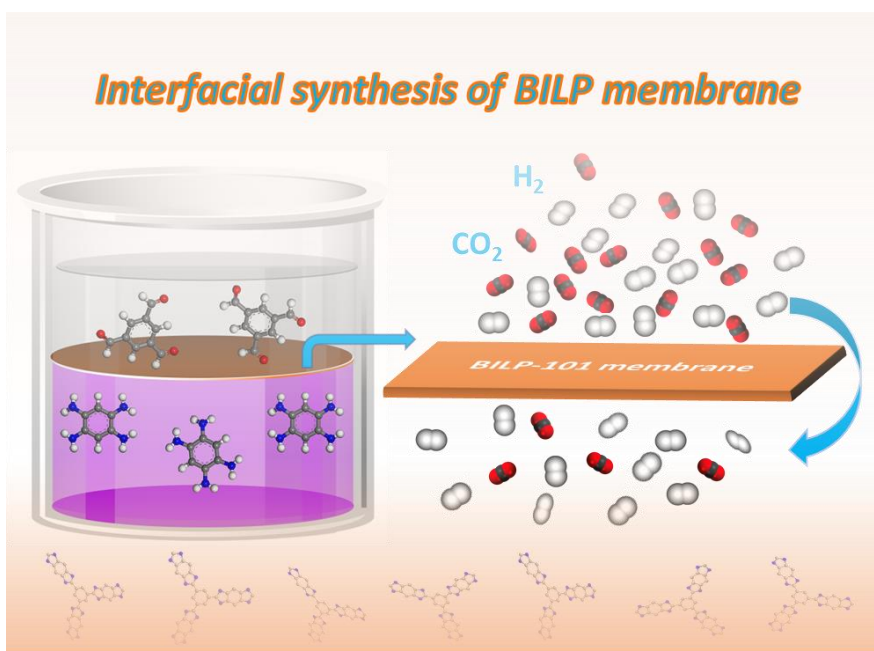
MMMs			Performance		Operation conditions			Reference
POF	Polymer	wt.% loading	$P_{CO_2}$ (Barrer)	$CO_2/N_2$ selectivity (-)	Type of analysis	T (K)	Feed P (bar)	
ACOF-1	Matrimid®	16	17.7	34.7	Mixed gas	308	2	3
	Polyactive™	0	147.5	42.8	"	"	"	
		16	98.9	44	"	"	"	
		6FDA-DAM	0	754.3	19.8	"	"	
	16		751.7	24	"	"	"	
BILP-101	Matrimid®	15	14	34.5	Single gas	295	0.2	4
BILP-4	Matrimid®	10	13.2	32	Single gas	"	"	
		15	14.9	38.9	"	"	"	
TpPa-1	PBI-Bul	0	2.3	25.6	Single gas	298	20	5
		20	2.8	21.4	"	"	"	
		40	5	20.9	"	"	"	
		50	13.1	2.5	"	"	"	
TpBD-1	PBI-Bul	20	4.3	19.9	"	"	"	
		40	6.6	21.5	"	"	"	
		50	14.8	23	"	"	"	
BILP-101	PIM	0	4700	19.3	Single gas	313	-	6
		17	6300	15.1	"	"	"	
		30	7200	15.3	"	"	"	
		40	5100	17.4	"	"	"	
SNW-1	PSF	0	12.5	17.5	Mixed gas	298	4.5	7
		5	16	26	"	"	"	
		8	21	33	"	"	"	
		12	27	40	"	"	"	
PAF-56P	PSF	0	67.5	11	Mixed gas	293	1.6	8
		1	90	17.5	"	"	"	
		3	100	22	"	"	"	
		5	132.2	38.9	"	"	"	
RT-BILP-101	Matrimid®	0	9.6	30	Mixed gas	308	2	This work
		16	17	31	"	"		
		24	27	29	"	"		
BILP-101		16	13	31	"	"		
		24	17	30	"	"		

- C1 T.-S. Chung, S. S. Chan, R. Wang, Z. Lu and C. He, *Journal of Membrane Science*, 2003, **211**, 91.
- C2 S. Kim, J. G. Seong, Y. S. Do and Y. M. Lee, *Journal of Membrane Science*, 2015, **474**, 122.
- C3 M. Shan, B. Seoane, E. Andres-Garcia, F. Kapteijn and J. Gascon, *Journal of Membrane Science*, 2018, **549**, 377.
- C4 T. D. M. Tessema, S. R. Venna, G. Dahe, D. P. Hopkinson, H. M. El-Kaderi and A. K. Sekizkardes, *Journal of Membrane Science*, 2018, **554**, 90.
- C5 U. K. Kharul, R. Banerjee, B. Biswal and H. D. Chaudhari, *Chemistry–A European Journal*, 2016, **22**, 4695.
- C6 A. K. Sekizkardes, V. A. Kusuma, G. Dahe, E. A. Roth, L. J. Hill, A. Marti, M. Macala, S. R. Venna and D. Hopkinson, *Chemical Communications*, 2016, **52**, 11768.
- C7 X. Gao, X. Zou, H. Ma, S. Meng and G. Zhu, *Advanced Materials*, 2014, **26**, 3644.
- C8 L. Meng, X. Zou, S. Guo, H. Ma, Y. Zhao and G. Zhu, *ACS Applied Materials & Interfaces*, 2015, **7**, 15561.



# Alumina Supported Porous Organic Framework Membranes for Pre-Combustion $\text{CO}_2$ Capture - Manufacture and Performance

5



This chapter is based on the following publication:

M. Shan, X. Liu, X. Wang, I. Yarulina, B. Seoane, F. Kapteijn and J. Gascon, Facile Manufacture of Porous Organic Framework Membranes for Precombustion  $\text{CO}_2$  Capture. *Sci. Adv.* **2018**, 4:eaau1698

---

**Abstract:** The development of new membranes with high H<sub>2</sub> separation performance under industrially relevant conditions (high temperatures and pressures) is of primary importance. Such membranes may facilitate the implementation of energy efficient pre-combustion CO<sub>2</sub> capture or reduce energy intensity in other industrial processes such as ammonia synthesis. In this chapter, a facile synthetic protocol based on interfacial polymerization is fabricated for the fabrication of supported benzimidazole-linked polymer (BILPs) membranes that display an unprecedented H<sub>2</sub>/CO<sub>2</sub> selectivity (up to 40) at 423 K together with high pressure resistance and long-term stability (> 800 h in the presence of water vapor).

---

## 5.1. INTRODUCTION

Separation processes, mostly based on distillation, account for 10-15% of the world energy consumption.<sup>1</sup> Membrane-based units offer several advantages, including a higher energy efficiency, smaller footprints, ease of operation and environmental friendliness. It is therefore not surprising that intense research has been devoted to the development of membrane modules able to efficiently separate complex gas mixtures. Among the different membrane materials, polymers still dominate the market due to their good processability and mechanical stability.<sup>2</sup> Nevertheless, conventional polymeric membranes suffer from a 'trade-off' between gas permeability and selectivity.<sup>3-5</sup> Extensive efforts have been put into the rational design and synthesis of novel microporous polymeric membranes to overcome this limit, including thermally rearranged (TR) polymers<sup>6</sup>, polymers of intrinsic microporosity (PIMs)<sup>7,8</sup> and porous organic frameworks (POFs) such as covalent organic frameworks (COFs)<sup>9</sup>, covalent triazine frameworks (CTFs)<sup>10</sup> or porous aromatic frameworks (PAFs)<sup>11</sup>. Even though some PIMs are highly soluble in common solvents and can be directly processed into membranes, PIM membranes suffer from moderate selectivity and serious aging issues. POFs are generally insoluble in most solvents, which greatly restricts their functionalization and post-processing into defect-free membranes.<sup>12</sup> The preparation of POF membranes has been achieved by direct growth on functional substrates,<sup>9</sup> assembly of porous nanosheets<sup>13</sup> or by mixing these porous fillers with non-structured and generally non-porous polymers in the form of mixed-matrix membranes (MMMs).<sup>11,14,15</sup> However, so far for POF-based membranes are far from ideal due to the relatively large pores of the selected POF frameworks and the challenge of preparing continuous defect-free membranes.

Benzimidazole-linked polymers (BILPs) are a new class of POFs, which are commonly synthesized *via* condensation of diamines with the respective aldehydes in N,N-dimethylformamide (DMF), resulting in amorphous powders with remarkable thermal and chemical stabilities as well as high CO<sub>2</sub> uptakes.<sup>16, 17</sup> Compared to other POFs, BILPs possess narrower pores due to their highly crosslinked interpenetrated networks,<sup>17, 18</sup> rendering them more suitable for the separation of small molecules. However, BILPs are non-soluble in most solvents, making the preparation of membranes highly challenging. In

this spirit, the development of more straightforward manufacturing processes for the large-scale production of continuous thin films is a must. Interfacial polymerization (IP)<sup>19-24</sup> is a facile and effective technique that allows the synthesis of large-area thin layers at the interface between two immiscible liquids. The IP method has been successfully applied for the synthesis of polyamide<sup>20, 21</sup> membranes on the bulk scale for water desalination and nanofiltration. Despite its potential, IP remains largely unexplored in the field of novel microporous polymer membranes for gas separation<sup>25, 26</sup>, although some COF films were recently synthesized following this approach for application in liquid phase nanofiltration<sup>27</sup>.

Herein, we circumvented the challenge of producing defect-free BILPs membranes (BILP-101<sup>18</sup>) by using a facile room temperature interfacial polymerization method. The resulting membranes display an excellent H<sub>2</sub>/CO<sub>2</sub> separation performance together with long-term stability under relevant separation conditions (pressure and water vapor presence) for pre-combustion CO<sub>2</sub> capture.

## **5.2. EXPERIMENTAL**

### **5.2.1. Materials**

1,3,5-triformylbenzene (TFB, 97 %), and 1,2,4,5-benzenetetramine tetrahydrochloride (BTA), Benzene (anhydrous, 99.8 %) were purchased from Sigma Aldrich and N,N-Dimethylformamide (anhydrous, 99.8 %) were ordered from Thermo Fisher. All the chemicals were used without further purification. Asymmetric  $\alpha$ -Al<sub>2</sub>O<sub>3</sub> disks ( $\gamma$ -Al<sub>2</sub>O<sub>3</sub> layer on top) with a diameter of 18 mm and thickness of 1 mm were purchased from Fraunhofer IKTS. The average pore size of  $\alpha$ -Al<sub>2</sub>O<sub>3</sub> and  $\gamma$ -Al<sub>2</sub>O<sub>3</sub> layer is *ca.* 2.5  $\mu$ m and 5 nm, respectively.

### **5.2.2 Synthesis of supported BILP-101 membranes**

Supported BILP-101 membranes with different monomer concentrations and different layers were prepared. Table 5.1 lists the conditions for each membrane and Fig. 5.1 shows pictures of prepared membranes. The membrane color becomes darker with the increase

**Table 5.1.** Summary of membrane preparation conditions. \* Two samples were prepared under A3 conditions, marked in the text as A3-1, A3-2 for distinction.

Membranes	Interfacial polymerization (IP) conditions			
	Aqueous amine phase [wt.%]	Aldehyde in benzene phase [wt.%]	IP time (min)	layers
<b>A1</b>	0.3	0.1	60	1
<b>A2</b>	0.75	0.25	60	1
<b>A3*</b>	1.5	0.5	60	1
<b>A4</b>	1.5	0.5	60	2

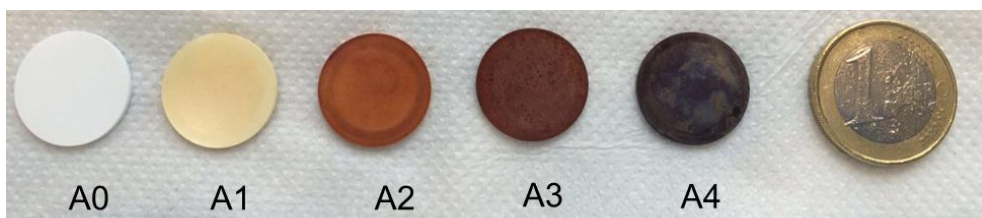


**Fig. 5.1.** Pictures of the prepared membranes under four different conditions (see table 5.1 for the details). A0 corresponds to the bare alumina support.

of monomer concentration. For the specific procedures, the alumina disks were firstly immersed in an aqueous BTA solution under reduced pressure (0.2 bar) for 20 min, dried with compressed air until no visible droplets were left on the surface and then contacted with TFB solution in benzene for 60 min (toluene as solvent also works). This procedure was repeated to prepare membranes with two layers of BILP. The membranes were left overnight and washed with benzene to remove the unreacted TFB, dried at room temperature for at least 16 h, and finally the membrane was put into a home-made permeation set-up for performance testing.<sup>15</sup>



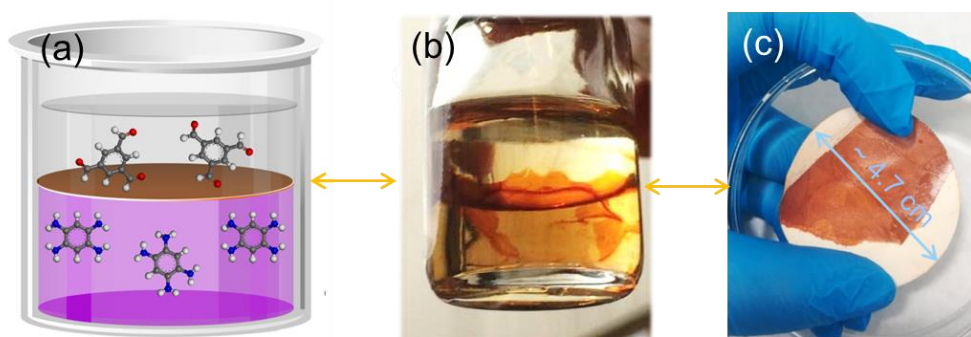


**Fig. 5.2.** (a). Description of free-standing BILP-101 film synthesis. (b) Photograph of the film formed at the water-benzene interface, and (c), the film supported on a nylon substrate. The diameter of nylon support is 4.7 cm.

### 5.2.3. Synthesis of BILP-101 film at the bulk liquid interface

An aqueous solution of BTA (*i.e.* 1.5 wt.%, 150 mg in 10 g de-ionized water) was poured into a small petri dish (inner Diameter  $\sim 5$  cm) and then a solution of TFB in benzene (0.5 wt.%, 44.7 mg in 8.7 g benzene) was gently spread on top of the BTA solution. After a few seconds, a brown layer was formed at the water-benzene interface. Fig.5.2a depicts the formation process. The film can be gently transferred to a nylon substrate (see Fig. 5.2c). Plenty of films were synthesized following this procedure and then washed with benzene, water, DMF and ethanol and finally dried under vacuum overnight at 393 K for further characterization. In order to get a clear view, a photo of a film synthesized in a small vial is presented in Fig. 5.2b.

### 5.2.4. Characterization techniques

Diffuse reflectance infrared Fourier transform (DRIFT) spectra of BILP-101 film was acquired in a Nicolet 8700 FT-IR (Thermo Scientific) spectrometer equipped with a high temperature cell with  $\text{CaF}_2$  windows (Praying Mantis<sup>TM</sup>). The samples were pretreated in He at 423 K for 30 min to collect the spectra.

Thermogravimetric analysis (TGA) of a BILP-101 film were performed on a Mettler Toledo TGA/SDTA851e apparatus by measuring the mass loss of the sample while heating the

prepared BILP film under air flow (100 mL min<sup>-1</sup>) from 303 K to 1073 K at a heating rate of 5 K·min<sup>-1</sup>.

Powder X-ray diffraction (PXRD) patterns of the prepared films were recorded using a Bruker-D8 Advanced diffractometer with Co-K $\alpha$  radiation ( $\lambda = 1.78897 \text{ \AA}$ ). The samples were scanned in the  $2\theta$  range of 5 – 80° using a step size of 0.02° and a scan speed of 0.4 s per step in a continuous scanning mode.

Scanning Electron Microscopy (SEM) micrographs of the freestanding film were acquired using a JEOL JSM-6010LA InTouchScope microscope. The images of the supported membranes were obtained using a DualBeam Strata 235 microscope (FEI) and an AURIGA Compact (Zeiss) microscope. Prior to the analyses, BILP-101 films and the supported membranes were sputter-coated with gold.

Atomic force microscopy (AFM) images were obtained by transferring the freestanding films to silica wafer and dried in an oven at 353 K for 1 h. The images were obtained using a Veeco Multimode Nanoscope 3A microscope operating in a tapping mode.

N<sub>2</sub> (77 K) and CO<sub>2</sub> (298 K) adsorption isotherms were recorded in a Tristar II 3020 (Micromeritics) instrument. Prior to the gas adsorption measurements, the samples were degassed at 423 K under N<sub>2</sub> flow for at least 16 h.

One-dimensional <sup>13</sup>C CP/MAS solid state NMR spectra were recorded on Bruker AVANCE III spectrometers operating at 600 MHz resonance frequencies for <sup>1</sup>H. Experiments at 600 MHz employed a conventional double-resonance 3.2 mm CP/MAS probe or a 2.5 mm double-resonance probe. Dry nitrogen gas was utilized for sample spinning to prevent degradation of the samples. NMR chemical shifts are reported with respect to the external references TMS and adamantane. For <sup>13</sup>C CP/MAS NMR experiments, the following sequence was used: 90° pulse on the proton (pulse length 2.4 s), then a cross-polarization step with contact time of typically 2 ms, and finally acquisition of the <sup>13</sup>C NMR signal under high-power proton decoupling. The delay between the scans was set to 5 s to allow the complete relaxation of the <sup>1</sup>H nuclei, and the number of scans ranged between 10000 and 20000. An exponential apodization function corresponding to a line broadening of 80 Hz was applied prior to Fourier transformation. The sample spinning frequency was 15 kHz and 20 KHz.

High resolution transmission electron microscopy (TEM) analysis was obtained using a JEOL JEM3200 FSC operated at 300 kV. Low resolution TEM images were acquired by a JEOL JEM1400 plus operated at 120 kV. Before TEM observation, the specimens were prepared by applying a few drops of a BILP-101 film ethanol suspension on a carbon-coated copper grid and letting it dry.

### 5.2.5. Gas permeation experiments

The supported BILP-101 membranes with an area of 1.33 cm<sup>2</sup> were mounted in a flange between Viton<sup>®</sup> O-rings. This flange fits in a permeation module, which was placed inside an oven in a home-made permeation setup. The diagram was shown in Scheme D1. The H<sub>2</sub>/CO<sub>2</sub> separation measurements were performed employing a 50:50 H<sub>2</sub>:CO<sub>2</sub> gas mixture (100 mL·min<sup>-1</sup> CO<sub>2</sub> and 100 mL·min<sup>-1</sup> of H<sub>2</sub>) as feed. Helium (4.6 mL·min<sup>-1</sup>) was used as sweep gas at the permeate side. The absolute pressure of the feed stream was adjusted in a range of 1 - 10 bar using a back-pressure controller at the retentate side, keeping the permeate side at atmospheric pressure. The temperature in the permeation module was adjusted from 298 K to 498 K through a convection oven. An on-line gas chromatograph (Interscience Compact GC) equipped with a packed Carboxen 1010 PLOT (30 m x 0.32 mm) column and TCD detector was used to periodically analyse the permeate stream. For single gas permeation tests, the feed flow rates were set at around 50 mL/min to keep 1 bar pressure drop between the feed and permeate side. The typical A3 membrane (Table 5.1) was synthesised two times to ensure reproducibility of the reported data. In all cases, gas separation performance was evaluated after ensuring steady state operation.

Gas separation performance was defined by the selectivity ( $\alpha$ ) and the gas permeance ( $P$ ) of the individual components. The permeance of component  $i$  ( $P_i$ ) was calculated as follows (Equation 5.1):

$$P_i = \frac{N_i}{\Delta p_i \cdot A} = \frac{F_i}{\Delta p_i} \quad (5.1)$$

where flux  $F_i$  denotes the molar flux of compound  $i$  ( $\text{mol m}^{-2} \text{s}^{-1}$ ),  $N_i$  is the permeate rate of component  $i$  ( $\text{mol s}^{-1}$ ),  $A$  is the membrane area and  $\Delta p_i$  is the partial pressure difference of component  $i$  across the membrane and it can be calculated according to Equation 5.2.

$$\Delta p_i = p_{\text{feed}} \times Y_{i,\text{feed}} - p_{\text{perm}} \times X_{i,\text{perm}} \quad (5.2)$$

where  $p_{\text{feed}}$  and  $p_{\text{perm}}$  represent the pressures at the feed and permeate sides and  $Y_{i,\text{feed}}$  and  $X_{i,\text{perm}}$  are the molar fractions of component  $i$  in the feed and permeate gas streams, respectively.

The SI unit for the permeance is  $\text{mol} \cdot \text{s}^{-1} \cdot \text{m}^{-2} \cdot \text{Pa}^{-1}$ . However, gas permeances are reported in the widely unit GPU (Gas Permeation Unit),

where  $1 \text{ GPU} = 3.3928 \times 10^{-10} \text{ mol} \cdot \text{s}^{-1} \cdot \text{m}^{-2} \cdot \text{Pa}^{-1}$ .

The separation factor or mixed gas selectivity ( $\alpha$ ) was calculated as the ratio of the permeance of the faster permeating component ( $\text{H}_2$ ), to the permeance of the less permeating component ( $\text{CO}_2$ ) (equation 5.3).

$$\alpha = \frac{P_{\text{H}_2}}{P_{\text{CO}_2}} \quad (5.3)$$

### 5.3. RESULTS AND DISCUSSION

The BILP-101 membrane was directly fabricated onto an  $\alpha\text{-Al}_2\text{O}_3$  porous support ( $\gamma\text{-Al}_2\text{O}_3$  on top, pore size of  $\gamma$  layer 5 nm) by interfacial polymerization (Fig. 5.3a).  $\alpha\text{-Al}_2\text{O}_3$  was selected due to its good thermal stability. Moreover,  $\gamma\text{-Al}_2\text{O}_3$  top layer offer a large volume of small hydrophilic pores, ideal for the IP process.<sup>26</sup> The BTA-containing aqueous solution was trapped into the small pores of the top layer of the asymmetric  $\text{Al}_2\text{O}_3$  support, which after drying the surface was further immersed in a 0.5 wt.% 1,3,5-triformylbenzene (TFB) benzene solution for 60 min (see details in experimental section). Upon contact with the TFB-containing solution, the amine groups of the trapped BTA monomer quickly react with the aldehyde moieties at the water/benzene interface, leading to the rapid formation of a brown layer at the interface. The growing film itself probably becomes a barrier for the contact between the two monomers and confines the reaction to the remaining defects, resulting in the formation

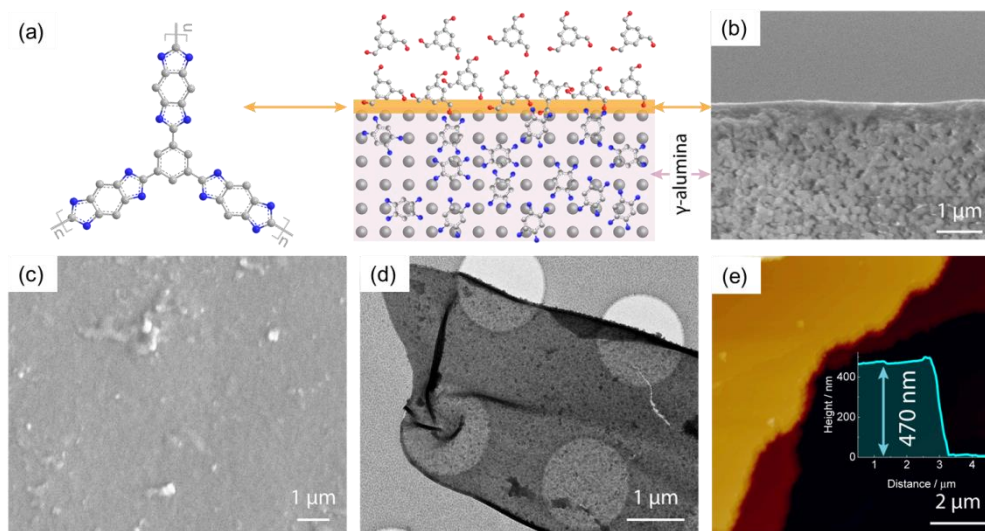


**Fig. 5.3.** (a) The alumina disk was first saturated with an aqueous BTA solution and then contacted with a benzene layer containing TFB, enabling the formation of BILP-101 membranes at the interface. (b and c) Cross-sectional and surface SEM images of a BILP-101 membrane,  $\sim 400$  nm thick, formed on alumina substrate. (d) TEM image of the free standing BILP-101 film. (e) AFM topographical image of the film on a silicon wafer. Inset shows the film height. The samples were prepared under the condition of 1.5 wt.% BTA-0.5 wt.% TFB-60 min (see experimental section).

of a continuous, defect-free layer at the support surface. Scanning electron microscopy (SEM) images were acquired from the cross-section and top surface of the membrane. A continuous membrane (Fig. 5.3c) with a thickness of around  $\sim 400$  nm (Fig. 5.3b) can be observed by SEM.

To gain insight into the structure of the membrane, free-standing films were prepared at the bulk liquid interface under identical conditions (see experimental part 5.2.3 for details). A film with lateral dimensions of up to several centimeters was transferred to a nylon substrate (Fig. 5.2c). The sheet-like morphology was further observed by transmission electron microscopy (TEM) (Fig. 5.3d, Fig. D1c and d). In some places, the layer was crumpled or scrolled, suggesting its high flexibility. Atomic force microscopy (AFM) images of a BILP film transferred onto a silicon wafer revealed a film thickness of  $\sim 470$  nm (Fig. 5.3e), which is consistent with the

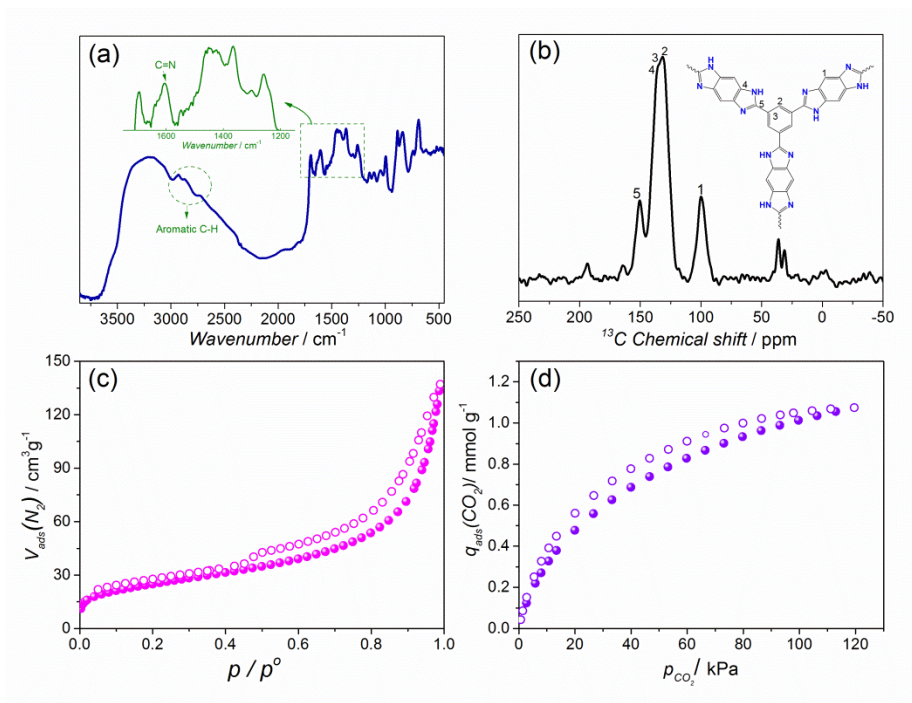


**Fig. 5. 4.** (a) DRIFT-IR and (b) <sup>13</sup>C CP/MAS spectra of films. (c) N<sub>2</sub> and (d) CO<sub>2</sub> adsorption (solid symbols) and desorption (open symbols) isotherms of the films at 77 and 298 K, respectively. The samples were prepared under the conditions of 1.5 wt.% BTA-0.5 wt.% TFB-60 min (see experimental section).

membrane thickness prepared on the alumina substrate. The formation of BILP-101 was confirmed by Diffuse Reflectance Infrared Fourier Transform Spectroscopy (DRIFTS) and <sup>13</sup>C Cross-Polarization Magic Angle Spinning (CP/MAS) NMR spectroscopy. Fig. 5.4a reveals a characteristic stretching band at 1610 cm<sup>-1</sup> (the C=N vibration) and bands at 1450, 1365, 1260 cm<sup>-1</sup>, which are assigned to the formation of the benzimidazole ring<sup>18, 29</sup>. The band at 1700 cm<sup>-1</sup> points to the presence of some residual aldehyde groups, further corroborated by a weak peak at  $\delta = 194$  ppm in the solid-state <sup>13</sup>C CP-MAS NMR spectrum (Fig. 5.4b). In line with the DRIFTS results, the <sup>13</sup>C CP-MAS NMR spectrum proves the successful condensation between TFB and BTA building units (Fig. 5.4b), giving rise to the appearance of a peak at a chemical shift of 150 ppm characteristic of the

benzimidazole ring. Signals centered at 130 and 100 ppm are characteristic of aromatic carbons, particularly those of the monomers. The full assignment of the peaks is shown on Fig. 5.4b. Thermogravimetric analysis (TGA) under air reveals that the film remains stable up to 523 K (Fig. D2).

The textural properties of the prepared film, were determined by N<sub>2</sub>, Ar and CO<sub>2</sub> adsorption isotherms, acquired at 77, 298 and 87 K, respectively. About N<sub>2</sub> adsorption, the BILP-101 film exhibits a type II isotherm together with a type III hysteresis loop.<sup>30</sup> The calculated Brunauer-Emmett-Teller (BET) area of BILP-101 film was 87 m<sup>2</sup>g<sup>-1</sup>, comprising a small amount of microporous (17 m<sup>2</sup>g<sup>-1</sup>) and mainly external surface area (70 m<sup>2</sup>g<sup>-1</sup>) according to the *t*-plot method. The micropores come from the internal structure of the film, while mesopores are expected to arise from the dense packing of film sheets. In line with N<sub>2</sub> adsorption results, Ar adsorption also shows only a small uptake at relatively low pressures together with similar hysteresis loop (Fig. D4), indicating its low accessibility towards Ar (~ 3.4 Å) and N<sub>2</sub> (~3.6 Å). Considering the high Lewis basic N/C ratio in the BILP-101x network, it should achieve a high CO<sub>2</sub> uptake at low pressures. However, CO<sub>2</sub> adsorption isotherms (Fig. 5.4d) shows a CO<sub>2</sub> uptake of ~22 cm<sup>3</sup> g<sup>-1</sup> at 1 bar and 298 K, which is much lower than reported BILP-101 powders<sup>18</sup>, indicating a higher degree of interpenetration in the prepared BILP-101 film. In the powder X-Ray diffraction patterns (PXRD) (Fig. D3), the film shows a single broad reflection at 30° with a *d* spacing of ~ 3.5 Å. The *d* spacing is usually considered as the packing distance of different polymer chains and the decrease in *d* is expected to increase the size-sieving ability of polymer membranes for gas separation. In our case, the small *d* spacing results in the high hydrogen selectivity, as discussed below. Both the value of *d* spacing and porosity of the as-synthesized BILP-101x films are different from the BILP-101 particles reported in Ref. 18. The method for the preparation of our films is different from the earlier approach, e.g., temperature, duration, solvent and the way of monomer addition. As noticed by Nguyen et al.<sup>31</sup> and El-Kaderi et al.<sup>29</sup>, the addition speed of monomers and the temperature will influence the formation of the oligomers at the beginning of the reaction, which are important factors affecting the overall porosity of BILPs.

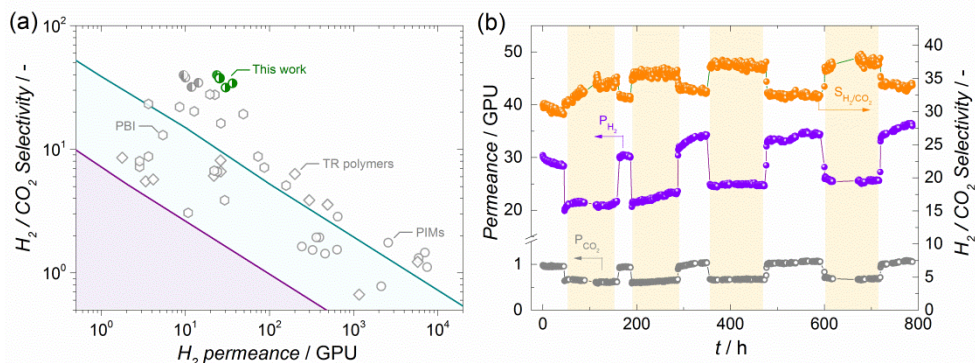


**Fig. 5.5.** (a) Comparison of H<sub>2</sub>/CO<sub>2</sub> separation performance with previously reported polymer membranes. The lines were drawn based on 2008 Robeson upper bound line by converting permeability to permeance assuming a membrane thickness of 50 μm (purple line) and 1 μm (green line). The membrane thickness is assumed as 1 μm for the typical PBI, TR polymers and PIMs. The green half-filled circles represent the BILP membrane performance developed in this work. For comparison, the predicted membrane performance (gray half-filled circles) of BILP with a membrane thickness of 1 μm is calculated. The details can be found in Table D5. (b) Long-term stability for H<sub>2</sub>/CO<sub>2</sub> separation under alternating dry and wet gas mixture (2.3 mol.% H<sub>2</sub>O, marked by light-yellow area) at 423 K. The samples were prepared under the conditions of 1.5 wt.% BTA-0.5 wt.% TFB-60 min (see details in Table 5.1).

The prepared BILP membranes were mounted into a Wicke-Kallenbach cell to evaluate their performance in the separation of equimolar H<sub>2</sub>/CO<sub>2</sub> mixtures at 423 K. Such separation is very relevant for pre-combustion CO<sub>2</sub> capture or H<sub>2</sub> production. An experiment using the bare α-Al<sub>2</sub>O<sub>3</sub> substrate showed a H<sub>2</sub> permeance of > 80,000 GPUs with a low H<sub>2</sub>/CO<sub>2</sub> selectivity of ~ 3. Hence, the support does not constitute a transport barrier. The supported BILP-101 membrane exhibits an excellent separation performance with a H<sub>2</sub>/CO<sub>2</sub> selectivity of 40 and a H<sub>2</sub> permeance of 24 GPU at 1 bar trans-membrane pressure difference, surpassing not only the H<sub>2</sub>/CO<sub>2</sub> separation limitation (*i.e.*, the 2008 Robeson upper bound line<sup>3</sup> in Fig. 5.5a) of conventional polymer membranes but also the performance of a wide range of new polymers such as PIM and TR polymers and most of the benchmarked polybenzimidazole (PBI) membranes.<sup>32</sup>



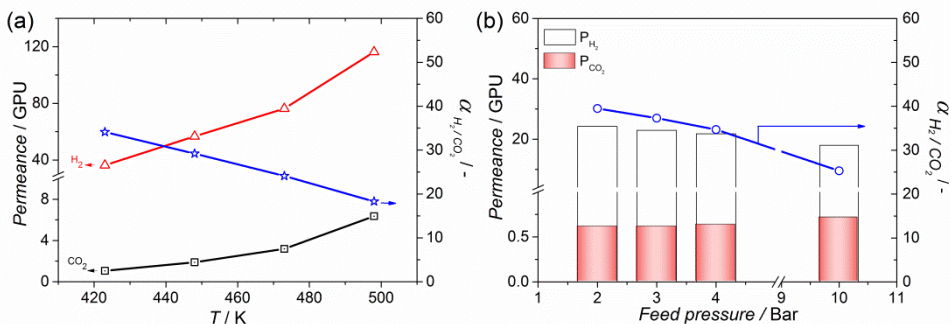


**Fig. 5.6.** (a) Effect of the temperature on the membrane separation performance for sample A3-2.  $H_2/CO_2$  feed ratio = 1, sweep gas helium, atmospheric pressure, no absolute pressure difference across the membrane. (b) Effect of absolute feed pressure on the membrane performance in the separation of  $H_2$  from an equimolar  $H_2/CO_2$  mixture at 423 K. Results are obtained from sample A3-1.

In a typical pre-combustion  $CO_2$  capture process,  $H_2$  is generated through stream reforming of fossil fuels followed by water-gas shift (WGS). As a result, a high pressure (up to  $\sim 35$  bar), high temperature ( $\sim 450$ - $530$  K) mixture of  $CO_2$  and  $H_2$  is generated.<sup>33</sup> In order to be able to selectively separate  $H_2$  and capture  $CO_2$ , membrane materials displaying high temperature and pressure resistance are required,<sup>5</sup> next to resistance against the water vapor presence from the WGS. The separation performance of the BILP-101 membranes was further evaluated under conditions relevant for this important separation.  $H_2/CO_2$  measurements at elevated temperatures (from 423 K to 498 K) are shown in Fig. 5.6a. It was found that the gas permeabilities increased with temperature for both  $CO_2$  and  $H_2$ , indicating an activated diffusion mechanism.

The apparent activated energy  $E_{act,i}$  for  $H_2$  and  $CO_2$  diffusion can be estimated by fitting the experimental gas permeance data to an Arrhenius equation 5.4.

$$P_i = A_i \exp\left(-\frac{E_{act,i}}{RT}\right)$$

$$\ln P_i = a - \frac{E_{act,i}}{R} \cdot \frac{1}{T} \quad (5.4)$$

Where  $E_{act,i}$  is the activation energy of gas component  $i$ .  $P_i$  ( $\text{mol m}^{-2} \text{s}^{-1} \text{Pa}^{-1}$ ) represents the gas permeance of component  $i$ ,  $A_i$  is the pre-exponential factor of gas component  $i$ ,  $T$

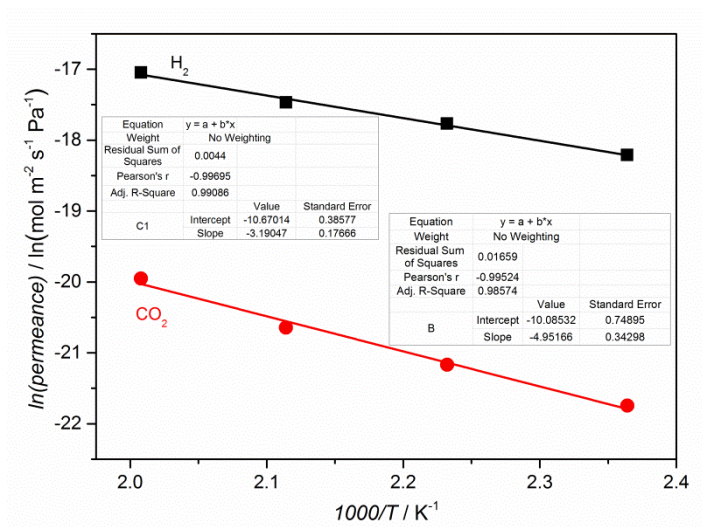


**Fig. 5.7.** Arrhenius temperature dependence of H<sub>2</sub> and CO<sub>2</sub> permeances for A3-1 membrane.

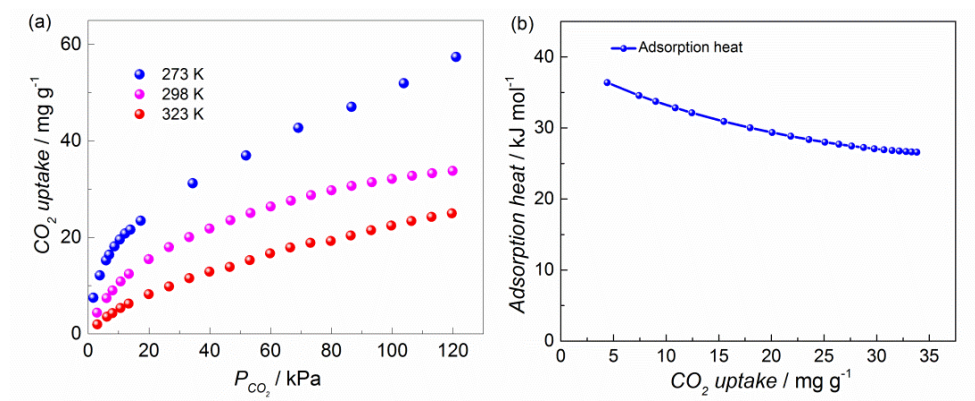


**Fig. 5.8.** (a) CO<sub>2</sub> adsorption isotherms of BILP-101 film at 273, 298 and 323 K. (b) Adsorption heat of CO<sub>2</sub> calculated by Virial equation.

is the absolute temperature (K) and  $R$  is the ideal gas constant,  $8.314 \text{ J mol}^{-1} \text{ K}^{-1}$ . The plot of  $\ln P_i$  versus  $1/T$  results in a straight line, whose slope can be used to calculate the apparent activation energy. As shown in Fig. 5.7, the activation energy for H<sub>2</sub> is 26.5, which is lower than CO<sub>2</sub>, 41.2  $\text{kJ mol}^{-1}$ , in agreement with that less permeable gases often possess higher activation energy. Thus, the less permeable CO<sub>2</sub> realize the relatively larger increase with temperature compared with that of H<sub>2</sub>, leading to the decrease in H<sub>2</sub>/CO<sub>2</sub>

selectivity. Despite the decrease in selectivity with temperature, the membrane still exhibits an excellent separation performance with a  $\text{H}_2/\text{CO}_2$  selectivity of 24 even at 498 K. Furthermore,  $\text{CO}_2$  adsorption isotherms at different temperatures (Fig. 5.8a) were measured to calculate the isosteric heat of adsorption ( $\Delta H_{ads}$ ) of BILP-101 film according to the common method Virial equation (Fig. 5.8b). The film showed a  $\Delta H_{ads}$  value of  $36 \text{ kJ mol}^{-1}$  for  $\text{CO}_2$ , which is similar to the reported BILP-101 powders ( $33 \text{ kJ mol}^{-1}$ ).<sup>18</sup> Thus, the diffusion activation energy for  $\text{CO}_2$  ( $E_{diff}$ ) is calculated by equation 5.5,

$$E_{act} = E_{diff} - \Delta H_{ads} \quad (5.5)$$

which value is  $77.1 \text{ kJ mol}^{-1}$ , further confirms the activated diffusion for  $\text{CO}_2$ .

High pressure measurements (Fig. 5.6b) indicate that the membrane still maintains a high  $\text{H}_2/\text{CO}_2$  selectivity ( $\sim 25$ ) even at 423 K and 10 bar absolute feed pressure in comparison with other reported membranes (see Table D5). Most conventional polymers either could not withstand such conditions or exhibit limited gas permeation performance at elevated temperatures.<sup>34</sup> Some emerging ultrathin 2D metal-organic frameworks (MOFs) and graphene oxide nanosheet membranes<sup>35-37</sup> could achieve a good  $\text{H}_2/\text{CO}_2$  separation performance at high temperatures. However, these ultrathin membranes are vulnerable to high pressures owing to the fragile nature of single 2D nanosheets and the weak interaction between layers.

Lack of stability is the biggest hurdle faced by  $\text{H}_2$  separation membranes.<sup>33</sup> Development of hydrothermally-stable membranes is highly desired since water is inevitably present in industrial  $\text{H}_2/\text{CO}_2$  separation processes. Accordingly, the long-term performance of our BILP-101 membranes under steam at 423 K was studied (Fig. 5.5b). Both,  $\text{H}_2$  and  $\text{CO}_2$  permeances decreased when introducing 2.3 mol.% water vapour in the feed, attributed to the competitive sorption of water molecules that increases diffusion resistance for both gases. Such a competitive effect has a more significant impact for the transport of bigger  $\text{CO}_2$  molecules, leading to an increased  $\text{H}_2/\text{CO}_2$  selectivity. Upon removing the water from the feed, the performance returns to that previously observed under dry conditions. During the 800 h hydrothermal cycling test, both the permeance and selectivity of BILP-101 membrane were slightly increased, probably due to the release of impurities. The high

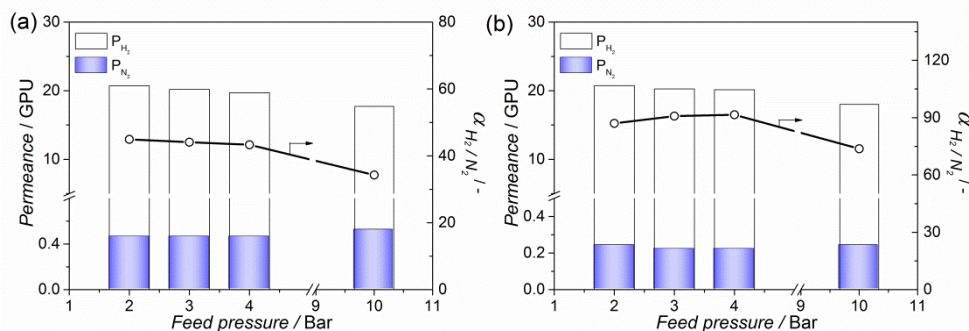


**Fig. 5.9.** Effect of absolute feed pressure on the membrane performance in the separation of H<sub>2</sub> from an equimolar H<sub>2</sub>/N<sub>2</sub> mixture at 423 K. Results are obtained from sample (a) A2 and (b) A3-1

H<sub>2</sub>/CO<sub>2</sub> separation performance combined with an excellent long-term hydrothermal stability place the supported BILP-101 membranes among promising candidates to be used for H<sub>2</sub> separation/purification under industrially relevant conditions.

Moreover, the BILP-101 membranes also hold great potential for H<sub>2</sub> recovery from ammonia production with high H<sub>2</sub>/N<sub>2</sub> selectivities (up to 87 for A3-1 membrane, Fig. 5.9, Table D4), which are higher than H<sub>2</sub>/CO<sub>2</sub> results, suggesting a molecular sieving mechanism. This is further supported by the PXRD of the film showing an average chain *d*-spacing of 3.5 Å (Fig. D3), consequently facilitating the diffusion of molecules with small kinetic diameters (H<sub>2</sub> ~ 2.9 Å) while hindering the transport of those with large diameter (CO<sub>2</sub> ~ 3.3 Å and N<sub>2</sub> ~ 3.6 Å). The different size of CO<sub>2</sub> and N<sub>2</sub> is indicative of the higher selectivity for H<sub>2</sub>/N<sub>2</sub> mixtures.

## 5.4. CONCLUSIONS

In summary, free standing POF films (specifically BILP-101) were successfully synthesized at the benzene-water interface. BILP-101 membrane films were further fabricated in a similar manner onto porous  $\alpha$ -Al<sub>2</sub>O<sub>3</sub> supports with a top layer of  $\gamma$ -Al<sub>2</sub>O<sub>3</sub>. The membrane demonstrates a high H<sub>2</sub> selectivity over both CO<sub>2</sub> and N<sub>2</sub> at elevated temperatures together with high-pressure resistance. In addition, the membrane performed stable during 800 h, and the separation performance even slightly improved during the 800 h hydrocycling test. These results demonstrate that interfacial polymerization offers great advantages for the preparation of defect free membranes based on porous organic

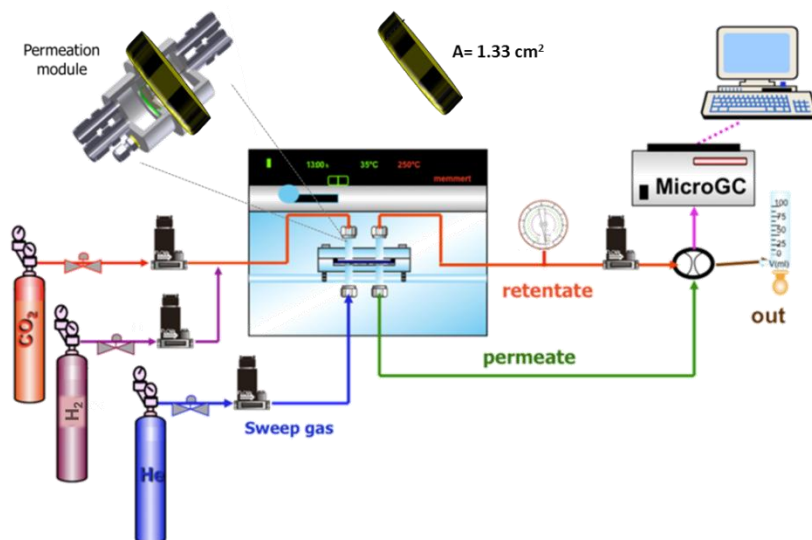
frameworks. The combination of such a simple preparation method with the rich chemistry of POFs is expected to result in the development of many more membranes with applications in a wide variety of separations.

## REFERENCES

- 1 D. S. Sholl and R. P. Lively, *Nature*, 2016, **532**, 435.
- 2 H. B. Park, J. Kamcev, L. M. Robeson, M. Elimelech and B. D. Freeman, *Science*, 2017, **356**, eaab0530.
- 3 L. M. Robeson, *Journal of Membrane Science*, 2008, **320**, 390.
- 4 T. Rodenas, I. Luz, G. Prieto, B. Seoane, H. Miro, A. Corma, F. Kapteijn, F. X. L. i. Xamena and J. Gascon, *Nature Materials*, 2015, **14**, 48.
- 5 B. Seoane, J. Coronas, I. Gascon, M. E. Benavides, O. Karvan, J. Caro, F. Kapteijn and J. Gascon, *Chemical Society Reviews*, 2015, **44**, 2421.
- 6 H. B. Park, C. H. Jung, Y. M. Lee, A. J. Hill, S. J. Pas, S. T. Mudie, E. Van Wagner, B. D. Freeman and D. J. Cookson, *Science*, 2007, **318**, 254.
- 7 M. Carta, R. Malpass-Evans, M. Croad, Y. Rogan, J. C. Jansen, P. Bernardo, F. Bazzarelli and N. B. McKeown, *Science*, 2013, **339**, 303.
- 8 M. D. Guiver and Y. M. Lee, *Science*, 2013, **339**, 284.
- 9 J. Fu, S. Das, G. Xing, T. Ben, V. Valtchev and S. Qiu, *Journal of the American Chemical Society*, 2016, **138**, 7673.
- 10 X. Zhu, C. Tian, S. M. Mahurin, S.-H. Chai, C. Wang, S. Brown, G. M. Veith, H. Luo, H. Liu and S. Dai, *Journal of the American Chemical Society*, 2012, **134**, 10478.
- 11 C. H. Lau, P. T. Nguyen, M. R. Hill, A. W. Thornton, K. Konstas, C. M. Doherty, R. J. Mulder, L. Bourgeois, A. C. Y. Liu, D. J. Sprouster, J. P. Sullivan, T. J. Bastow, A. J. Hill, D. L. Gin and R. D. Noble, *Angewandte Chemie International Edition*, 2014, **53**, 5322.
- 12 N. Chaoui, M. Trunk, R. Dawson, J. Schmidt and A. Thomas, *Chemical Society Reviews*, 2017, **46**, 3302.
- 13 G. Li, K. Zhang and T. Tsuru, *ACS Applied Materials & Interfaces*, 2017, **9**, 8433.
- 14 Z. Kang, Y. Peng, Y. Qian, D. Yuan, M. A. Addicoat, T. Heine, Z. Hu, L. Tee, Z. Guo and D. Zhao, *Chemistry of Materials*, 2016, **28**, 1277.
- 15 M. Shan, B. Seoane, E. Rozhko, A. Dikhtiarenko, G. Clet, F. Kapteijn and J. Gascon, *Chemistry-A European Journal*, 2016, **22**, 14467.
- 16 M. G. Rabbani and H. M. El-Kaderi, *Chemistry of Materials*, 2012, **24**, 1511.
- 17 M. G. Rabbani, T. E. Reich, R. M. Kassab, K. T. Jackson and H. M. El-Kaderi, *Chemical Communications*, 2012, **48**, 1141.
- 18 A. K. Sekizkardes, J. T. Culp, T. Islamoglu, A. Marti, D. Hopkinson, C. Myers, H. M. El-Kaderi and H. B. Nulwala, *Chemical Communications*, 2015, **51**, 13393.

- 19 M. J. T. Raaijmakers, M. A. Hempenius, P. M. Schön, G. J. Vancso, A. Nijmeijer, M. Wessling and N. E. Benes, *Journal of the American Chemical Society*, 2014, **136**, 330.
- 20 S. Karan, Z. Jiang and A. G. Livingston, *Science*, 2015, **348**, 1347.
- 21 M. Elimelech and W. A. Phillip, *Science*, 2011, **333**, 712.
- 22 M. F. Jimenez-Solomon, Q. Song, K. E. Jelfs, M. Munoz-Ibanez and A. G. Livingston, *Nature Materials*, 2016, **15**, 760.
- 23 A. J. Brown, N. A. Brunelli, K. Eum, F. Rashidi, J. R. Johnson, W. J. Koros, C. W. Jones and S. Nair, *Science*, 2014, **345**, 72.
- 24 R. Ameloot, F. Vermoortele, W. Vanhove, M. B. J. Roeffaers, B. F. Sels and D. E. De Vos, *Nature Chemistry*, 2011, **3**, 382.
- 25 Z. Ali, F. Pacheco, E. Litwiller, Y. Wang, Y. Han and I. Pinnau, *Journal of Materials Chemistry A*, 2018, **6**, 30.
- 26 J. Sánchez-Laínez, L. Paseta, M. Navarro, B. Zornoza, C. Téllez and J. Coronas, *Advanced Materials Interfaces*, 2018, 1800647.
- 27 K. Dey, M. Pal, K. C. Rout, S. Kunjattu H, A. Das, R. Mukherjee, U. K. Kharul and R. Banerjee, *Journal of the American Chemical Society*, 2017, **139**, 13083.
- 28 E. Maaskant, P. de Wit and N. E. Benes, *Journal of Membrane Science*, 2018, **550**, 296.
- 29 M. G. Rabbani, A. K. Sekizkardes, O. M. El-Kadri, B. R. Kaafarani and H. M. El-Kaderi, *Journal of Materials Chemistry*, 2012, **22**, 25409.
- 30 M. Thommes, K. Kaneko, A. V. Neimark, J. P. Olivier, F. Rodriguez-Reinoso, J. Rouquerol and K. S. W. Sing, *Pure and Applied Chemistry*, 2015, **87**, 1051.
- 31 P. Pandey, A. P. Katsoulidis, I. Eryazici, Y. Wu, M. G. Kanatzidis and S. T. Nguyen, *Chemistry of Materials*, 2010, **22**, 4974.
- 32 T. Yang, Y. Xiao and T.-S. Chung, *Energy & Environmental Science*, 2011, **4**, 4171.
- 33 N. W. Ockwig and T. M. Nenoff, *Chemical Reviews*, 2007, **107**, 4078.
- 34 H. Lin, E. Van Wagner, B. D. Freeman, L. G. Toy and R. P. Gupta, *Science*, 2006, **311**, 639.
- 35 X. Wang, C. Chi, K. Zhang, Y. Qian, K. M. Gupta, Z. Kang, J. Jiang and D. Zhao, *Nature Communications*, 2017, **8**, 14460.
- 36 Y. Peng, Y. Li, Y. Ban, H. Jin, W. Jiao, X. Liu and W. Yang, *Science*, 2014, **346**, 1356.
- 37 H. Li, Z. Song, X. Zhang, Y. Huang, S. Li, Y. Mao, H. J. Ploehn, Y. Bao and M. Yu, *Science*, 2013, **342**, 95.

## Appendix D



**Scheme D1.** Diagram of gas permeation apparatus used in this work.

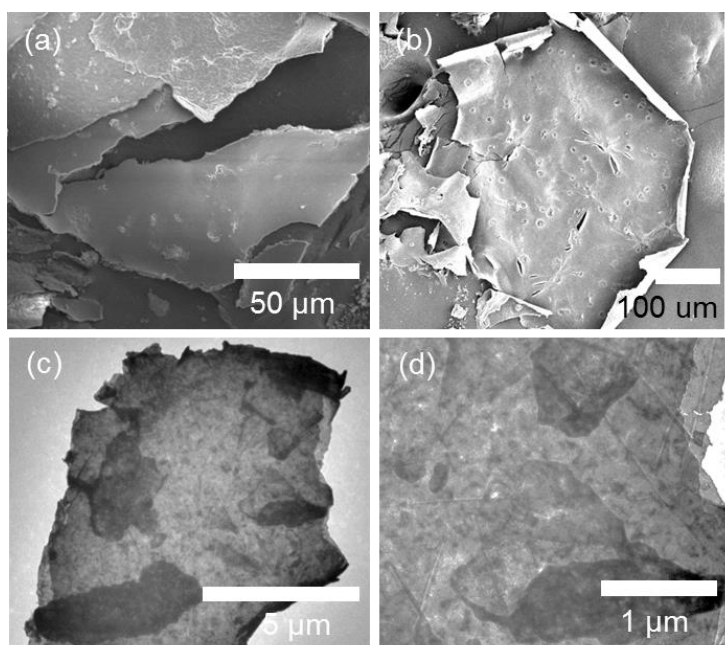


**Fig. D1.** (a) and (b) are low resolution SEM images of the films. (c) and (d) are low resolution TEM images.



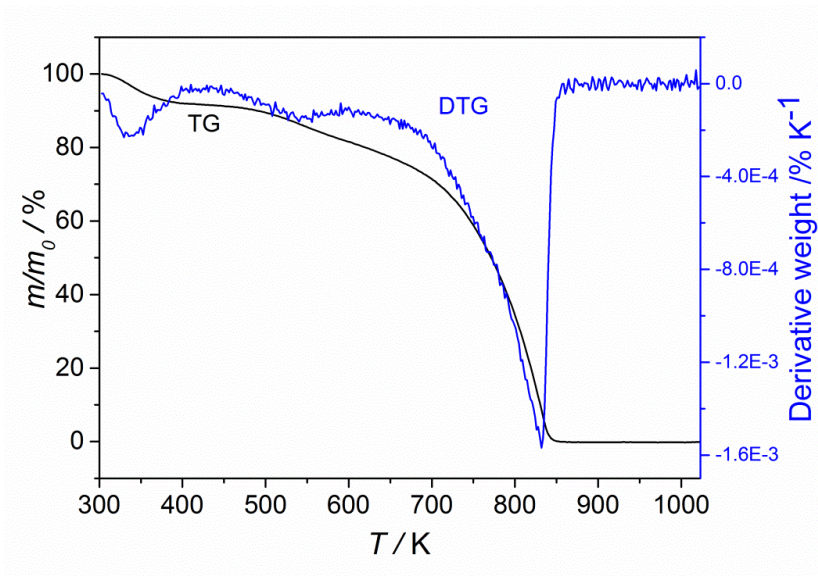


**Fig. D2.** TG and DTG profile of BILP-101 film under air flow (100 mL/min) at a heating rate of 5 K/min.

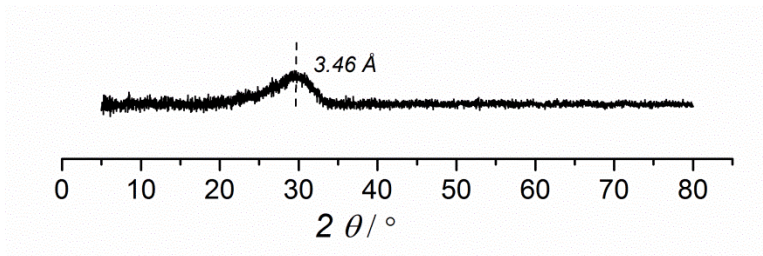


**Fig. D3.** Powder X-ray diffraction pattern of the free standing BILP-101 film.

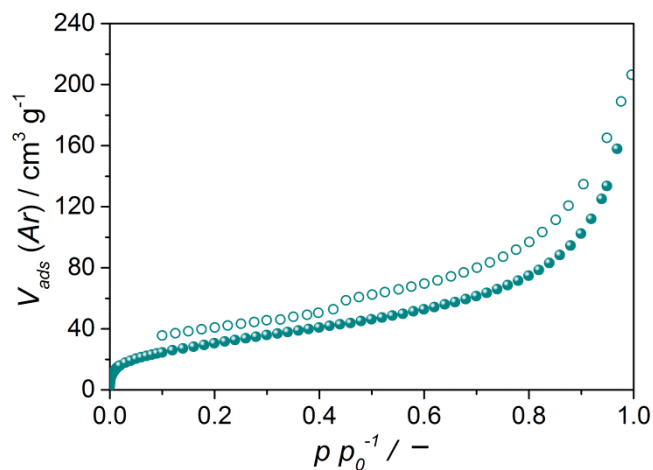


**Fig. D4.** Argon adsorption isotherms of BILP-101 film at 87 K.

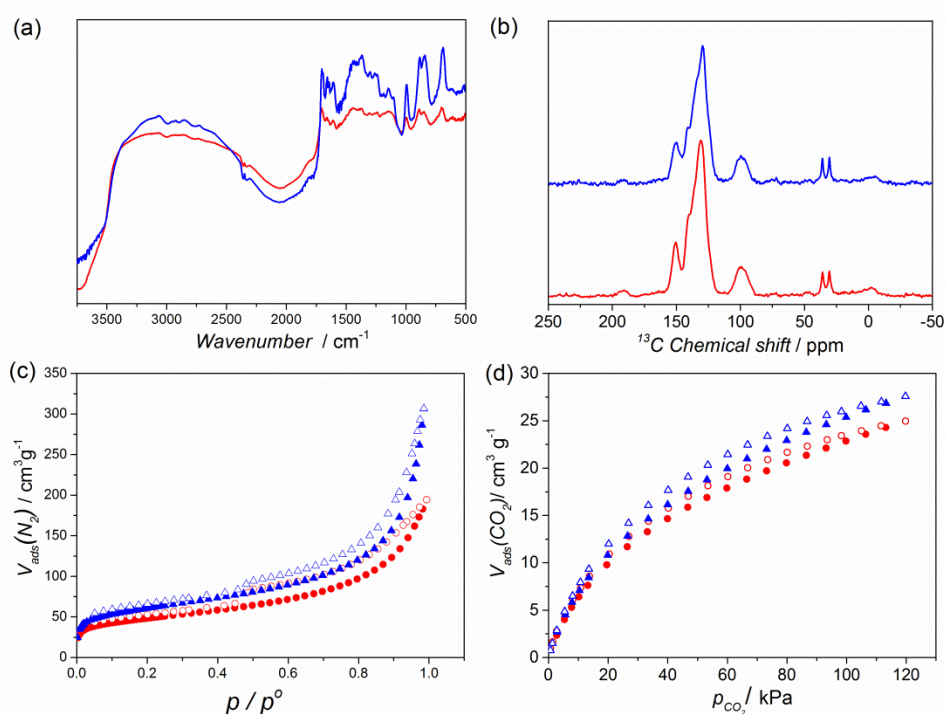


**Fig. D5.** Characterization of BILP-101 film prepared under A1 and A2 conditions. (a and b) DRIFT-IR and <sup>13</sup>C CP/MAS spectra of films. (c and d) N<sub>2</sub> and CO<sub>2</sub> adsorption (solid symbols) and desorption (open symbols) isotherms of the films at 77 and 298 K, respectively. Red and blue corresponds to samples A1 and A2, respectively.

**Table D1.** Summary of BILP-101 membranes' performance tested for different membranes in the H<sub>2</sub> separation of a 50:50 H<sub>2</sub>/CO<sub>2</sub> equimolar mixture at 423 K and different feed pressure conditions. Permeate side at atmospheric pressure with helium as sweep gas.

Membrane	Sample A1			
$PH_2$ [GPU]	$PN_2$ [GPU]	$PCO_2$ [GPU]	Selectivity H <sub>2</sub> /CO <sub>2</sub> [-]	Selectivity H <sub>2</sub> /N <sub>2</sub> [-]
18397	5508	5298	3.5	3.3

Membrane	Sample A2			
Feed pressure [bar]	2	3	4	10
$PH_2$ [GPU]	24	23	23	21
$PCO_2$ [GPU]	2.4	2.4	2.5	2.4
Selectivity H <sub>2</sub> /CO <sub>2</sub> [-]	10	9.6	9.2	8.8

Membrane	Sample A3-1			
Feed pressure [bar]	2	3	4	10
$PH_2$ [GPU]	24	23	22	18
$PCO_2$ [GPU]	0.61	0.61	0.63	0.71
Selectivity H <sub>2</sub> /CO <sub>2</sub> [-]	40	38	35	25

Membrane	Sample A4		
Feed pressure [bar]	2	3	4
$PH_2$ [GPU]	15	14	13
$PCO_2$ [GPU]	0.68	0.67	0.68
Selectivity H <sub>2</sub> /CO <sub>2</sub> [-]	22	20	19

Single gas permeation tests indicate that Sample A1 shows a characteristic of Knudsen diffusion, therefore a mixed-gas test was not performed. For membrane A4, a second layer was grown on top of the first layer (See details in experimental section). As expected, the H<sub>2</sub> permeance decreased due to the thicker layer. For A1, A2 and A3 membranes, the CO<sub>2</sub> permeance decreased with increasing monomer concentration, reflecting the formation of more dense membranes. DRIFT-IR and <sup>13</sup>C CP/MAS spectra of films confirm a similar composition (Fig. D5a and b). Interestingly, the relative intensity of aldehyde groups (~ 1700 cm<sup>-1</sup>) compared to the -C=N- (~1610 cm<sup>-1</sup>) in the imidazole ring in A1 and A2 samples is higher than that in sample A3 (Fig. 5.4 A), indicating more missing links exist in their structures which explains the lower selectivity for sample A1 and A2. This is further supported by the higher porosity of samples A1 and A2 (Fig. D5) compared to sample A3 (Fig. 5.4C). Overall, the membrane prepared under A3 conditions exhibits the best performance. Thus, we mainly focus on the discussion of membrane A3 in the main text. Only membranes A2 and A3-1 were further tested for H<sub>2</sub>/N<sub>2</sub> separation.

**Table D2** Summary of BILP-101 membranes' performance tested at different temperatures under 1 bar absolute feed pressure in the H<sub>2</sub> separation of a 50:50 H<sub>2</sub>/CO<sub>2</sub> equimolar.

Membrane	Sample A3-1			
Temperature [K]	423	448	473	498
$PH_2$ [GPU]	36	57	76	116
$PCO_2$ [GPU]	1.1	1.9	3.2	6.4
Selectivity H <sub>2</sub> /CO <sub>2</sub> [-]	34	29	24	18

**Table D3** Summary of BILP-101 membranes’ performance tested under different absolute feed pressures at 423 K in the H<sub>2</sub> separation of a 50:50 H<sub>2</sub>/CO<sub>2</sub> equimolar.

Membrane	Sample A3-1			
Temperature [K]	423	448	473	498
$PH_2$ [GPU]	24	23	22	18
$PCO_2$ [GPU]	0.61	0.61	0.63	0.71
Selectivity H <sub>2</sub> /CO <sub>2</sub> [-]	40	37	35	25

**Table D4.** Summary of BILP-101 membranes performance data for the H<sub>2</sub> separation of a 50:50 H<sub>2</sub>/N<sub>2</sub> equimolar mixture at 423 K and different feed pressure conditions. The data were obtained for different membranes under several feed pressure conditions. Permeate side at atmospheric pressure with helium as sweep gas.

Membrane	Sample A2			
Feed pressure [bar]	2	3	4	10
$PH_2$ [GPU]	21	20	20	18
$PN_2$ [GPU]	0.46	0.46	0.46	0.52
Selectivity H <sub>2</sub> /N <sub>2</sub> [-]	45	44	43	34

Membrane	Sample A3-1			
Feed pressure [bar]	2	3	4	10
$PH_2$ [GPU]	21	20	20	18
$PN_2$ [GPU]	0.24	0.22	0.22	0.24
Selectivity H <sub>2</sub> /N <sub>2</sub> [-]	87	92	91	75

**Table D5.** Membrane performance of typical PIM, TR-polymer, PBI and BILP presented in Fig. 5.5a. The membrane thickness was assumed to be 1  $\mu\text{m}$  when converting the permeability to permeance.

Membrane material		Performance		Operation conditions		Reference		
		$P_{H_2}$ (GPU)	$H_2/CO_2$ selectivity (-)	Type of analysis	$T$ (K)		Absolute Feed Pressure $P$ (bar)	
PIMs	PIM-EA-TB	7760	1.09	Single gas	298	1	(1)	
		7310	1.43	Single gas				
		6155	1.29	Single gas/aged 24h				
	PIM-SBI-TB	2200	0.76	Single gas	298	2	(2)	
		TPIM-1	2666	1.72				Single gas
		TPIM-2	655	1.51				"
	CoPI-TB-1	249	1.6	Single gas	308	1	(3)	
		CoPI-TB-2	403	1.9				"
		CoPI-TB-3	371	1.9				"
		CoPI-TB-4	667	2.8				"
		CoPI-TB-5	334	1.5				"
		CoPI-TB-6	472	1.4				"
TR Polymer	TR-1	1200	0.65	Single gas	298	1	(4, 5)	
	TR-6	6000	1.2	"				
	<i>m</i> PBO	206	6.2	Single gas	483	-	(6)	
	<i>p</i> PBO,	305	3.8	"				
	6 <i>f</i> PBO	505	3.5	"				
	PHBOA(8:2)	1.8	8.4	Single gas	308	10	(7)	
	PBOA(8:2)	3.4	5.4	"				
	PBOA(5:5)	4.2	5.6	"				
	PHBOA(8:2)	26.8	8	Single gas	483			
	PBOA(8:2)	22.3	6	"				
PBOA(5:5)	26.9	6.5	"					
PBI		0.09	9	Single gas	293	3.4	(8, 9)	
		13	20	Mixed gas	433			
		11	3	"	623			
		3.7	8.6	Single gas	308	3.5	(10)	
		2.9	7.1	Mixed gas	308	7		
		75	8.6	"	453	"	(11)	
		30	3.8	Mixed gas	423	5		
		2.9	7.9	Single gas	373	5-8	(13)	
		5.5	12.8	"	473			
		8.7	21.7	"	573			
		22.9	27.3	"	673			
		27	16	Single gas	423	8	(14)	
		50	19	Single gas	623~723	7		
		20	27.5	Single gas	623~723		(15)	
		162	5	Single gas	523	3.5		
		89	7	"			(16)	
		24.5	6.5	"				
		22.5	6.6					
		3.7	23					
		35.6	20.3	Mixed gas	523	6	(17)	
	BILP-101 (400 nm)	Fresh A3-1	24.2	39.5	Mixed gas	423	2	This work
Fresh A3-2		30.1	31.6	"		1		
A3-2 <sup>a</sup>		36.4	34.2	Dry gas mixture				
A3-2 <sup>b</sup>		25.6	37.6	Wet gas mixture				
BILP-101 (assumed 1 μm thickness)	A3-1	9.7	39.5	Mixed gas	423	2		
	A3-2	12.0	31.6	"		1		
	A3-2 <sup>a</sup>	14.6	34.2	Dry gas mixture				
	A3-2 <sup>b</sup>	10.2	37.6	Wet gas mixture				

<sup>a</sup> and <sup>b</sup> correspond to A3-2 sample measured after ~800 h on stream under alternating dry gas and wet gas

**References**

- D1 M. Carta, R. Malpass-Evans, M. Croad, Y. Rogan, J. C. Jansen, P. Bernardo, F. Bazzarelli and N. B. McKeown, *Science*, 2013, **339**, 303.
- D2 B. S. Ghanem, R. Swaidan, X. Ma, E. Litwiller and I. Pinnau, *Advanced Materials*, 2014, **26**, 6696.
- D3 Y. Zhuang, J. G. Seong, Y. S. Do, W. H. Lee, M. J. Lee, Z. Cui, A. E. Lozano, M. D. Guiver and Y. M. Lee, *Chemical Communications*, 2016, **52**, 3817.
- D4 H. B. Park, S. H. Han, C. H. Jung, Y. M. Lee and A. J. Hill, *Journal of Membrane Science*, 2010, **359**, 11.
- D5 H. B. Park, C. H. Jung, Y. M. Lee, A. J. Hill, S. J. Pas, S. T. Mudie, E. Van Wagner, B. D. Freeman and D. J. Cookson, *Science*, 2007, **318**, 254.
- D6 S. H. Han, H. J. Kwon, K. Y. Kim, J. G. Seong, C. H. Park, S. Kim, C. M. Doherty, A. W. Thornton, A. J. Hill, A. E. Lozano, K. A. Berchtold and Y. M. Lee, *Physical Chemistry Chemical Physics*, 2012, **14**, 4365.
- D7 Y. S. Do, J. G. Seong, S. Kim, J. G. Lee and Y. M. Lee, *Journal of Membrane Science*, 2013, **446**, 294.
- D8 D. R. Pesiri, B. Jorgensen and R. C. Dye, *Journal of Membrane Science*, 2003, **218**, 11.
- D9 C. A. Scholes, K. H. Smith, S. E. Kentish and G. W. Stevens, *International Journal of Greenhouse Gas Control*, 2010, **4**, 739.
- D10 T. Yang, G. M. Shi and T.-S. Chung, *Advanced Energy Materials*, 2012, **2**, 1358.
- D11 T. Yang, Y. Xiao and T.-S. Chung, *Energy & Environmental Science*, 2011, **4**, 4171.
- D12 J. Sánchez-Laínez, B. Zornoza, S. Friebe, J. Caro, S. Cao, A. Sabetghadam, B. Seoane, J. Gascon, F. Kapteijn, C. Le Guillouzer, G. Clet, M. Daturi, C. Téllez and J. Coronas, *Journal of Membrane Science*, 2016, **515**, 45.
- D13 S. C. Kumbharkar, Y. Liu and K. Li, *Journal of Membrane Science*, 2011, **375**, 231.
- D14 L. Zhu, M. T. Swihart and H. Lin, *Energy & Environmental Science*, 2018, **11**, 94.
- D15 R. Singh, G. Dahe, K. Dudeck, C. Welch and K. Berchtold, *Energy Procedia*, 2014, **63**, 153.
- D16 X. Li, R. Singh, K. Dudeck, K. Berchtold, B. Benicewicz, *Journal of Membrane Science*, 2014, **461**, 59
- D17 J. Sánchez-Laínez, B. Zornoza, C. Téllez and J. Coronas, *Journal of Membrane Science*, 2018, **563**, 427.





# SUMMARY

Membrane-based separation has become a promising alternative to traditional separation processes to capture CO<sub>2</sub> owing to the great features such as energy efficiency and environmental friendliness. Polymers are easy to process and have been commercialized. However, most commercial polymer membranes suffer from a trade-off relation between gas permeability and selectivity, expressed as the Robeson upper bound<sup>1</sup>. Porous organic frameworks (POFs) are an emerging class of microporous polymers, which may have high CO<sub>2</sub> permeability and selectivity when being processed into membranes due to their intrinsic porosity and strong CO<sub>2</sub> adsorption ability. However, using POFs as membranes are still at the infancy stage due to their insolubility in most common solvents.

Thus, this thesis focusses on the development of porous organic frameworks (POFs) membranes for various CO<sub>2</sub> separation applications, including biogas upgrading, (Chapter 2), post-combustion CO<sub>2</sub> capture (Chapter 3 and 4) and pre-combustion capture (Chapter 5). The fully organic nature together with the excellent thermal and chemical stabilities make POFs promising to be used as membranes for CO<sub>2</sub> separation.

**Part I (Chapter 1)** gives an introduction on different types of POFs along with their structures and applications in gas separation either in the form of mixed-matrix membranes (MMMs) or pure POF membranes. Some basic definitions and separation mechanisms are also discussed for better understanding the following chapters. POFs can have a crystalline or amorphous structure, thus we choose two types of POFs for membrane preparation. One is a crystalline POF, azine-linked covalent organic frameworks (ACOF-1) (**Part II**) and the other is an amorphous POF, benzimidazole-linked polymers (BILP-101) (**Part III**).

**Part II** includes **Chapter 2** and **3**. In Chapter 2, we first focus on the synthesis and characterization of an ACOF-1. ACOF-1 was chosen because of its relatively small pore size (~ 9.4 Å) and high CO<sub>2</sub> adsorption capacity. Diffusion reflectance infrared Fourier transform (DRIFT) and solid-state <sup>13</sup>C cross-polarization magic-angle spinning (CP/MAS) NMR spectroscopy confirms the successful synthesis of ACOF-1 with the

formation of characteristic C=N band. N<sub>2</sub> adsorption suggests a microporous structure. powder X-ray diffraction (PXRD) pattern reveals the good crystallinity. The CO<sub>2</sub> uptake of ACOF-1 at 1 bar, 3.92 mmol·g<sup>-1</sup>, is much higher than that of CH<sub>4</sub>, 0.92 mmol·g<sup>-1</sup>, which demonstrates its selectivity towards CO<sub>2</sub>. ACOF-1 was incorporated into Matrimid® to prepare MMMs. Cross-sectional scanning electron microscopy (SEM) images and Raman spectroscopy of the resulting membranes indicate a good dispersion of ACOF-1 in the polymer matrix. The ACOF-1 containing mixed-matrix membranes (MMMs) were tested for CO<sub>2</sub>/CH<sub>4</sub> separation at 308 K. The gas permeability increases with ACOF-1 loading and the 16 wt.% COF loading MMM shows an increase of more than doubling of the CO<sub>2</sub> permeability compared to the bare Matrimid® membrane, together with slightly higher CO<sub>2</sub>/CH<sub>4</sub> selectivities. The increase in gas permeability is attributed to the additional gas transport pathways introduced by the porous ACOF-1 network, while the slightly higher CO<sub>2</sub>/CH<sub>4</sub> selectivities can be rationalized by the selective adsorption of CO<sub>2</sub> over CH<sub>4</sub> in the N-rich ACOF-1 through dipole-quadrupole interactions.

In Chapter 3, ACOF-1 was further incorporated into 3 different polymer matrices (low flux-mid selectivity Matrimid®, mid flux-high selectivity Polyactive™ and high flux-low selectivity 6FDA:DAM) to investigate the influence of polymeric components on post-combustion CO<sub>2</sub> capture. For Matrimid® and 6FDA:DAM, an overall enhancement of the polymer's separation properties could be achieved, in case of Polyactive™ penetration of the more flexible polymer into the COF porosity resulted in a decreased membrane permeability. The best improvement was obtained for Matrimid®-based MMMs, for which the CO<sub>2</sub>/N<sub>2</sub> selectivity increases from 29 to 35, together with an enhancement in CO<sub>2</sub> permeability from 9.5 to 17.7 Barrer for 16 wt.% COF loading, was observed. All the composite membranes show a higher selectivity, which is attributed to the favorable CO<sub>2</sub> adsorption ability of ACOF-1. This chapter demonstrates that the combination of the filler-polymeric matrix pair chosen is crucial for POF based MMMs. Overall, **Part II** presents ACOF-1 as an interesting candidate to prepare MMMs for CO<sub>2</sub> separation.

**Part III** comprises **Chapter 4 and 5**. In this part, the main focus is on the development of BILP membranes for post-combustion (Chapter 4) as well as for pre-combustion (Chapter 5). BILP-101 was selected because of its ultra-microporous structure (reported pore size ~

5.4 Å) and high stability. In Chapter 4, BILPs with high and low porosity (BILP-101 and RT-BILP-101) were synthesized through controlling the initial polymerization rate. RT-BILP-101 with lower porosity was synthesized at room temperature, increasing the nucleation rate and resulting in smaller particle size and porosity. The incorporation of both BILPs into Matrimid® to prepare MMMs resulted in an increased gas permeability with loading for both CO<sub>2</sub> and N<sub>2</sub>, attributed to the introduction of fast transport ways by porous BILPs. MMMs fabricated with RT-BILP-101 exhibits a higher gas permeability than BILP-101 MMMs at the same loading. The best improvement was achieved by 24 wt.% RT-BILP-101 MMMs, for which the CO<sub>2</sub> permeability increases 2.8 times, from 9.6 to 26.5 Barrer. The selectivity remained constant upon BILP addition and is still determined by the polymer matrix.

**Chapter 5** describes the further engineering of BILP-101 into pure POF membranes. Using the interfacial polymerization method, free standing BILP-101 films were formed at a benzene-water interface. DRIFTS and <sup>13</sup>C CP/MAS) NMR spectroscopies confirm the same chemical connectivity as BILP spherical particles synthesized in Chapter 4. SEM, TEM and AFM supported the formation of sheet-like morphology. BILP-101 membrane films were further fabricated in a similar manner onto porous α-Al<sub>2</sub>O<sub>3</sub> supports with a top layer of γ-Al<sub>2</sub>O<sub>3</sub>. The obtained membranes demonstrated a high potential for pre-combustion CO<sub>2</sub> capture with an ultrahigh H<sub>2</sub> selectivity (up to 40) at elevated temperature (423 K) together with high-pressure resistance. Even at 10 bar absolute feed pressure and 423 K the membrane still exhibits a H<sub>2</sub>/CO<sub>2</sub> selectivity of 25. In addition, the membrane remained stable under alternating dry and humidified gas mixtures at 423 K during 800 h of operation. The separation performance was even slightly improved during this 800 h long hydrocycling test. The supported BILP membranes were also selective in the H<sub>2</sub>/N<sub>2</sub> separation with selectivity values up to 87. All results point to the interpretation that these membranes are operated by molecular sieving and can be used for a wider range of gas separation applications.

## ***Summary***

---

Overall, the obtained results in this thesis demonstrate that POFs are promising candidates to be applied in membrane fields for CO<sub>2</sub> separation. The fully organic nature makes POFs attractive and easy to be incorporated into polymers to prepare defect-free MMMs due to their excellent compatibility. Another alternative method, interfacial polymerization, offers an interesting outlook for the preparation of defect-free pure POF membranes. The combination of the above two preparation methods with the rich chemistry of POFs may open the door to the rational design of versatile POF membranes for a wide range of separations.

1. L. M. Robeson, *Journal of Membrane Science*, 2008, 320, 390.

# Samenvatting

Membraanscheiding is een veelbelovend alternatief geworden voor traditionele scheidingsprocessen om CO<sub>2</sub> af te vangen. Dit komt doordat membraanscheiding energie-efficiënt en milieuvriendelijk is en een kleine fysieke 'footprint' heeft. De meeste membranen zijn gebaseerd op polymeren. Polymeren zijn gemakkelijk te verwerken en reeds gecommercialiseerd. Echter, de meeste commerciële polymeermembranen vertonen een negatieve correlatie tussen de gaspermeabiliteit en selectiviteit, wat tot uitdrukking komt in the zogenaamde 'Robeson limit'<sup>1</sup>. Porous Organic Frameworks (POF's) zijn een opkomende klasse van microporeuze polymeren, die een hoge CO<sub>2</sub> permeabiliteit en selectiviteit kunnen vertonen wanneer ze worden verwerkt in membranen vanwege hun intrinsieke porositeit en sterk CO<sub>2</sub>-adsorptievermogen. Echter, het gebruik van POF's in of als membranen staat nog steeds in de kinderschoenen vanwege hun onoplosbaarheid in de meeste oplosmiddelen.

Dit proefschrift richt zich daarom op de ontwikkeling van Porous Organic Framework (POF) membranen voor een variëteit aan CO<sub>2</sub> scheidingstoepassingen, waaronder: biogas zuivering (Hoofdstuk 2), CO<sub>2</sub> afvang uit rookgas ('post-combustion', Hoofdstuk 3 en 4) en uit synthesegas ('pre-combustion', Hoofdstuk 5). De volledig organische aard samen met de goede thermische en chemische stabiliteit maken POF's veelbelovend om te gebruiken voor CO<sub>2</sub>-scheiding.

**Deel I (Hoofdstuk 1)** introduceert de verschillende typen POF's samen met bijbehorende structuren en toepassingen in gasscheiding, zowel in de vorm van mixed-matrix membranen (MMMs) als zuivere POF membranen. Enkele basisdefinities en scheidingsmechanismen worden toegelicht voor beter begrip van de volgende hoofdstukken. POF's hebben een kristallijne of een amorfe structuur, dus er zijn twee typen POF's voor membraan bereiding. De kristallijne POF is een azine-linked covalent organische framework (ACOF-1) (**Deel II**) en de amorfe POF is een benzimidazole-linked polymeer (BILP-101) (**Deel III**).

**Deel II** omvat **Hoofdstuk 2 en 3**. In hoofdstuk 2, wordt eerst de synthese en karakterisering van een ACOF-1 beschreven. ACOF-1 is gekozen vanwege zijn relatief kleine poriegrootte ( $\sim 9.4$  Å) en hoge CO<sub>2</sub> adsorptie capaciteit. Diffuse reflectance infrared Fourier Transform (DRIFT) spectroscopie en solid-state <sup>13</sup>C cross-polarization magic-angle spinning (CP/MAS) NMR spectroscopie bevestigen de succesvolle synthese van ACOF-1 aan de hand van de vorming van de karakteristieke C=N verbinding. N<sub>2</sub> adsorptie suggereert een microporeuze structuur. Poeder X-ray diffractie (PXRD) patronen tonen een goede kristalliniteit aan. De CO<sub>2</sub> opname van een ACOF-1 bij 1 bar is met 3.92 mmol·g<sup>-1</sup> veel hoger dan die van CH<sub>4</sub>, 0.92 mmol·g<sup>-1</sup>, wat de selectiviteit voor CO<sub>2</sub> demonstreert. MMMs zijn bereid door ACOF-1 in te bedden als 'filler' in Matrimid®. Cross-sectional scanning electron microscopy (SEM) afbeeldingen en Raman spectroscopie van de membranen indiceren een goede dispersie van ACOF-1 in de polymeer matrix. De ACOF-1 bevattende mixed-matrix membranen (MMM's) zijn getest op CO<sub>2</sub>/CH<sub>4</sub> scheiding bij 308 K. De gas permeabiliteit neemt toe met de ACOF-1 belading en de 16 wt.% beladen MMM heeft een meer dan dubbele CO<sub>2</sub> permeabiliteit dan het Matrimid® membraan en een iets hogere CO<sub>2</sub>/CH<sub>4</sub> selectiviteit. De toename in gaspermeabiliteit wordt toegeschreven aan de extra gastransportwegen geïntroduceerd door de poreuze ACOF-1 netwerken, terwijl de enigszins hogere CO<sub>2</sub>/CH<sub>4</sub> selectiviteit kan worden verklaard door de selectieve adsorptie van CO<sub>2</sub> over CH<sub>4</sub> door dipool-quadrupole interacties in de N-rijke ACOF-1.

In **Hoofdstuk 3**, is ACOF-1 ingebed in 3 verschillende polymeer matrices (lage flux-gemiddeld selectief Matrimid®, gemiddelde flux-hoog selectief Polyactive™ en hoge flux-laag selectief 6FDA:DAM) om de invloed van polymeercomponenten op de CO<sub>2</sub> afvang uit rookgas (post-combustion CO<sub>2</sub> capture) te onderzoeken. Voor Matrimid® en 6FDA:DAM, werd een algehele verbetering van de scheidingseigenschappen van het polymeer bereikt. In het geval van Polyactive™ resulteerde penetratie van dit meer flexibele polymeer in de poreuze COF in een verminderde membraanpermeabiliteit. De grootste verbetering werd gemaakt met de Matrimid® gebaseerde MMM's waarbij de CO<sub>2</sub>/N<sub>2</sub> selectiviteit toeneemt van 29 tot 35, tezamen met een verhoging van de CO<sub>2</sub> permeabiliteit van 9.5 tot 17.7 Barrer voor 16 wt.% COF belading. Alle composietmembranen vertonen een hogere

selectiviteit, die wordt toegeschreven aan het selectieve CO<sub>2</sub> adsorptievermogen van ACOF-1. Dit hoofdstuk laat zien dat de combinatie van het gekozen filler-polymeer matrix paar cruciaal is voor op POF gebaseerde MMM's. Deel II laat zien dat ACOF-1 een interessante kandidaat is voor de bereiding van MMM's voor CO<sub>2</sub>-scheiding.

**Deel III** omvat **hoofdstuk 4 en 5**. In dit deel ligt de nadruk op de ontwikkeling van BILP-membranen voor post-combustion CO<sub>2</sub> capture (hoofdstuk 4) en voor pre-combustion CO<sub>2</sub> capture (hoofdstuk 5). BILP-101 werd geselecteerd vanwege zijn ultra-micro poreuze structuur (gerapporteerde poriegrootte ~ 5.4 Å) en hoge stabiliteit. Voor Hoofdstuk 4 zijn BILP's met hoge en lage porositeit (BILP-101 en RT-BILP-101) gesynthetiseerd door de initiële polymerisatiesnelheid te regelen. RT-BILP-101 met lagere porositeit werd gesynthetiseerd bij kamertemperatuur, waardoor de nucleatiesnelheid toenam, resulterend in kleinere deeltjesgrootte en lage porositeit. Het inbedden van beide BILP's in Matrimid® om MMM's te bereiden resulteerde in een toename van gaspermeabiliteit met belading voor zowel CO<sub>2</sub> als N<sub>2</sub>, toegeschreven aan de introductie van transport snelwegen door poreuze BILP's. MMM's gefabriceerd met RT-BILP-101 vertonen een hogere gaspermeabiliteit dan BILP-101 MMM's bij dezelfde belading. De beste verbetering werd bereikt met 24 gew.% RT-BILP-101 MMM's, waarbij de CO<sub>2</sub>-permeabiliteit 2.8 maal toeneemt, van 9.6 tot 26.5 Barrer. De selectiviteit bleef constant bij toevoeging van BILP en wordt nog steeds bepaald door de polymeermatrix.

**Hoofdstuk 5** beschrijft de verdere engineering van BILP-101 in pure POF-membranen. Door toepassing van de grensvlakpolymerisatiemethode werden vrijstaande BILP-101-films gevormd op het grensvlak tussen benzeen en water. DRIFTS en <sup>13</sup>C (CP/MAS) NMR-spectroscopie bevestigen dezelfde chemische bindingen als in de bolvormige BILP deeltjes gesynthetiseerd in hoofdstuk 4. SEM, TEM en AFM ondersteunen de vorming van een gelaagde morfologie. BILP-101 membraanfilms zijn verder op vergelijkbare wijze vervaardigd op poreuze α-Al<sub>2</sub>O<sub>3</sub> dragers met een toplaag van γ-Al<sub>2</sub>O<sub>3</sub>. De verkregen membranen zijn zeer interessant voor pre-combustion CO<sub>2</sub> afvang, zij combineren een ultrahoge H<sub>2</sub>-CO<sub>2</sub> selectiviteit (tot 40) bij verhoogde temperatuur (423 K) met mechanische weerstand tegen hoge druk. Zelfs bij een absolute voedingsdruk van 10 bar en 423 K vertoont het membraan nog steeds een H<sub>2</sub>/CO<sub>2</sub> selectiviteit van 25. Bovendien



bleef het membraan stabiel onder alternerende droge en bevochtigde gasmengsels bij 423 K gedurende een duurttest van 800 uur. De scheidingsprestatie verbeterde zelfs lichtjes tijdens deze 800 uur lange hydro-cycling-test. De gedragen BILP-membranen waren ook selectief in de  $H_2/N_2$  scheiding met selectiviteitswaarden tot 87. Alle resultaten wijzen erop dat deze membranen werken op basis van moleculair zeven en dat ze kunnen worden gebruikt voor een breder scala aan toepassingen in gasscheiding.

Over het algemeen laten de verkregen resultaten in dit proefschrift zien dat POF's veelbelovende kandidaten zijn om voor  $CO_2$ -scheiding in membraan systemen te worden toegepast. De volledig organische aard en hun uitstekende compatibiliteit maakt POF's aantrekkelijk om ze eenvoudig in polymeren te verwerken tot defectvrije MMM's. Een andere alternatieve methode, grensvlakpolymerisatie, biedt interessante perspectieven voor de bereiding van defectvrije zuivere POF-membranen. De combinatie van de bovenstaande twee bereidingsmethoden met de rijke chemie van POF's kan de deur openen naar het rationele ontwerp van veelzijdige POF-membranen voor een breed scala aan scheidingen.

1. L. M. Robeson, *Journal of Membrane Science*, 2008, 320, 390.

# Acknowledgements

Looking back on the past four years, I thank God for bringing me to this beautiful country and guiding me in the whole journey of my PhD study. At first, I was a bit nervous about the numerous challenges I was facing and experienced depression and anxiety. Finally, the journey turns out to be exciting and enjoyable with the help and encouragement from many people, my supervisors, my colleagues, my friends and my family. Thus, I would like to take the opportunity to thank all of them for their contribution to this work.

My supervisor and promotor Prof. dr. Jorge Gascon, thanks for your swift reply and accept me as a PhD candidate when I send you the first email, which made me believe next four years I would spend in Delft. Thanks for your constant encouragements during these years. Since I had no background in chemistry and no working experience in the lab, I felt frustrated when just starting my PhD, but your encouragement and trust really helped me a lot. I still remember your words “no problem, you can learn” in the first meeting. I admire your optimistic attitude and smart reaction towards research. When I got lost, you were always in the position to give me insightful suggestions to try again which makes my research goes smoothly. My sincere thanks also go to my promotor Prof. dr. Freek Kapteijn for his critical, professional supervision and deep discussion on my thesis. I admire your sensitivity towards mistakes. You can always point out the mistakes in the manuscript. Your serious and responsible attitude towards science will influence me the whole life. By the way, I like the sentence you send me “stay focus till the end”. I also enjoy the conference we spent together in Dalian, you are more like a friend rather than a promotor.

I would also like to thank all the co-authors in my paper. Thanks Elena for teaching me every detail in the lab when I just started my PhD. Beba, my deep thanks for your supervision during the four years, especially on chapters 2, 3 and 4. You led me through the membrane area. You taught me every detail in preparing MMMs, operating the permeation setup and data analysis. I also appreciate the manuscript revision notes you

gave me which helped me improving my writing skills. Even though sometimes we had different ideas, you were always so kind to listen and explain to me. Hope we will have more collaboration in the future. Xinlei, thank you so much for your immense help and guidance on Chapter 5. I start to know how to prepare pure membranes and go deeper in the membrane field. Without your help, I am sure that I could not finish Chapter 5 that fast. I admire your solid knowledge and rich experience on membranes. I really learnt a lot from you! Xuerui, I appreciate your help on fixing my setup. You are the “second Bart” in the lab! Thanks also for your artwork contribution on my thesis. Xinlei & Xuerui, both of you helped me a lot in the lab, thank you for your patience with all my annoying questions! In addition, your dedicated attitude towards science also influenced me a lot! Surely, I hope to have more collaboration with you in the future and keep learning from both of you! Alla, you have talent in designing. Thank you so much for building such a beautiful COF network and cover page for me. Irina, thanks for taking care of my samples in KAUST. I appreciate your kind contribution and nice suggestions on Chapter 4 and 5. Eduardo, thank you for the long time measurement on N<sub>2</sub> and CO<sub>2</sub> adsorption. Alexey, your kind discussion and help on Chapter 4 was great for me. I admire your solid background in chemistry! Besides science, thank you for making a cheerful atmosphere in the lab! You always break the silence in the lab with Chinese old stories! Nastya, thank you for teaching me how to make CTFs. Although I do not have results to publish, I learnt a lot from you! Liangyong, we are from the same group and knew each other before. Thanks for your suggestion for choosing TUD. I appreciate your kind help and discussion on AFM!

My PhD research could not be smoothly completed without the assistance of technicians. I would like to thank Bart for the help to check and fix my permeation setup and also for the guidance in using TGA, and DRIFTS. I have never seen you in a bad mood, that’s why I always asked your help from time to time. Thank you for your patience! In addition, my sincere thanks to you and your daughter for help translating the summary! I would also like to give thanks to Willy for the kind and patient help in N<sub>2</sub>, CO<sub>2</sub>, CH<sub>4</sub> and Ar adsorption measurements and detailed data explanation. Harrie, thanks for the help in the old building for checking the setup, ordering and moving chemicals. Liliana, thanks for the help in GC analysis. Besides our lab, I am also grateful for the help of technicians outside

CE. Marcel, Duco and Ben, I am grateful to your patient training in AFM, SEM and XRD measurements. Thanks to Wiel and Stephen for their help on TEM and NMR analysis. I also appreciate the help from gas team member Erwin. You are always so kind and efficient to check the gas supply, so that I could always run the set-up.

I also would like to thank the secretaries in our group. Els, thank you so much for the help to arrange everything on the administrative issues. Caroline, thank you so much for help me deliver chemicals

Further, I want to thank all the members in the catalysis engineering group. Thank you all for providing me with a friendly environment for research and life. Xiaohui, thanks for guiding me to know new study environment in the early stages. Sonia and Alma, thanks for the help and discussion on COF synthesis. Ana, thanks for sharing your experience on using the permeation setup and nice coffee talks on life! Miren, I appreciate your help in calibrating the GC and your nice suggestions on preparing PBI membranes! Martijn, thanks for teaching me some modeling methods! Maria, thanks for helping me sending samples to Spain. Jara, your accompany in Edinburgh was great and thanks for sharing your PhD research experience! Eli, thanks for explaining GC to me when I just started my PhD and also for your great talk in Dalian! Riming, you are so kind to help me carry the luggage in France! Thanks Ina for sharing your life and research when we eat dinner together. Agi, your nice reminders for Friday drinks are great! Dima, you are always in good mood! Thanks for your nice greetings! I would also like to thank my students, Hodayfa, Pim, Ravi, Zhongping, Raoul, Liset, Berend, Danique. Thanks also to Yixiao, Guanna, Tim, Prof. Xu, Adrian, Constantino, Robert, Lide, Rupali, Rob, Chuncheng, ... for the nice time in the CE group!

Further, thanks to my other friends outside the lab. Juan, my best friend, you are right, we already studied together for 11 years! Thank you for your accompany during these years. When I feel depressed about research and life, you are always the person I want to share my feelings. Your suggestions and encouragement really helps me a lot! you are always independent and decisive, you teach me a lot! Surely, I will continue bothering you even though you are already in China! Haiyan, we started the PhD almost at the same time in Delft! Thanks for sharing your research and life to me! Thanks for listening my

weakness and encouraging me when I got lost. Prof. Xue, thank you for teaching me how to do research and your kind encouragement during these years! Ming, Anping, Rong, Yujie, Fan, Yaya, Yiming, Kai (Z & L), Qian, Dengyang, Wuyuan, Min, Jingyu, Zhi, Yuan, Tiantian, ... Thank you all for being my friends in Delft and share the great time with me! I owe my special thanks to my friends from Delft fellowship, Lulu, Yanchun, Haiyan, Nelly, Yuting, Chengcheng, Yingzhu, Jingwen, Ting, Tianmu, Xuan, Feifei, Michelle, Shangyu, Liang, Weiyan, Philip, Ou, Zanni, Pan, Yan, Renshi, Yonghui, Ye, Xuanyu, Fei, Yi, Siqi, Chao, Maokun, brother Pan and Weiwei, Uncle Li and Aunt Li, Pastor Cai (sorry I cannot list all the names here). Thank you all for your help, prayer and accompany. We are brothers and sisters, really like one family. I really enjoyed every weekend during these four years and learnt a lot from all of you!

I am grateful to my family in China. Thank you for your support and love. I will write in Chinese, sorry for the inconvenience.

谢谢我亲爱的爸爸妈妈，让我一直读书读到现在，谢谢你们深深的爱。我知道在国外这几年你们没少挂念，没少为我祈祷，谢谢你们默默的支持！谢谢你们的养育，教导，支持，使我得以在学业路上走的更远。姐姐，姐夫，哥哥，嫂子，谢谢你们无微不至的照顾爸妈，谢谢你们为家里所做的一切，我才可以无负担无压力地在这里学习！谢谢你们每一次宝贵的建议以及每次回国的照顾与宴请！谢谢公公婆婆的理解与支持，谢谢你们每次回国对我的照顾和关爱！谢谢“家人微信群里”的各位，不一一列出了，谢谢你们时时分享故乡的照片和可爱的宝宝们！确实减缓了我的思乡之情！很遗憾在我即将交论文时公公和外婆相继离开，留给我深深的亏欠与无奈！我不得不承认四年其实也是一段很长的人生路。。。

Last but not least, I want to express my deepest appreciation for my husband Chenghai, whom I met when I just entered the university. Thank you for waiting for me for such long time! Despite the time difference, you are always there to listen to me, encouraging me, comfort me and cheer me up when I am down. Sorry for disturbing your rest when I feel upset! Thank you for your full understanding, support and love during these years! Thank you for preparing everything for our home. Looking forward to experience all the moments with you coming soon!

# List of publications

## Publications related to this thesis:

1. **M. Shan**, B. Seoane, E. Rozhko, A. Dikhtiarenko, G. Clet, F. Kapteijn, J. Gascon, Azine-Linked Covalent Organic Framework (COF)-based Mixed-Matrix Membranes for CO<sub>2</sub>/CH<sub>4</sub> Separation. *Chemistry—A European Journal*, 2016, 41, 14467-14470. (**Hot paper, Inside Cover, highlight by ChemViews**)
2. **M. Shan**, B. Seoane, E. Andres-Garcia, F. Kapteijn, J. Gascon, Mixed-matrix Membranes Containing an Azine-Linked Covalent Organic Framework: Influence of the Polymeric Matrix on Post-Combustion CO<sub>2</sub>-Capture, *Journal of Membrane Science*, 2018, 549, 377-384.
3. **M. Shan**, B. Seoane, A. Pustovarenko, X. Wang, X. Liu, I. Yarulina, F. Kapteijn, J. Gascon, Benzimidazole Linked Polymers (BILP) in Mixed-Matrix Membranes: Influence of Filler Porosity on the CO<sub>2</sub>/ N<sub>2</sub> Separation Performance, *Journal of Membrane Science*, 2018, 566, 213-222.
4. **M. Shan**, X. Liu, X. Wang, I. Yarulina, B. Seoane, F. Kapteijn, J. Gascon, Facile Manufacture of Porous Organic Framework Membranes for Pre-Combustion CO<sub>2</sub> Capture, *Science Advances*, 2018, 4, eaau1698.

## Other publications

5. **M. Shan**, X. Liu, X. Wang, H. Lziyi, J. Gascon, F. Kapteijn, High Performance Ultrathin Polybenzimidazole Membranes Formed by Interfacial Polymerization for H<sub>2</sub>/CO<sub>2</sub> Separation. (*In preparation*)
6. **M. Shan**, Q. Xue, N. Jing, C. Ling, T. Zhang, Z. Yan, J. Zheng, Influence of Chemical Functionalization on the CO<sub>2</sub>/N<sub>2</sub> Separation Performance of Porous Graphene Membranes, *Nanoscale*, 2012, 4, 5477–5482.
7. **M. Shan**, Q. Xue, T. Lei, W. Xing, Z. Yan, Self-Assembly of Helical Polyacetylene Nanostructures on Carbon Nanotubes, *The Journal of Physical Chemistry C*, 2013, 117, 16248-16255.

8. A. Cao, **M. Shan**, L. Paltrinieri, W.H. Evers, L. Chu, L. Poltorak, J. H. Klootwijk, B. Seoane, J. Gascon, E. J.R. Sudhölter, L. CP. Smet, Enhanced Vapour Sensing using Silicon Nanowire Devices Coated with Pt Nanoparticle Functionalized Porous Organic Frameworks, *Nanoscale*, 2018, 10, 6884-6891 (**Cover paper**)
9. A. Pustovarenko, M. G. Goesten, S. Sachdeva, **M. Shan**, Z. Amghouz, Y. Belmabkhout, A. Dikhtiarenko, T. Rodenas, D. Keskin, I. K. Voets, B. M. Weckhuysen, M. Eddaoudi, L. CPM Smet, E. JR Sudhölter, F.Kapteijn, B. Seoane, J. Gascon, Nanosheets of Nonlayered Aluminum Metal–Organic Frameworks through a Surfactant Assisted Method, *Advanced Materials*, 2018, 30, 1707234.
10. X. Liu, X. Wang, A Bavykina, L. Chu, **M. Shan**, A. Sabetghadam, H. Miro, F. Kapteijn, J. Gascon, Molecular-Scale Hybrid Membranes Derived from Metal–Organic Polyhedra for Gas Separation, *ACS Applied Materials & Interfaces*, 2018, 10, 21381–21389.
11. X. Wang, P. Karakiliç, X. Liu, **M. Shan**, A. Nijmeijer, L. Winnubst, J. Gascon, F. Kapteijn, *ACS Applied Materials & Interfaces*, Accepted, DOI: 10.1021/acsami.8b12613
12. Q. Xue, **M. Shan**, Y. Tao, Z. Liu, C. Ling, Y. Du, N-Doped Porous Graphene for Carbon Dioxide Separation: A Molecular Dynamics Study, *Chinese Science Bulletin*, 2014, 59, 3919-3925.
13. Y. Tao, Q. Xue, Z. Liu, **M. Shan**, C. Ling, T. Wu, X. Li, Tunable Hydrogen Separation In Porous Graphene Membrane: First-Principle and Molecular Dynamic Simulation, *ACS Applied Materials & Interfaces*, 2014, 6, 8048-8058.
14. T. Wu, Q. Xue, C. Ling, **M. Shan**, Z. Liu, Y. Tao, X. Li, Fluorine-Modified Porous Graphene as Membrane for CO<sub>2</sub>/N<sub>2</sub> Separation: Molecular Dynamic and First-Principles Simulations, *The Journal of Physical Chemistry C*, 2014, 118,7369-7376.
15. C. Lv, Q. Xue, **M. Shan**, N. Jing, C. Ling, X. Zhou, Z. Jiao, W. Xing, Z. Yan, Self-Assembly of Double Helical Nanostructures Inside Carbon Nanotubes, *Nanoscale*, 2013, 5, 4191–4199. (**Cover Paper**)
16. Q. Xue, C. Lv, **M. Shan**, H. Zhang, C. Ling, X. Zhou, Z. Jiao, Glass transition temperature of functionalized graphene–polymer composites, *Computational Materials Science*, 2013, 71, 66-71
17. T. Zhang, Q. Xue, **M. Shan**, Z. Jiao, X. Zhou, C. Ling, Z. Yan, Adsorption and Catalytic

Activation of O<sub>2</sub> Molecule on the Surface of Au-doped Graphene under an External Electric Field, *The Journal of Physical Chemistry C*, 2012, 116, 19918–19924.

18. J. Li, Q. Xue, **M. Shan**, S. Wang, Y. Zhen, Z. Han, Room-Temperature Hydrogen-Sensitive Characteristics of Pd/boron Doped Amorphous Carbon Film/n-Si Structure, *Sensors and Actuators B: Chemical*, 2012, 161, 1102–1107.

19. N. Jing, Q. Xue, C. Ling, **M. Shan**, T. Zhang, X. Zhou, Z. Jiao, Effect of Defects on Young's Modulus of Graphene Sheets: A Molecular Dynamics Simulation, *RSC Advances*, 2012, 2, 9124–9129.

20. C. Ling, Q. Xue, D. Xia, **M. Shan**, Fullerene Filling Modulates Carbon Nanotube Radial Elasticity and Resistance to High Pressure, *RSC Advances*, 2014, 4, 1107–1115.

21. Z. Liu, Q. Xue, T. Zhang, Y. Tao, C. Ling, **M. Shan**. Carbon Doping of Hexagonal Boron Nitride by using CO Molecules, *The Journal of Physical Chemistry C*, 2013, 117, 9332–9339.

## Patent

J. Gascon, **M. Shan**, X. Liu, F. Kapteijn, Method for the Fabrication of Supported Benzimidazole-Linked Polymer (BILP) Membranes and Application, *US Patent*, 62/659,271.

## Presentations

**M. Shan**, B. Seoane, G. Clet, F. Kapteijn, J. Gascon, Azine-linked Covalent Organic Frameworks (COFs) based Mixed Matrix Membranes for CO<sub>2</sub> separation, 7<sup>th</sup> International Zeolite Membrane Conference, Dalian, China, August 2016 **(Oral)**

**M. Shan**, B. Seoane, F. Kapteijn, J. Gascon, Covalent Organic Frameworks as Fillers in Mixed Matrix Membranes for Efficient CO<sub>2</sub> Capture, Dutch Membrane Day, Venue De St@art Apenheul, Apeldoorn, The Netherlands, June 2016 **(Poster)**

**M. Shan**, B. Seoane, F. Kapteijn, J. Gascon, Covalent Organic Frameworks based Mixed Matrix Membranes for CO<sub>2</sub> Separation, New Directions for Porous Material-Faraday Discussion, Edinburgh, UK, June 2017 **(Poster)**

**M. Shan**, B. Seoane, F. Kapteijn, J. Gascon, Mixed Matrix Membranes containing Azine-linked Covalent Organic Frameworks (ACOF-1) as Filler in Different Polymers for CO<sub>2</sub> Separation. EuroMOF2017, Delft, The Netherlands, October 2017 **(Poster)**



**M. Shan**, B. Seoane, F. Kapteijn, J. Gascon, Mixed-Matrix Membranes Containing an Azine-Linked Covalent Organic Framework for CO<sub>2</sub> Separation, Euromembrane2018, Valencia, Spain, July 2018 **(Oral)**

# Curriculum Vitae

Meixia Shan was born on November 19, 1988 in Shangqiu, Henan province, China. She received her bachelor's degree in Applied Physics from college of Science at China University of Petroleum (Huadong) in 2011. Afterwards, she continued her masters study in Materials Science and Engineering at the same university under the supervision of Prof. dr. Qingzhong Xue. Her bachelor thesis, entitled 'Hydrogen Gas Sensing Properties of Pd/boron Doped Amorphous Carbon Film/n-Si Structure' resulted in



her first co-authorship research paper. Her master thesis, entitled "Molecular Dynamic Simulation of Gas Separation Performance of Graphene Membranes" was awarded as the outstanding thesis of Shandong Province. In September 2014, she moved to the Netherlands and started her PhD project under the supervision of Prof. dr. Freek Kapteijn and Prof. dr. Jorge Gascon in the group of Catalysis Engineering at the Department of Chemical Engineering, Faculty of Applied Sciences at the Delft University of Technology. This project was focused on the application of porous organic framework membranes for CO<sub>2</sub> separation.

Currently, she works as a post-doc in the Transport Phenomena group at the Department of Chemical Engineering, Faculty of Applied Sciences at the Delft University of Technology under the supervision of Dr. Ir. David A. Vermaas, working on metal organic framework (MOF) based mixed matrix membranes for post-combustion CO<sub>2</sub> capture.